

AALBORG UNIVERSITY

MASTER THESIS REPORT

---

# Experimental and numerical investigation of the powder die filling process

---

*Authors:*

Dimitra ALEXOULI

Lisa R. BØYSTRUP

*Supervisor:*

Benny Ø. ENDELT

June the 1<sup>st</sup>, 2018



**AALBORG UNIVERSITET**



**Title:**

Experimental and numerical investigation of the powder die filling process

**Theme:**

Master Thesis

**Project period:**

1<sup>st</sup> of February - 1<sup>st</sup> of June 2018

**Project group:**

Group 14.35-e

**Group members:**

---

Dimitra Alexouli



---

Lisa Rydahl Bøstrup

**Supervisor:**

Benny Ørtoft Endelt

**Examiner:**

Lars Erik Bräuner

**Pages:** 97

*By signing this document, each member of the group confirms participation on equal terms in the process of writing the project. Thus, each member of the group is responsible for the all contents in the project.*



# Resumé

---

Processen med at fylde en form med metalpulver fra en fyldesko, efterfulgt af komprimering af pulveret i formen og sintring af den komprimerede del har været i brug til fremstilling af metalkomponenter i mange år. Metoden "pres og sintring" foretrækkes i forhold til andre produktionsmetoder, fordi det er en hurtig og forholdsvis nem metode, som kan give fordelagtige egenskaber til komponenterne. Slutprodukterne anvendes hovedsageligt inden for bil, medicin og fødevarerindustrien.

Dette projekt er udviklet i samarbejde med Sintex A / S, der bruger "presse- og sintringsmetoden" til at producere dele til en lang række kunder og brancher. Pulvermetallurgiindustrien, såvel som den akademiske verden, mangler en absolut forståelse af fyldningsprocessen, og dermed er en optimering af processen problemfyldt.

Fyldningstrinnet i processen anses for at have stor indflydelse på slutproduktet. Det argumenteres at være fordi, at egenskaberne af slutproduktet (såsom homogen tæthed) er arvet fra fyldningsfasen. De fleste numeriske modeller, der er udviklet til processen hidtil, går ind fra et akademisk synspunkt og ikke et industrielt, og et flertal er begrænset til 2D-simuleringer på grund af de store beregningsmæssige omkostninger.

Derfor er fokuset i denne undersøgelse på at forstå fyldningsprocessen og dens underliggende mekanismer på et dybere niveau. Desuden er en numerisk model udviklet til at imødekomme denne forståelse, samt muligvis optimere nogle procesparametre. Samtidig udformes og udføres eksperimenter for at lette modellens validering såvel som procesobservationer.

Derfor kan projektets titel formuleres som følger:

## *Eksperimentel og numerisk undersøgelse af pulver form fyldning*

Undersøgelser af fyldningsprocessen fremhæver vigtigheden af fyldningshastighed, formgeometri, dvaletid og pulverhøjde som indflydelsesrige parametre. Disse parametre undersøges eksperimentelt gennem massefyldeindikationer og pulverstrømningsobservationer ved anvendelse af en gamma-densitometri-maskine og et højhastighedskamera, og der er gjort en indsats for at få en dybere forståelse af pulveradfærden under fyldning. Sammenfattet kan det ses, at dvaletiden, skohastigheden og formgeometrien har en vigtig

indvirkning på pulverstrømmen såvel som på slutdensiteten af pulveret i formen efter fyldning.

3D-numeriske modeller udvikles ved hjælp af LS-DYNA til at undersøge pulverstrømningen og aflejringen, og et forsøg på at medtage luften i processen er lavet, da nyere undersøgelser understreger dens betydning for fyldningsprocessen. Der er gjort en indsats for at verificere de udviklede numeriske modeller ved sammenligning med de eksperimentelle pulverstrømnings- og tæthedsresultater, men de har ikke været frugtbare.

Sammenfattet konkluderer denne rapport, at pulverstrømningen er uregelmæssig, da flere af resultaterne af undersøgelsens parametre er uventede.

# Abstract

---

The process of filling a die with metal powder from a moving shoe, followed by compaction of the filled die, and sintering of the compacted part, has been in use for the production of metal components for many years. The "press and sinter" method is preferred over other production methods, because it is a fast and comparatively easy method, which can also grant advantageous properties to the components. End products are mainly used in the automotive, medical and food industries, among others.

This project is developed in cooperation with Sintex A/S, which uses the "press and sinter" method to produce parts for a variety of customers and industries. The Powder Metallurgy industry, as well as the academia, lack an absolute understanding of the die filling process, and thus its optimization is doubtful.

The die filling step is considered to be of high influence on the final product. That is because, it is argued that properties of the end product (such as homogeneous density) are inherited from the filling stage. Most numerical models developed for the process so far, approach it from an academic point of view and not an industrial one, and their majority is very often limited to 2D simulations due to the necessarily high computational times involved.

Thus, the focus of this study is to understand on a deeper level the filling process and its underlying mechanisms. Moreover, a numerical model is developed to accommodate this understanding, as well as possibly optimize some process parameters. Simultaneously, experiments are designed and conducted to facilitate the model's validation as well as process observations.

Therefore, the study's title can be formulated as follows:

*Experimental and numerical investigation of the powder die filling process*

Studies of the die filling process highlight the importance of the filling shoe speed, die geometry, dwell time and powder height as influential parameters. These parameters are investigated experimentally through density measurements and powder flow observations, with the use of a gamma densitometry machine and a high speed camera, and an effort to deeper understand the powder behaviour during filling has been made. Summarily, it

can be seen that the dwell time, the shoe speed and the die geometry have an important effect on the powder flow as well as on the final density of the powder inside the cavity after filling.

3D numerical models are developed using LS-DYNA to investigate the powder flow and deposition, and attempts to account for the air included in the process are made, since recent studies underline its importance on the filling process. Efforts have been made to verify the developed numerical models through comparison with the experimental powder flow and density results, however they have not been fruitful.

Summarily, this report concludes that the powder flow is irregular, as some of the results of investigating its influencing parameters are unexpected.

# Preface

---

This master thesis report is written by VT4-Group 14.35-e from Aalborg University's Manufacturing Technology programme. The project is conducted during the spring semester between the 1<sup>st</sup> of February and the 1<sup>st</sup> of June 2018. Information regarding the scope of the project, the literature study conducted, the experiments performed, the numerical models developed as well as conclusion and recommendations can be found in this report. The project builds upon the work conducted by Dimitra Alexouli in her 3<sup>rd</sup> semester academic internship project.

The master thesis is presented in one main report with the appendix located in the end, which is referred to throughout the report, as needed.

Each source will be represented by a corresponding number in square brackets, and all of them collectively can be found organized in [ref.], which refers to the bibliography.

Figures, tables and sections are numbered with reference to the chapter, i.e., the first figure in Chapter 4 uses the numbering 4.1, the second figure 4.2, etc. All units are stated in *SI* base units, or by using *SI* prefixes, unless otherwise stated.

The report is composed in L<sup>A</sup>T<sub>E</sub>X and the numerical model is developed and solved in LS-DYNA software. The high speed camera recordings of the die fillings conducted can be found in this link: [https://aaudk-my.sharepoint.com/:f/g/person/dalexo16\\_student\\_aaau\\_dk/EkPQd-nA86RFnY65hvRSWuQBvygJQ2Eayn4MnrPj1deQqA?e=JcxWWH](https://aaudk-my.sharepoint.com/:f/g/person/dalexo16_student_aaau_dk/EkPQd-nA86RFnY65hvRSWuQBvygJQ2Eayn4MnrPj1deQqA?e=JcxWWH)

The authors would like to express their great appreciation towards Sintex A/S for providing needed time and resources in order to assist this project. Additionally, personal thanks are expressed towards the very helpful and insightful supervisor Benny Endelt, the very supportive connection with the company Peter Kjeldsteen, and Radoslav Darula for his insightful and creative ideas.



# Contents

---

<b>1</b>	<b>Introduction</b>	<b>1</b>
<b>2</b>	<b>Process Theory</b>	<b>3</b>
2.1	Process history . . . . .	3
2.2	The process today . . . . .	6
2.3	The press and sinter method . . . . .	6
2.4	The die filling stage . . . . .	8
<b>3</b>	<b>Problem approach</b>	<b>11</b>
3.1	Problem statement . . . . .	11
3.2	Variables and parameters involved in the process . . . . .	11
3.3	Solution approach . . . . .	16
3.4	Experiments . . . . .	17
3.5	Simulations . . . . .	17
3.6	Validation methods . . . . .	18
<b>4</b>	<b>Experiments</b>	<b>27</b>
4.1	Purpose . . . . .	27
4.2	Industrial set-up . . . . .	28
4.3	Experimental set-up . . . . .	28
4.4	Parameters investigated . . . . .	31
4.5	Experimental methodology summary . . . . .	38
4.6	Density measuring experiments . . . . .	39
4.7	Flow observation experiments . . . . .	46
<b>5</b>	<b>Experimental Results</b>	<b>49</b>
5.1	Powder flow observation . . . . .	49
5.2	Density measurements in points of the powder mass . . . . .	57
5.3	Average density . . . . .	63
<b>6</b>	<b>Numerical Simulations</b>	<b>67</b>
6.1	Purpose . . . . .	67
6.2	Introductory information . . . . .	67
6.3	3D simulations . . . . .	69

6.4	Simulation methods . . . . .	70
6.5	Description of the model . . . . .	73
6.6	The computational fluid dynamics method . . . . .	82
6.7	Model description - ICFD . . . . .	84
6.8	Validation of the numerical models . . . . .	87
6.9	Computational cost . . . . .	93
<b>7</b>	<b>Conclusive Remarks</b>	<b>95</b>
7.1	Reflections on the experimental results . . . . .	95
7.2	Reflections on the simulations . . . . .	96
7.3	Industrial applications and future work . . . . .	97
	<b>Bibliography</b>	<b>99</b>
	<b>Appendices</b>	<b>105</b>
<b>A</b>	<b>ARDUINO scripts</b>	<b>105</b>
<b>B</b>	<b>Numerical models' diagram</b>	<b>111</b>
<b>C</b>	<b>ICFD numerical model keyword</b>	<b>117</b>
<b>D</b>	<b>Graphs and pictures from the experiments conducted</b>	<b>119</b>
<b>E</b>	<b>Die geometries</b>	<b>125</b>
<b>F</b>	<b>Numerical model keyword</b>	<b>127</b>

# Introduction

---

# 1

Sintex A/S is located in Hobro and has existed since 1997. It is one of the leading experts on sintering technology and it originates from Grundfos A/S. The initial idea was to utilise the knowledge, materials and processes employed in Grundfos A/S in other industries too. Throughout the years Sintex A/S has expanded from being a Grundfos' department consisting of 6 employees, to becoming a self-standing company in the Grundfos Group having 160 employees.



*Figure 1.1.* The facilities of Sintex A/S in Hobro. Source: [1].

In the branch of sintering technology Sintex expertises in sintered metal, metal injection moulding, magnetic technologies, and metal spraying. It has costumers in the automotive, motor and pumps, medtech, food, energy, and electronics industries.

Sintex is interested in obtaining a deeper understanding of the process of producing sintered products; in particular within the traditional "press and sinter" method, which involves die filling and compaction of powder followed by sintering. That understanding is of interest so that quality problems are predicted and avoided, and hence process limits are pushed and high quality products are produced faster.

Generally, the sintering industry is founded on empirical knowledge, and even though academic research have been conducted on the topic, little attention has been given to approaches from an industrial perspective. Consequently, the industry is still greatly relying on experience as well as preliminary experiments, when a new part is to be produced. This procedure of primary experiments requires multiple adjustments along the way, and is thus expensive, time demanding and inconsistent. Therefore, an interest in predictive models from a production oriented perspective rose. Furthermore, increased knowledge together with the possibility of predicting the outcome could potentially lead to the production process obtaining new capabilities, i.e. producing more complex products.



**Figure 1.2.** Parts manufactured by metal injection moulding and the press and sinter method from Sintex A/S. Source: [1].

## Process Theory

# 2



**Figure 2.1.** End products of the press and sinter method. Source: [1].

Powder metallurgy (PM) processes are widely employed by a great number of industries today. Some of the biggest advantages of powder metallurgy are the low production costs involved, and the opportunity to apply different additives to the raw material, which in turn grants various mechanical properties and different degrees of porosity to the end products.

### 2.1 Process history

*The course of events seen in this Section originates from the ASM Handbook [2], unless otherwise stated.*

Powder metallurgy (PM) is an old branch of metal manufacturing, and has gone through a great development since its origin, to end up as the competitive manufacturing process it is today. The key events within the development of powder metallurgy can be seen in the time-line in Figure 2.3.

The main characteristic of the powder metallurgy processes is the shaping of powder materials into metallic parts without melting. Powder metallurgy principles can be dated back to 3000*B.C.*, when sponge iron was used by the Egyptians (among others) for jewellery and weapons. The sponge iron was produced by heating iron oxide in a charcoal and shell fire, with air blown in from beneath. The resulting hot sponge iron was then



**Figure 2.2.** Delhi iron pillar. Source: [3].

hammered, in order to weld the particles together, and finally forged to obtain the desired shape. An example of this procedure in use is the monumental Delhi iron pillar, seen in Figure 2.2, which was created in around 300*C.E.* with an estimated weight of 6 tons [4]. This method of producing and handling sponge iron led to one of the methods used in its production today. Currently, a viable method for producing high quality iron powder is by grinding sponge iron, and heating it in hydrogen to remove oxides.



**Figure 2.3.** History of the PM processes development.

One of the largest steps forward in the history of powder metallurgy is considered to be related to the discovery of, and progress in, the platinum metallurgy during the 18th and 19th centuries in Europe. In 1829 an article by Wollaston was published, which describes a method developed by him 16 years earlier. This method had wet powder mass being pressed and dried, in order to obtain malleable ingots from platinum ore. The Wollaston process, as well as the investigation of the properties of metal powders conducted in parallel, were the foundations of the modern PM techniques. The above-mentioned process was widely in use until 1859, when Sainte-Claire Deville and Debray developed the platinum fusion procedure, which proved to be both cheaper and of higher

quality.

Due to the development of furnaces capable of melting metals with high melting temperatures, the PM process was completely replaced and forgotten. The beginning of the PM processes being employed in a commercial level started with the development of the lamp filaments. In the late 19th century several patents were granted for different filaments; for example carbon and osmium filament. However, it was Coolidge's ductile tungsten filament, developed in 1909 for General Electric, the one that secured the entry of the incandescent light bulb and became a large commercial success.

Several areas of PM gained an increasing amount of attention in the early 20th century. These areas are cemented carbides, composite metals, as well as porous metals, which in the 1920's led to self-lubricating bearings and metallic filters. Moreover, the automotive industry has been one of the most important contributors to the development of PM. During World War II paraffin-impregnated sintered iron replaced the copper-zinc alloys for the production of driving bands for military projectiles. Thus, PM products were produced extensively in Germany at that period. After the end of the war, fields such as aerospace and nuclear have been considered as main contributors to the further evolution of the process.

As seen in this Section, the PM industry includes many different production methods. One more of them is metal injection moulding (MIM), which was originally developed for ceramics, and was adapted to metal powders in the end of the 1970s. Furthermore, on its first steps MIM was utilizing the injection moulding machines that were used in the plastics industry. Even though it is considerably more expensive than the more traditional PM process, it can mass produce significantly more complex geometries than other PM processes are able to, in a variety of raw materials, and in a cheaper way

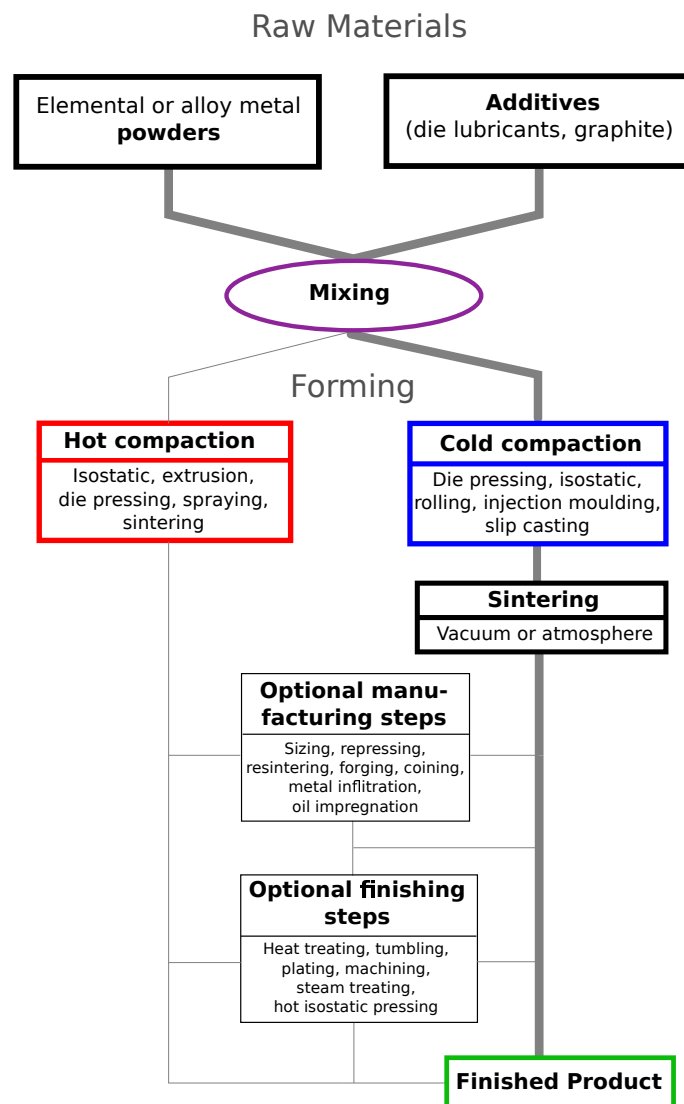


*Figure 2.4.* Powder metallurgy process diagram.

than machining. Despite the MIM end products being very small, it has been growing as a business with around 10% rate every year for the last decade. [5]

## 2.2 The process today

An overview of the modern powder metallurgy processes is presented in Figure 2.4, and its steps depend on the desired end product. The latest additions to the additive manufacturing processes of the PM industry are the Selective Laser Sintering (SLS) and Selective Laser Melting (SLM), in which a laser sinters on specified points, which binds the material together to create the final part. Some of the other PM methods used today are the hot pressing (which combines compaction and sintering in one step), isostatic pressing (which involves powder receiving isostatic pressure by being immersed in a liquid, and is gaining popularity) and high velocity compaction (which includes compaction in less than 20 *ms* and can be used for the production of components of up to 5*kg*). [5]

Currently, most PM products are produced for the automotive industry, and a modern car contains double the mass of PM products in relation to a car produced in 1990, as seen in [6]. Iron and steel hold the lion's share of the PM industry, and copper, stainless steel and aluminium are other very frequently utilized materials.

## 2.3 The press and sinter method

Summarily, the press and sinter method, which is the PM process of interest of this study, consists of 3 steps. It starts with a die being filled with powder from a filling shoe. Subsequently, the filled die is uni-axially pressed, and the outcome is a brittle part, called the 'green part'. After compaction, the green parts have to be strong enough to withstand the ejection from the press' die, and some necessary handling, before they enter the sintering furnaces. Finally, the green part gets sintered, so that the powder particles' pores get eliminated and they bond together (Figure 2.5). At this point the product has its end properties, and post-process procedures as machining or rolling may be implemented thereafter.

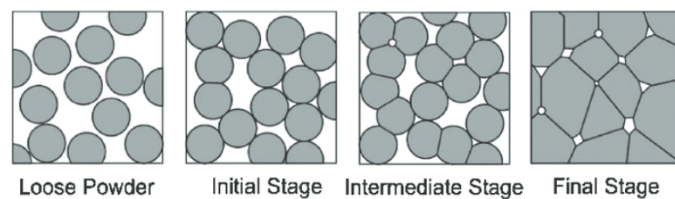


**Figure 2.5.** Stages of the sintering process of aluminium oxide. Source: [7].

Apart from metals, the 'press and sinter' method applies also to ceramics. This is almost a different process, because due to the substantially different raw material, different laws and parameters govern it. One of the latest innovations in the ceramics world is the vibratory pressing. There, the compaction takes place in special press, which result in the powder receiving vibrations during the pressing stage.

The focus of this project can be found in the introductory step of the forming process

(Figure 2.4). The step of the press and sinter method that is of interest is chronically placed after the mixing and before the cold compaction; more specifically, it regards the die filling with metal powder. The project is based on the production procedure at Sintex A/S, which is located in Hobro, Denmark.

The raw material of the process is the metal powder, and thus it is a very important factor, influential on both the end product properties and quality, as well as on the



**Figure 2.6.** Metal powder. Source: [8].

process' progress. Some of the most important characteristics of the powder, as seen in [6], are its apparent density, tap density, flowability, compressibility and compactibility. Where, the apparent density is very important as it directly affects the strength of the green part. The flowability is influenced by the particle characteristics (shape, size, etc.), by humidity and by the inter-particle friction. Flowability is also significant, as it straightforwardly influences the die filling step. Furthermore, compressibility and compactibility are two very important characteristics when talking about the compaction step. The compressibility is a gauge of how susceptible the powder is to reducing its volume when pressured, and is affected by particle characteristics, hardness and possible lubricants. Lastly, the compactibility expresses the powder's competence to be compressed to a green part with a particular strength.

Furthermore, because a big variety of end products with different characteristics can be produced from the press and sinter method, various materials and compaction pressures are in use. For example, porous filters usually require 40-70 MPa, while high density steel 700-1.700 MPa, [6].

The final step of the process is the sintering, which is an integral part of it. During sintering temperatures of 60-90% of the material's melting point are reached, where atomic diffusion takes place. The sintering takes place in a controlled atmosphere (very often hydrogen), so as to prevent oxidation, and to promote the reduction of surface oxides, [5]. It is interesting to note that the sintering furnaces in Sintex A/S are of their own manufacturing (Figure 2.7).



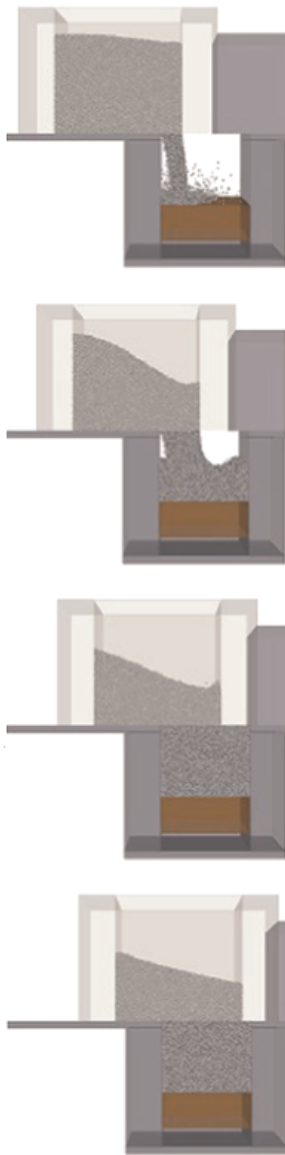
**Figure 2.7.** Parts entering the sintering furnace. Source: [1].

Figure 2.7).

## 2.4 The die filling stage

The press and sinter method is very widely used because it can produce strong parts, with complex geometries and good dimensional accuracy in a cheap way. Therefore, it is very important that those attributes are indeed present in its end products.

A funnel which is placed on top of a press, gets filled with metal powder. From there, the powder gets transferred to the filling shoe through a plastic tube. The filling shoe is a container with an open bottom side, which is placed on the same level with the top side of the die. It moves back and forth on crossing the die's opening, hence powder flows out of it (with the help of gravity) and in the die (Figure 2.8). The filling process comprises from the back and forth movement



**Figure 2.8.** Simulation of the die filling process. Adapted from [9].

of the filling shoe, during which powder flows out of it and settles inside the die. Therefore, the only way to modify or adjust the final powder deposition and density homogeneity before the compaction, is to alter shoe movement parameters. Thus, the operator does not have direct control on how the flow progresses or how the powder is settled in the die. Depending on the specific part geometry and press utilized, the filling process usually has an average duration of less than 2 seconds.

The concept of vibrations implemented in the shoe movement can be found in industrial environments. That is when the filling shoe moves rapidly back and forth over a short distance when above the die, for a specified number of times. When something in the production changes (e.g. new geometry, new press, new powder batch) that causes quality problems, shoe vibrations might be employed to solve them. Brewin et. al. in [10] and Burch in [11] studied shoe vibrations and they concluded that they can indeed increase the average density of a die. However, that is (mainly) due to surface densification that occurs on the top of the die. Surface densification increases because the filling shoe moves on top of the filled die many times back and forth, and therefore the

powder receives more shear effects and friction, from both the powder mass in the shoe and the shoe itself.

On the other hand Bierwisch et. al in [12] argue that for specific frequencies, shoe vibrations do not alter the average density of the die, but die oscillations do (Figure 2.9). They also point out parameters that should be considered when vibrations are implemented, i.e. a beneficial oscillation frequency should be chosen, and the oscillations' movement should respect the dies' geometry. In this study vibrations were not explored, since the experimental set-up did not allow to control the filling shoe's movement that precisely.

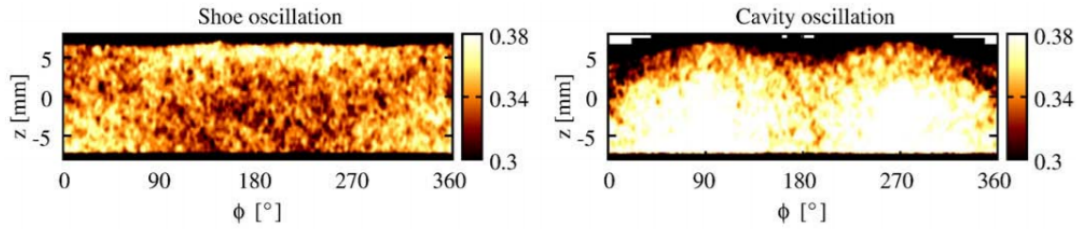


**Figure 2.9.** The density distribution in a narrow ring cavity, when the shoe or the die has been oscillated. Source: [12].

Researchers have also studied consecutive shoe passages, to conclude on whether they assist or not in having a homogeneous density distribution in the die (Figure 2.10). Bierwisch et. al. in [12] state that the extra shoe passages do indeed cause particle rearrangement, but only localized. This affect is said to be restricted only down to a certain depth under the shoe-die contact plane, and to do not extend to the whole die's depth. Moreover, this effect is weaker on the side of the die the shoe crosses first, thus it is very localized. Finally, the researchers argue that dies which received extra shoe passages require less pressure during compaction, which could prove to be profitable. Even though consecutive shoe passages can be studied with the experimental set-up developed for this study, they will not, since they are only of academical interest and are not used in production.

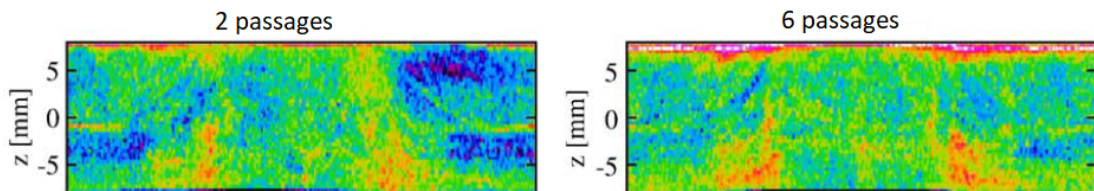


**Figure 2.10.** Experimental results of the density distribution of a narrow ring cavity, after two and six shoe passages. Adapted from [12].



# Problem approach

---

# 3

## 3.1 Problem statement

Inhomogeneously filled dies may transfer non-uniform powder density distribution to the compaction and sintering stages, causing the final parts to be problematic or scrapped. As stated in [13], the filling stage alone can cause up to 5% difference in the mass of the compacted part. Thus, homogeneously filled dies facilitate improved quality end products from a very early production stage. To ensure homogeneously filled dies, and thus also a smoother and faster production process, the deposition uniformity has to be controlled. The last years there have been interesting and fruitful studies about the die filling process; however, some of them lack the industrial aspect, by mainly addressing academic interests. Therefore, it is important, to keep in mind that the end goal of researching the deposition uniformity and density distribution is to be able to apply the gained knowledge to an industrial set-up.

## 3.2 Variables and parameters involved in the process

In this section information regarding variables and parameters involved in the die filling process will be presented, alongside a small discussion about their importance.

### 3.2.1 Powder

As metal powder is the raw material of the process, it greatly affects it. For example, in production sites it can be seen that, alterations in the process parameters may be required, when a new batch of powder is introduced to the production line. Moreover, due to the fact that the packing behaviour of powders is irregular, differences from experiment to experiment with set parameters are not uncommon, as seen in [13].

Powder characteristics (i.e. particle size, particle size distribution, and particle shape.) depend on the way it is produced. There are various ways to produce metal powder such as solid and liquid comminution techniques, electrolysis and thermal decomposition. For example in liquid comminution, a molten metal stream is hit by a fluid, and it disperses into droplets that solidify as irregularly shaped particles. Powders with irregular particles

have lower apparent density, undergo increased reduction of volume during compaction, and thus portray greater green part strength, [5]. The main reason why spherical powders are not preferred in compaction processes is that they create parts with poorer green strength, which often leads to parts being BROKEN?/scraped? during handling and transportation to the sintering stage.

The powder used in this study is called STX2000 and is produced by Höganäs. It is a 430L ferritic stainless steel and it comes pre-mixed with 1% lubricant. It is produced by water atomization (a comminution technique), and it is irregularly shaped to ensure more strength and easier binding for the particles. 90% of its particles have less than 150  $\mu\text{m}$  diameter.

### 3.2.2 Powder flow

The powder flow is an important factor in the filling process, as it involves the notions of filling rate and powder deposition. Filling rate is the rate with which the powder falls in the cavity, and thus directly connected with the time required for a die to be filled. Powder deposition has to do with the way that the powder settles in the die, which directly depends on the way it has been discharged in the die.

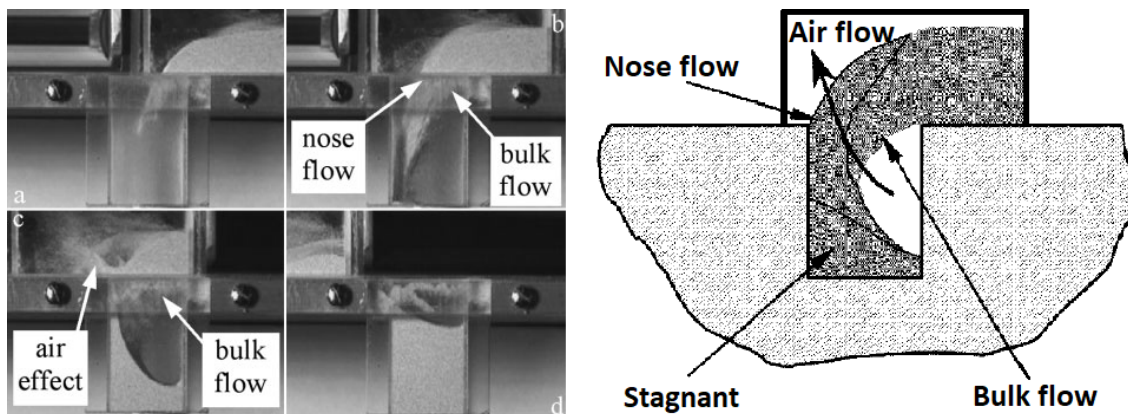


**Figure 3.1.** Powder flow types witnessed in experimental die fillings (left), and a graphical representation of filling features (right). Adapted from: [14].

In [15] Alexouli studied various researches on die fillings, and it is seen that researchers acknowledge three distinct powder flow types. Firstly, there is the nose flow, which is more often seen in low shoe speeds, larger die openings and less powder in the shoe. During the accelerating phase of the shoe's movement, the powder mass gathers in the back side of the shoe, and only powder particles on top of that mass can fall in the cavity by sliding on its surface. Those particles that roll on the surface of the powder mass create a nose-shaped profile, and the academia has not concluded yet on whether that type of flow assists or jeopardizes a higher filling rate.

Secondly, there is the bulk flow, which is described by powder bulks detaching from the powder mass' bottom and falling in the cavity. It is considered to occur in higher shoe

speeds and dies with narrow openings. In those cases the nose flow's tip quickly crosses the die's opening, and thus does not have enough time to dominate. It is also believed that bulk flow reduces flow rate, as during the powder mass flowing in the die, the air inside the cavity can only escape through the powder mass itself. Finally, there is the intermittent flow, which is irregular, occurs because of powder instabilities and is described by powder agglomerates flowing in the cavity randomly.

### 3.2.3 Filling shoe movement

The filling shoe movement highly affects on the end product of the press and sinter method, and one this Subsection some of its influencing parameters.

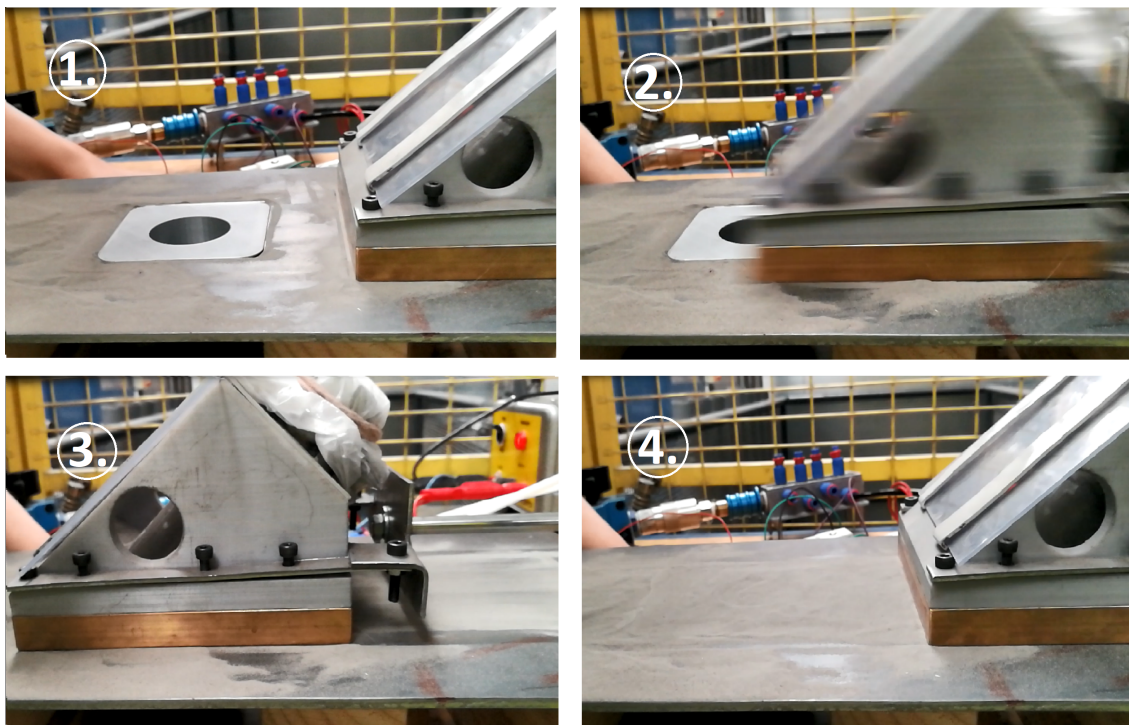


*Figure 3.2.* The filling shoe movement. 1. starting position, 2. forward moving position, 3. filling position, 4. end position.

### Speed

High shoe speeds are of interest in the industry, since they lead to higher production rates, which in turn increases the profit. However, the higher the speed is, the less time the powder has to fall out of the shoe and in the die; which in turn means that above a threshold shoe velocity, the die does not get fully filled. Moreover, it is very important to assure that the shoe speed allows not just for a fully filled die, but also for a homogeneous fill. Lack of a uniform powder deposition might lead to densification in some points of the part after compaction, as well as in-part density variations, and thus an imbalanced part that has different features at points. Those are not acceptable, as they can lead to micro-cracks or even failures under loading.

Higher shoe speeds also have proven to result in lower filling rates [15]. When it comes to density though, the academia has not reached an agreement, on whether higher shoe speeds assist or obstruct higher densities. It has been proven though, that more shallow and wide dies are easier to fill with higher speeds [15]. Moreover, low shoe speeds are argued to transfer more shear forces to the powder mass, which can lead to surface densification.

### **Vibrations**

The parameters of the filling process that are most commonly or frequently tuned in industrial environments are the filling shoe speed, and also whether or not there will be vibrations added in its movement. It is said that vibrations are implemented in the shoe's movement, when it moves rapidly back and forth for a short time and over a short distance for a specified number of times, when on top of the die (filling position in Figure 3.2). Both the industry and the academia argue that the average density of the powder inside the cavity increases with the implementation of vibrations. On the other hand, caution should be given to the vibration settings, because as stated in [15], for some frequencies adverse effects on density might be observed, due to fluidization occurring.

### **Repetitive fillings**

The academia has also expressed an interest in repetitive fillings<sup>1</sup>, as researchers have investigated them. repetitive fillings are proven to increase the average density, but also the powder on the surface of the die to be more compacted, which jeopardizes the end product, by increasing the risk for shape defects to appear [15]. In the industrial environment repetitive fillings are not in use, according to the authors' knowledge.

### **Dwell time**

Finally, there is also the shoe pause method, where the shoe stops, when on top of the die, for a predetermined amount of time. This period of time when the shoe does not move is called dwell time, and researches have investigated it. Here again there is a controversy in the academia, as some researchers defend that implementing dwell time increases the average density [15], while others support that it does not affect it [16].

#### **3.2.4 Die geometries**

The end parts of the press and sinter method are supplied to various industries, who require a plethora of parts with geometries varying from simple to very complex ones. Based on the die's geometry, different settings for parameters are required; for example, deep dies need more powder to fill, and thus usually more time for powder transfer, which can be achieved by lowering the shoe speed. The clients' needs can not be altered, so the die geometries is not something that can be altered, but a better understanding of how it influences the filling process and the end product with its features is of interest.

---

<sup>1</sup>the shoe repeats its back and forth movement on top of the die more than once before compaction

The majority of the literature studied, deals with simple die geometries (cuboids, disks, rings), however there are a few researchers that occupied themselves with more challenging geometries too. In [15] Alexouli studied various researches on die fillings, and summarily concluded that any type of complexity in a die's geometry (e.g. sharp corners, small openings, long thin sections) can endanger its density. Likewise, when it comes to density distribution, circular dies promote a uniform fill more than rectangular ones do.

One of the most interesting studies of complex geometries is [9], where Tsunazawa et. al. studied four dies in total, two of which have complex inlets inside them. The two dies in Figure 3.3 have the same dimensions, but case 4 die has a geometrically complex inlet inside it. It is easily distinguished that the die geometry significantly influences the filling process, as case 1 die is filled at  $t=0.30$  s, but case 4 die is not.

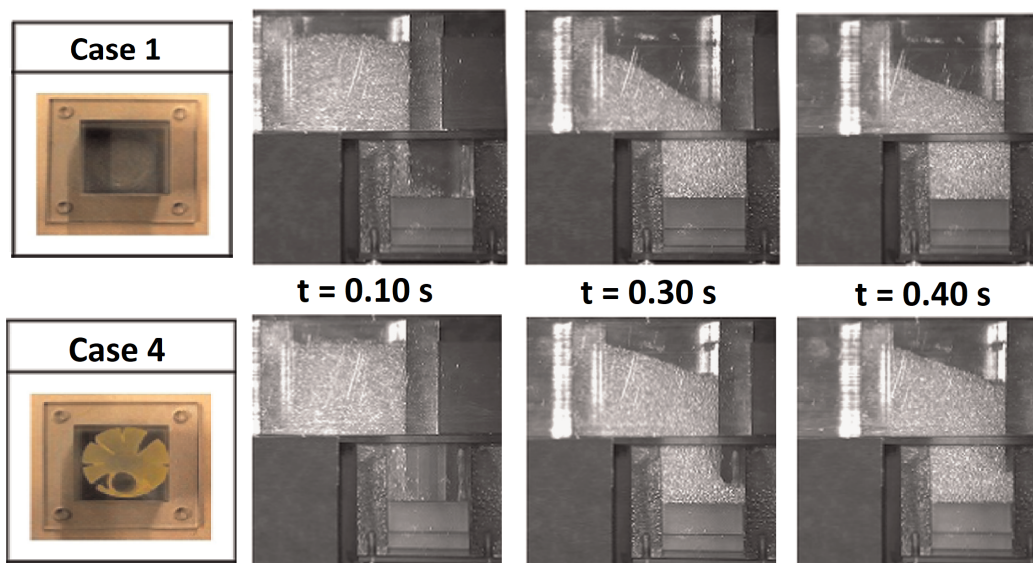


*Figure 3.3.* Experiments with different dies. Adapted from [9].

### 3.2.5 Density

The density and density distribution in the cavity are of utmost importance, since they are the variables that dictate the features and the quality of the end products. Nonetheless, they cannot be predicted, or directly controlled, thus more importance has been given into manipulating the parameters involved with the process, in order to acquired the required density and density distribution. An uneven density distribution can lead to local strengthening, and micro-cracks among others, which constitute the produced parts scrap. It has been experimentally proven that there is not a significant difference in the density between the die's left and right side. However, the first side of the die that the shoe crosses, portrays higher density than the second one [16].

### 3.2.6 Filling shoe geometry

The filling shoe comprises of a brass plate on the bottom, and a body on top of it (Figure 3.2). With the innovations in the 3D printing industry, many factories have now their own 3D printers and can thus print various shoe body geometries. Their influence though on the powder flow has not been assessed. On the other hand, a few studies have been conducted regarding the shoe's cross section (here brass plate geometry).

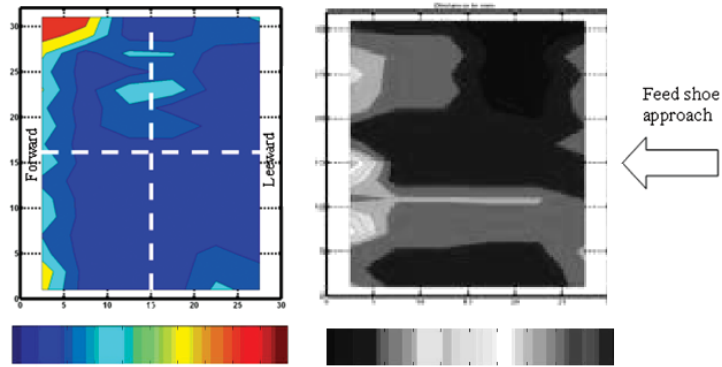


**Figure 3.4.** Contour plots of pressure as equivalent height for rectangular dies filled from shoes with different cross sections. Adapted from [17] and [18].

Roudsari and Puri in [17], [19] and [18] had some interesting results regarding the influence of different filling shoes cross sections on the powder density. By varying only the shoe cross section, and keeping all the other parameters stable, density distribution variations were eminent in their experiments (Figure 3.4).

### 3.2.7 Powder height in the shoe

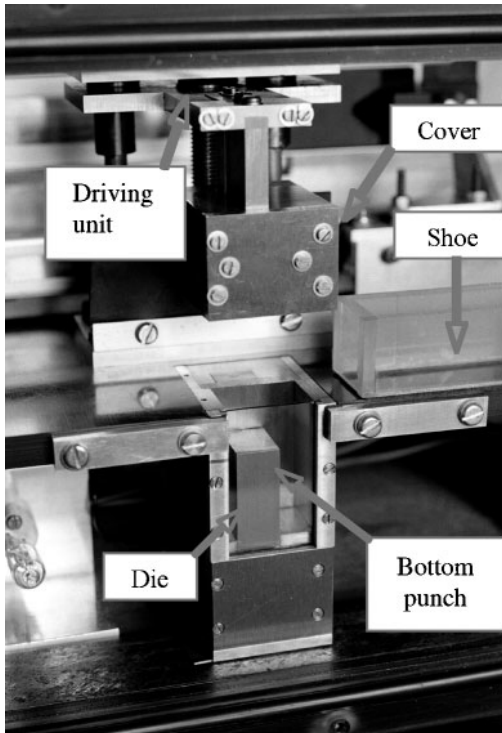


**Figure 3.5.** A typical experimental setup for die fillings. Source: [20].

Whether the powder height in the filling shoe influences the powder flow and deposition or not, has been of interest in the academic world, and researchers have investigated it, without conclusive results though. For example, Hjortsberg and Bergquist in [13], experimented with various powder heights in the shoe (from 2.5 up to 15 cm), and concluded that the density of the filled die is not affected by those different powder heights. On the other hand, Xie and Puri argued in [16], that a completely filled shoe might decrease the powder flow rate.

## 3.3 Solution approach

The purpose of this study is to deeper understand the powder flow and deposition, which will be achieved by observing the flow process under different parameter settings (i.e. exploring various die geometries, shoe speeds, etc.).

When that is achieved, control over the powder's density distribution in the die is the next target, so as to further ensure highest quality end products. Experiments with different parameter settings where the powder behaviour during filling and deposition are explored, are expected to assist in achieving the target of this project. In addition to that, numerical model simulations are expected to allow for further understanding of and experimentation with the filling process, as well as for exploring its limits.

### 3.4 Experiments

An important part of this study is to develop an experimental set-up which describes the industrial die filling process so accurately, that it can be used instead of latest for the purposes of this project. Firstly, for a better understanding of the process the macroscopic flow of the powder should be observed under various process parameters. Furthermore, combinations of different die geometries, shoe speeds and dwell times will be investigated, to give an overview of their influence on the powder settlement. Finally, additional die fillings will be performed, where the density in points of the powder mass in the die will be of interest. This information will supplement the above-mentioned observations, and together they will give a better overview of the powder's behaviour during flow and settlement. The end goal is to decipher powder's behaviour during flow and settlement, so as to be able to foresee its density distribution, and thus gain more control over the process.

More details about the experiments, as well as about their set-up and results can be found in Chapter 4.

### 3.5 Simulations

Process simulations have some very useful advantages. One of them is that since real life barriers do not exist there, they allow a deeper investigation of processes. For the die filling process, a real life limitation is that the duration of the process is very short, which minimizes the things an observer can perceive. Another real-life restraint that exists is the scale and external environment which are involved with the process (Figures 3.6 and 3.7). In the industrial set-up the

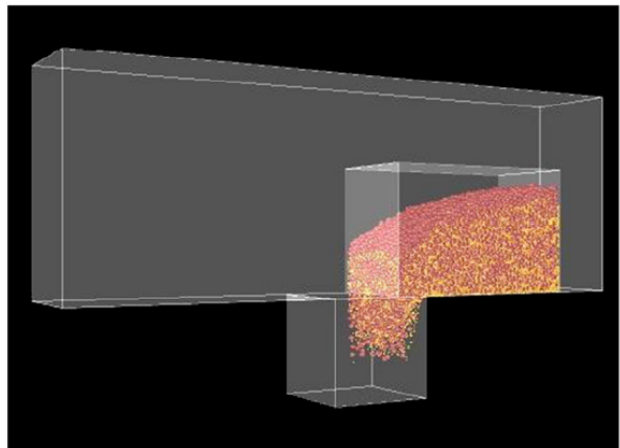


*Figure 3.6.* A typical simulation for die fillings. Source: [21].

die is surrounded by the press "punches", thus the powder flow and settlement are not visible. If they were visible, there would still be a perception problem, since the dies are maximum a few centimetres long and the powder particles less than  $150 \mu m$ . Finally,

things as density distribution, stresses and energies are from difficult to impossible to measure in real life set-ups; however, a user can calculate them with the push of some buttons when post-processing simulation results.

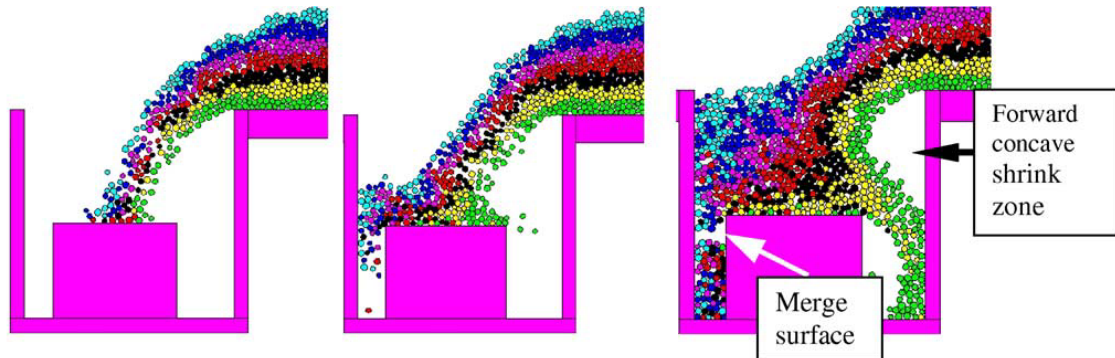


**Figure 3.7.** A simulation of a stepped die being filled. Phenomena that are not visible when observing the industrial process (e.g. shrink zones) can be distinguished here. Adapted from [22].

Moreover, simulations grant the ability to experiment with various variables and parameters of the process fast and without halting the production. This can be of help to the PM industry for example every time a new geometry is considered, or some optimization is of need. Simulations can be very profitable in those cases, since usually the extremely time consuming "trial and error" method is utilized instead.

More details about the numerical model and its development can be found in Chapter 6.

### 3.6 Validation methods

To be able to harvest all the benefits from the simulations, the developed numerical model should be reliable, thus validated. To develop a model a lot of input data are required, from e.g. the process steps, materials utilized, moving objects velocity curves. For the output of the simulation to be able to mimic the real life process accurately, some comparisons in points between the real and the modelled process must be made. For example a validation point could be that the powder flow in the simulation very accurately describes the powder flow observed in the experiments, as seen in Figure 3.8 from Tsunazawa et. al. for the validation of their model in [9]. More points of validation give more certainty for the results, as their accuracy gets further verified.

Hereunder, a discussion on validation methods for the die filling process found in the literature research and possible validation methods considered for this study are presented

- Data obtained from previously conducted studies
- Particle velocity and macroscopic observations

- Coloured powders
- Pressure sensors - strain gauges
- Average density
- Powder height and powder mass surface shape in the die
- X-Ray CT scanning and gamma densitometry
- Measurements on compacted parts

### 3.6.1 Data obtained from previously conducted studies

The conduction of experiments is a challenging process, that as a rule is time consuming and expensive. There has to be access to various types of tools, machinery and equipment too. For example, high speed cameras (more than 250 *frames/s*) that are commonly used for the powder flow observation, are expensive and thus not commonly found. To avoid all those downsides and obstacles, some studies have used experimental results from previously conducted studies as validation points for their numerical models.

### 3.6.2 Particle velocity and macroscopic observations

In 2015, Y. Tsunazawa et al. published a paper [9] in which the validation and results of a coupled discrete element method and signed distance function (DEM/SDF) numerical model are presented. The purpose of the model is to investigate the powder flow in complex shaped dies. Besides powder mass comparison for the validation of the model, they also use particle image velocimetry (PIV). The basic principle of PIV is to recognise the same particle in two images (taken at specified time points), and from its spatial data difference to calculate an approximate velocity. Tsunazawa et al. used PIV to validate the spatial velocity distribution of the powder flow, and some of

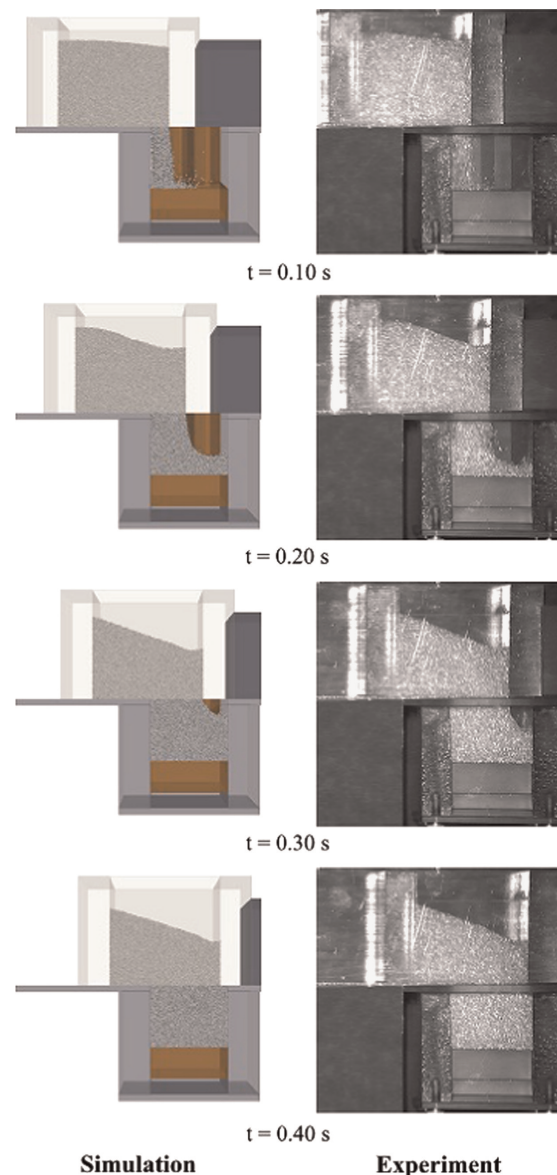


**Figure 3.8.** Qualitative comparison of the die filling process between experiment and simulation. Source: [9].

their results are shown in Figure 3.9. Furthermore, the edge point position of the middle of the powder bed was compared to the average velocity in the bottom neighbourhood of the die at specified times. Finally, they also used the angle of slope of the powder bed inside the filling shoe and the projection area of the shoe to compare the experimental to the numerical results. Similarly to that, Bierwisch et. al in [23] also cared about the angles of repose<sup>2</sup> as a means of validation.

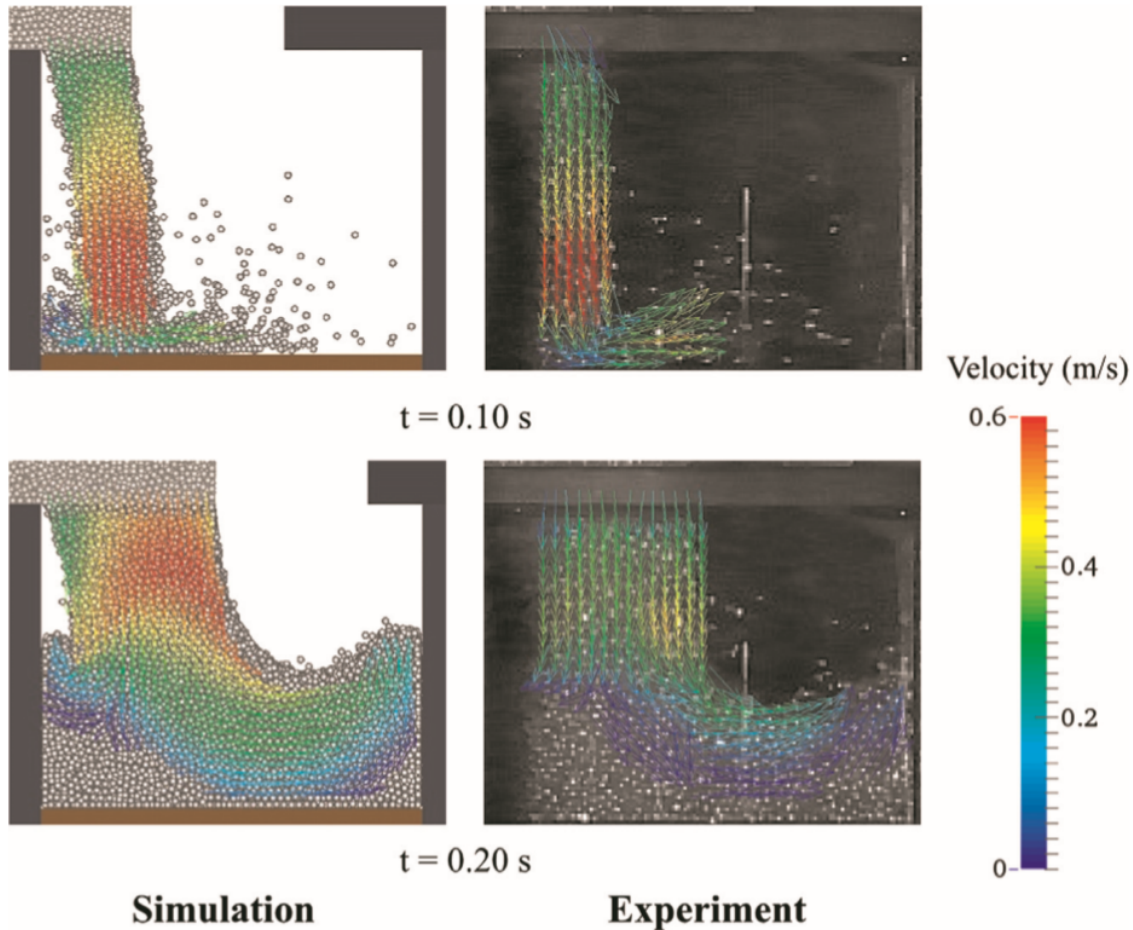


**Figure 3.9.** Example of velocity distributions, from a simulation and PIV experiments. Source: [9].

In order to create an experimental set-up for PIV measurements of powder flow in a die, transparent dies and a high speed camera are existential. The more frames per second the high speed camera can record, the easier it is for the PIV to be fruitful. This is because the closer in time two successive images are, the more accurate the results are, and the easier it becomes to distinguish individual particles. One way of identifying particles is to apply a pattern recognition algorithm, so that a pattern of a particle cluster can be identified, assuming that neighbouring particles have similar flow. Another possibility is to colour individual particles, which makes them easier to track. However, this method is

<sup>2</sup>Angle of repose is the angle between the powder heap slope and the parallel to the ground axis on its basis.

mostly applied when larger particles are investigated, as there is a risk of the colour mass significantly influencing the particles' flow. In addition to that, the cameras' vision of the coloured particle might be blocked by the thousands upon thousands of fine particles involved in the process.

PIV was not considered in this study because, but experiments with a high speed camera are conducted, so that the flow of the powder and its deposition in the die are investigated.

### 3.6.3 Coloured powders

In [24] Aole, Jain and Bruhis experimented with filling shoes filled with differently coloured layers and columns (Figure 3.10). They coloured salt with food colouring, and iron powder by lightly oxidizing it. Even though they did not develop numerical models, a few other researchers used the "coloured powder" technique in their simulations to observe better the powder behaviour. It would be interesting to see the "coloured powder" technique to be used combined in experiments and simulations, as a means of validation for the latest.

The researchers varied the filling shoe speed and the powder height inside the filling shoe, and they also experimented with a perforated plate placed on the bottom of the filling shoe (Figure 3.11). In the experiments with the simple filling shoe and higher shoe speed (385 mm/s) a distinguishable rotational flow was observed in the die (Figure 3.11). Moreover, they found out that the perforated plate assists a uniform powder distribution and packing pressure. However, with the higher shoe speed tested, this type of filling shoe seemed to depress the powder flow in comparison to the simple filling shoe, which could fill the die in shorter time.

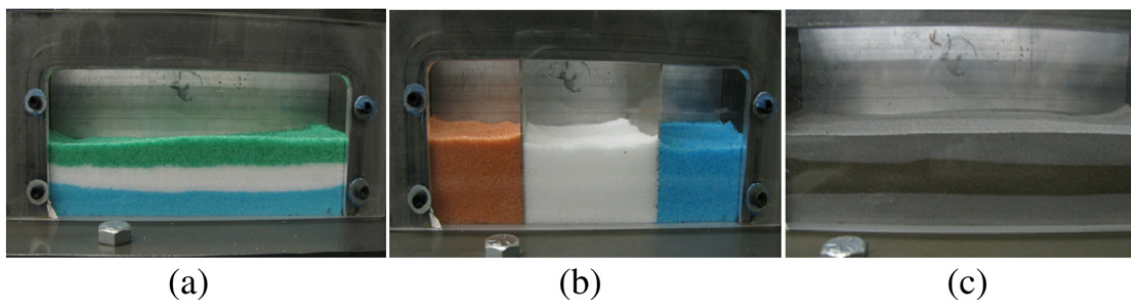


**Figure 3.10.** Filling shoes filled with: (a) three layers of coloured salt, (b) three columns of coloured salt, (c) three layers of iron powder. Source: [24].

Nonetheless, the perforated plate appears to be something that could be interesting to investigate. As the researchers state in [24], there should be some experimentation with different hole sizes, hole orientations and plate thicknesses. In this study coloured layers and columns were not considered, because it has been suggested that the paint might affect the very small steel particles.

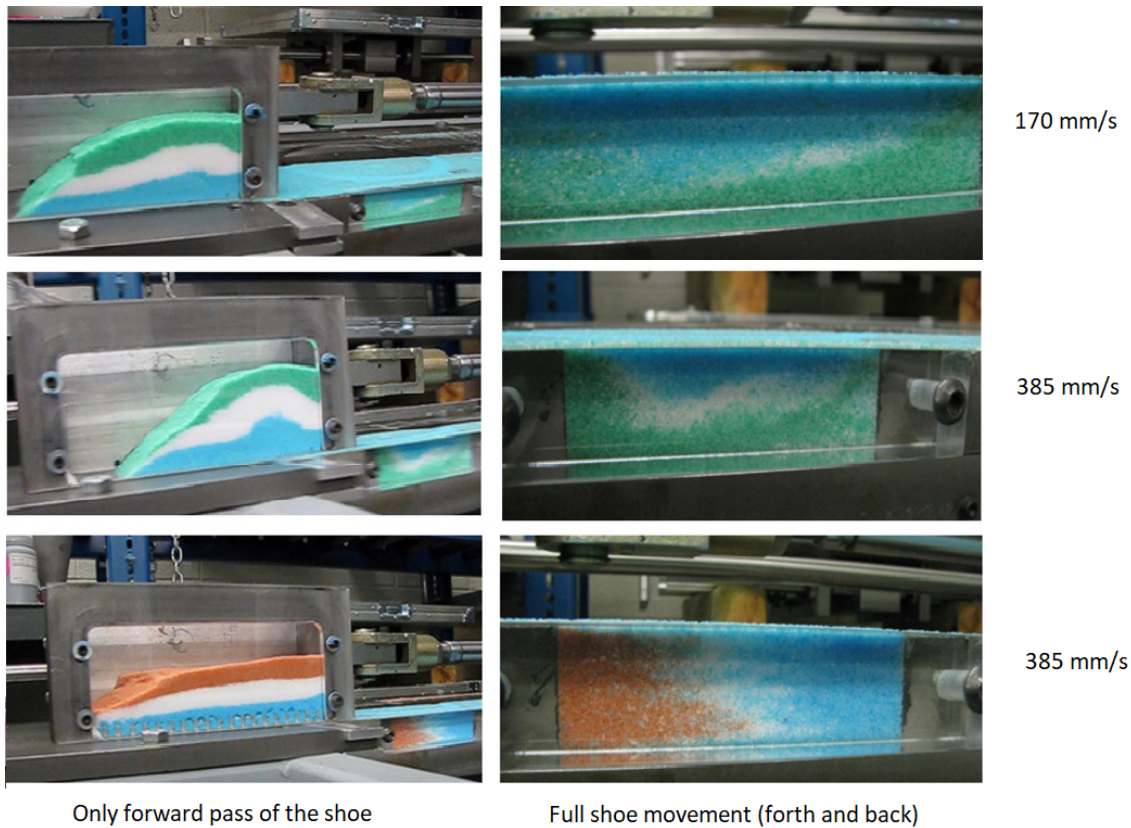


**Figure 3.11.** Filled dies and filling shoes from three different experiments. In the experiment of the last row the perforated plate is utilized in the shoe. Adapted from [24].

### 3.6.4 Pressure sensors - strain gauges

Investigations based on data from mass and pressure deposition testers in the bottom of dies have been carried out in some studies found. The first one was carried out by P. S. Dahora and V. M. Puri with a self-developed mass deposition tester, and is presented in their paper from 1998 [25]. Later in 2006, X. Xie developed and evaluated a new pressure deposition tester for his Ph.D. thesis [26], which showed satisfactory results with more precise measurements of the pressure distribution in the bottom of a die. The pressure deposition tester consists of 16 pressure sensors, placed in line in one pressure sensor strip. However, none of the investigations could evaluate the direct mass density distribution. That is because deep dies were employed in the experiments, and thus the measured values were strongly influenced by bridging effects, powder internal friction, particle-particle friction, and air pressure inside the dies.

In 2010 S. S. Roudsari and V. M. Puri published a two part article ([17] and [19]), where they investigated powder deposition in a rectangular and a circular die, respectively, from a shoe with a circular cross section. One year later they published one more paper [18] where they investigated powder deposition in rectangular and circular dies from a filling shoe with a rectangular cross section. One of the key findings of all three studies, was that for all tested dies, shoe cross sections and powders, higher shoe speeds (from 20  $mm/s$  to

100  $mm/s$ ) resulted in more uniformly distributed powder. The researchers stated that this is possibly because the extra kinetic energy that gets transferred into the die collapses existing powder bridges.

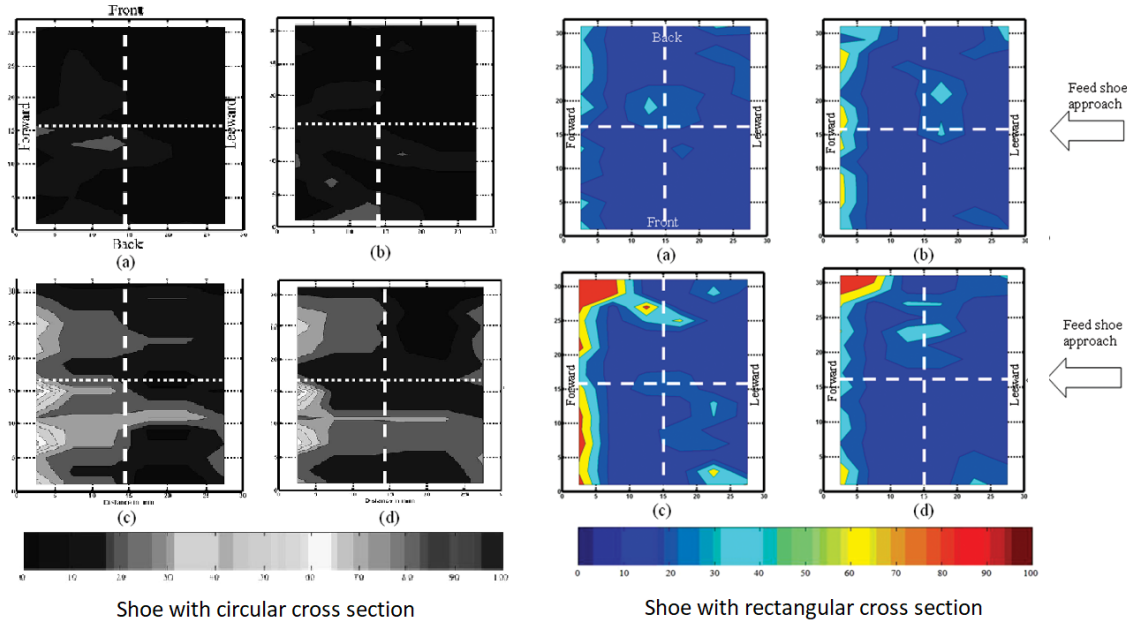


**Figure 3.12.** Contour plots of pressure as equivalent height for Avicel powder (a)20 $mm/s$  (b)100 $mm/s$ , and for BPM powder (c)20 $mm/s$  (d)100 $mm/s$ . Sources: [17] and [18].

The experiments were conducted using the pressure deposition tester developed by X. Xie. Multiple experiments were conducted, where the pressure strip was repositioned in order to get measurements of the whole plane of the bottom of the die. Shallow dies with a depth of 6.5  $mm$  were used, to disregard the parameters influencing the powder distribution measurements in deep dies. In Figure 3.12, the contour plots of the pressure values are shown as equivalent height ( $pressure/(particle\ density * gravity)$ ) for two different powders and shoe velocities. Moreover, the researchers used many more methods to study deeper the settled powder. Summarily those are: symmetry analysis (analysis of the pressure distribution in the filled dies), variance metrics (study of statistical parameters), Gini coefficient (in simple words it is approximately the percentage of non-uniformity), and uniformity analysis (uniformity in pressure distribution).

Attempts to employ strain gauges have been made during this study, but they have not been fruitful. What is of interest is to have measurements of various points from one die, and thereafter compare them to each other, so as to have a relevant evaluation of the density distribution. The problem with the sensors found in the market is that because of their accuracy in such low masses, it is doubtful whether there would be a difference in the values between points, and if yes, whether or not that could be trusted as realistic.

### 3.6.5 Average density

By measuring the powder mass in the die, and dividing that by the volume of the die (given the fact that the die is filled, and thus the die volume equals the powder volume) the average density of the powder in the die is obtained. Therefore, the average density is one easy -but also relevantly inaccurate- way to examine whether simulation results correspond to experimental ones. The average density as a means of validation is being utilized in this study. However, it does not give any details about the density distribution and thus is not enough to deduce on the similarities and differences of the die fillings.

Moreover, Guo et. al. in [27] displayed graphs of the cumulative powder mass in the die over time (Figure 3.13). This is an interesting method to be used as a validation means, but because of lack of the necessary equipment, it was not utilized in this study.

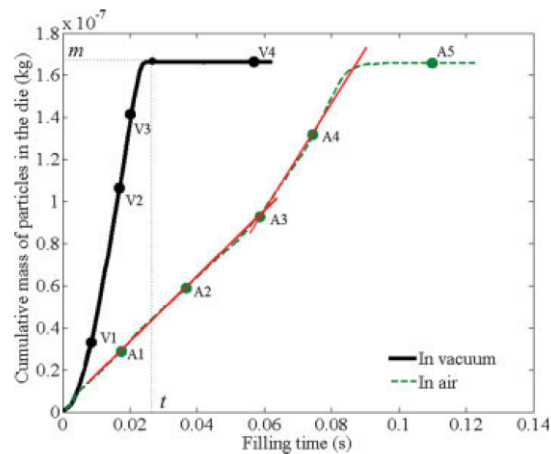


**Figure 3.13.** Graph of cumulative powder mass inside the cavity, over time. Source: [27].

### 3.6.6 Powder height and powder mass surface shape in the die

Another observational method that can be used as a qualitative validation method is the calculation of the powder height in the die after filling. This method is much more meaningful when the dies are not fully filled, and thus there are discernible differences between the powder height in points. On top of that, a visual observation of the shape of



**Figure 3.14.** A close up picture of a not fully filled die.

the powder mass in the die can yield some qualitative information about the flow and the powder deposition. Differences in the front, middle and back sides of the die may appear. It has been observed that depending on parameters as shoe speed and dwell time, the surface of the powder in the die might resemble for example a concave surface (see Figure 3.14) or a tilted plane.

With the necessary equipment very precise results can be obtained, which when thoroughly analysed can also yield important results about the powder behaviour during flow and its deposition. Bierwisch et. al in [23] pinpointed the significance of the powder height as a means of validations. They argued that it

describes both how the powder enters in the cavity and how it settles inside it. The powder height and the shape of the powder surface are utilized in this study as methods for the validation of the numerical models.

### 3.6.7 X-Ray CT scanning and gamma densitometry

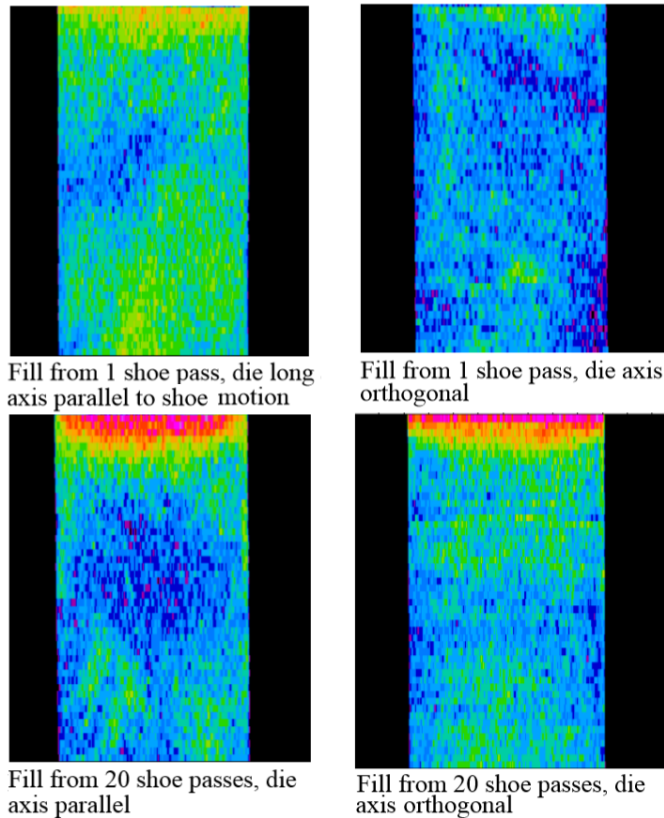


**Figure 3.15.** Vertical CT sections of a rectangular die filled with distaloy AE powder under different filling conditions. Source: [11].

X-ray and gamma densitometry methods have been applied to compacted parts for years, mostly on quality and end product investigations. Those methods have not seen wider spread as they require expensive equipment and they are time-consuming. As seen in [28] the first time that an industrial machine was created that allowed for gamma ray densitometry to be applied to powder compacts was in 1986, at the International Powder Metallurgy Conference and Exhibition in Dusseldorf, Germany. Both X-ray and gamma-ray techniques provide a variety of aperture diameters and shapes, and their accuracy increases with measuring time. They are generally very accurate and give very helpful insights on powder behaviour under compaction and end-product quality.

When talking about obtaining density distribution data of loose powder in a die, the use of X-Ray CT (Computerized Tomography) scanners can provide the required information. Those scanners facilitate the obtaining of 3D CT data, which subsequently enable the investigation of the density distribution in parts, and the differences of the powder density distributions between parts. That 3D data provide also information about the powder flow and powder deposition too when analysed. However, in order to scan loose powder in a die, the die should be made from low X-Ray attenuation material. This method was applied by S.F. Burch et al. among others, and their work was published in 2007 [11] and [10]. Vertical CT sections results from a rectangular die with a varied number of passes and die orientations are shown in Figure 3.15.

Gamma densitometry is a method similar in a way to the X-ray CT scan, as by utilizing

gamma rays it can measure average density in columns/points. Sintex A/S has a Gammadensomat (densomat), produced by Radec (Figure 4.16). The densomat receives as input the material and height of an object, as well as coordinates of various points on it, and it outputs the average density (in depth) of the part on those points. The densomat is utilized in this project as both a validation method, and as a way to deeper understand the powder behaviour under different circumstances.

### 3.6.8 Measurements on compacted parts

In many studies, in order to overcome the barrier of the loose powder, researchers compacted the dies, and tested the green parts with various methods to deduce on the density distribution. For example, Hrairi and Chtourou in [30] correlated Vickers hardness measurements to approximate (with  $\pm 1\%$  accuracy for densities up to 86%) the density distribution of compacted parts.

Furthermore, in [29] Tweed et. al. mention various ways to measure density. To start with, they mention a study where the researchers compacted the filled die, and then sectioned the green part, just before calculating the density of the sectioned parts using a densimetric balance. Furthermore, they add that depending on the raw material, some light sintering might also be needed. Furthermore, they mention a method used by the University of Leicester, where filled dies were lightly sintered at  $900^{\circ}\text{C}$  under nitrogen, and then sectioned so that they can be scanned in the X-ray CT machine available (Figure 3.16). Moreover, they give different alternatives for getting density results for specific types of material. For instance, for hardmetal they mention the use of paraffin wax to close the pores of the compacted part, followed by density measurements according to the Archimedes method. Generally, they also suggest hardness measurements, metallography and gamma densomat or X-ray CT methods for more accurate results.

In this report no compacted parts were examined, as experiments involving compaction of dies were not a possibility.

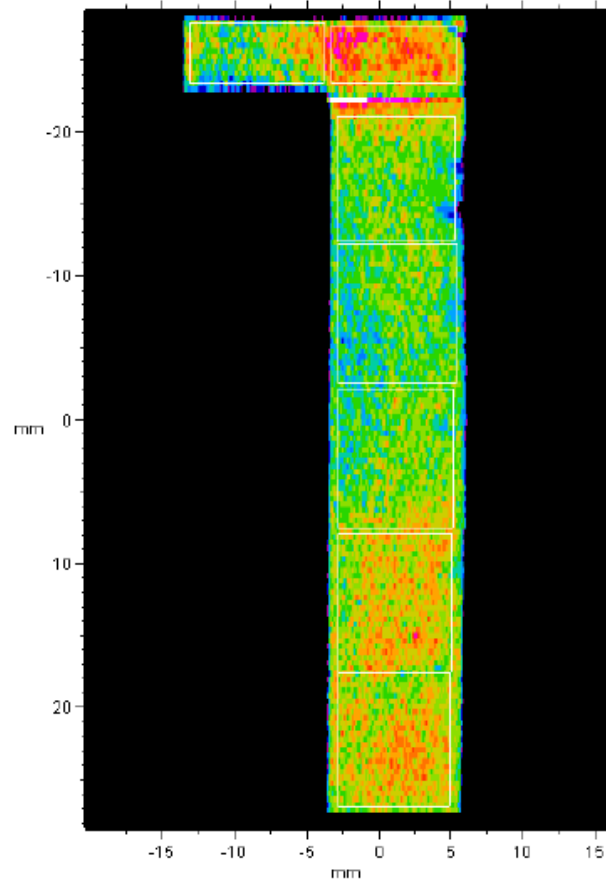


**Figure 3.16.** X-ray CT scan result for a lightly sintered part sectioned in seven pieces. Source: [29].

# Experiments

# 4

In this chapter, the experimental set-up developed will be analysed. Variables and parameters investigated will be discussed next to the reasons why they are important. Moreover, difficulties faced when managing them and experimental results will be presented and explained.

## 4.1 Purpose

A few of the studies found in the extensive literature research of the die filling process developed numerical models, but did not conduct experiments alongside. In those cases, the experimental results needed for the numerical models validation, are based on previously conducted studies. While this method proves efficient in specific cases, experimental databases existing from previous studies are considered insufficient for the purpose of this study, where experimenting with different parameters is considered crucial. Therefore, experiments are conducted to facilitate the targets of this project.

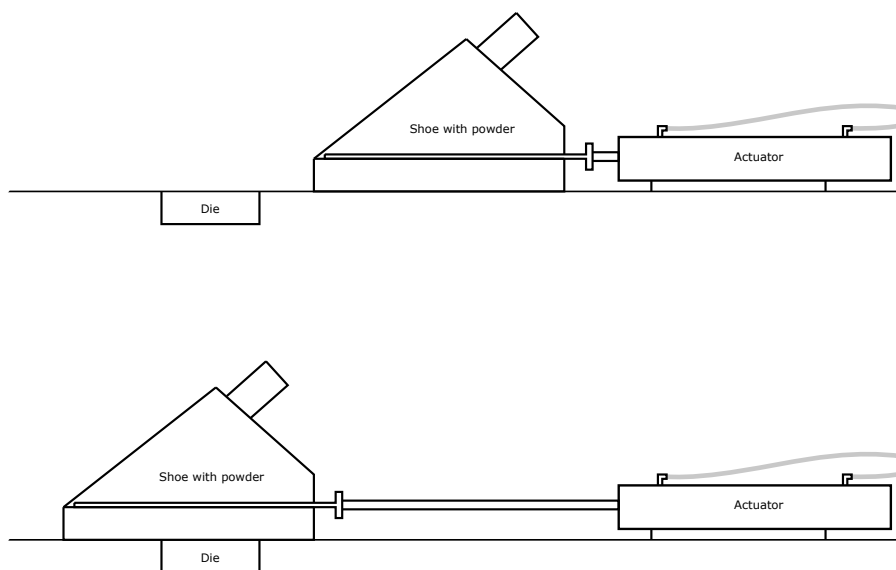


*Figure 4.1.* Schematic representation of the experimental setup developed, where the actuator is extracted and the filling shoe placed above the die.

In this study, experiments were planned and performed to provide the most information possible for the deeper understanding of the process as well as for the validation of the numerical models. The experimental set-up developed for those reasons, is limited to portray the die filling step only, and does not include neither the powder supply system nor the subsequent steps of compaction and sintering.

The aim of the developed experimental set-up is to be able to capture the main parameters influencing the production set-up process. A graphical representation of the experimental set-up is shown in Figure 4.1. The filling shoe is pushed forwards and pulled backwards by a double acting pneumatic actuator. When the actuator is fully extended, with a stroke length of  $130\text{mm}$ , the shoe is located above of the die. After a specified dwell time that the shoe is above the die, the actuator is retracted, so that the shoe returns to its original position. The powder is able to flow from the shoe down into the die during the full period that the shoe opening is above of the die.

## 4.2 Industrial set-up

The industrial set-up in Sintex A/S, involves dies being filled with suction filling. Suction filling is the process that has the bottom part of the die moving downwards when the shoe is placed on top of it, to aid the powder flow (Figure 4.2). This way of filling, apart from being faster in comparison to the traditional filling, can also lead to more powder being transferred in the die during that shorter time, as stated by Wu and Guo [31]. They also argue that when the bottom of the die moves (relatively) faster downwards, the powder has an even higher flow rate. Furthermore, Bierwisch et. al. in [12] state that suction filling assists in more homogeneous density distribution in the die.

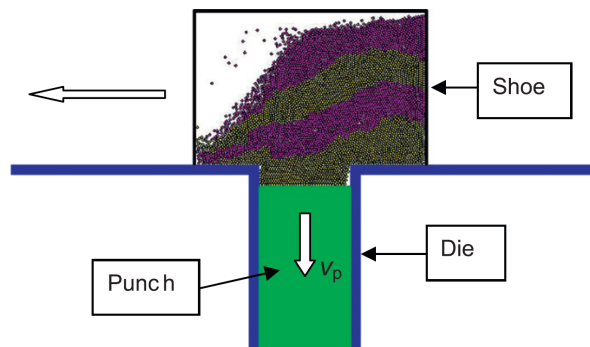


*Figure 4.2.* 2D numerical model of suction filling.  
Source: [31].

In this study suction filling is not considered, as an experimental set-up of it could not be developed.

## 4.3 Experimental set-up

In Figure 4.3 the experimental set-up developed can be seen, and summarized information regarding its parts can be found underneath it.

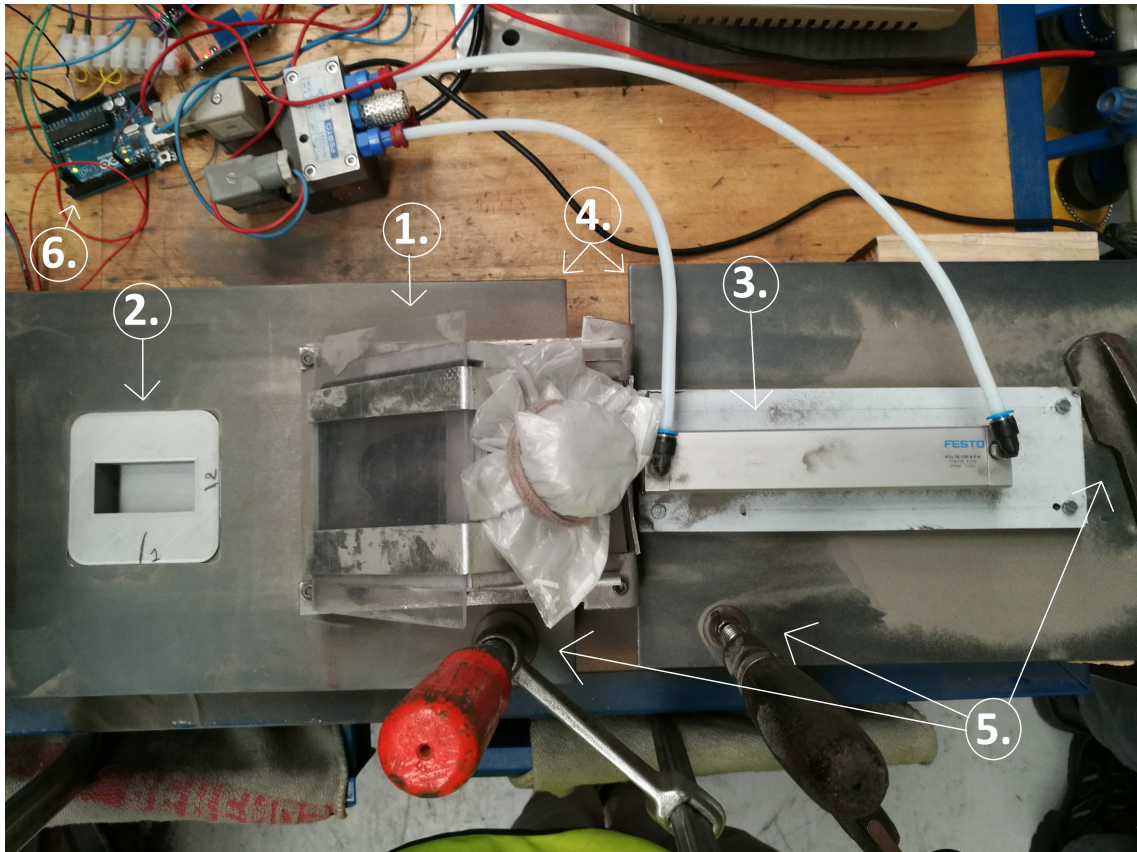


*Figure 4.3.* A picture of the die filling experimental setup developed.

1. **Filling shoe:** It consists of a plastic 3D printed body, a brass rectangular plate attached under it, and a metal filling tube attached on its top, acquired from Sintex A/S. Moreover, a mounting structure is manufactured and attached to it, so that it can seamlessly obey in the actuator's forced movement.
2. **Die:** 3D printed cavities in three different geometries are used as dies.
3. **Actuator:** A FESTO ADN-16-130-A-P-A double acting pneumatic actuator with 130 mm stroke, provided by Sintex A/S.
4. **Metal plate:** A 4mm steel plate, CNC milled to facilitate the placement of the die, so that the die's plate top plane is adjacent to the metal plate's top plane (Figures 4.4 and 4.5). After some initial experiments, it was cut in half, so that the shocks created from the actuators move do not pass directly through it from the actuator to the die, but only indirectly through the table where everything is mounted on.
5. **Stabilizing tools:** For the metal plate with the die attached to it to be able to receive, damp and endure the shock of the actuators movement, the plate has to be very well mounted.

6. **Electronics:** An ARDUINO board to facilitate the control of the shoe movement, as well as data collection from a distance measuring sensor. More on those can be found in Subsection 4.4.2.

### 4.3.1 Filling shoe - actuator mounting

The main body of the actuator receives the air input, and pushes out or pulls in, accordingly, a bar. That bar transfers the movement to the shoe, which can be mounted on the threads on the bar's end (Figure 4.6). A direct mounting of the shoe on those threads was impossible, as the shoe body is brittle, and any attempt to create a hole on it, results on it cracking. The filling shoe has to follow the straight movement imposed by the actuator without diverging, which is considered difficult, when considering forces as friction, its weight (approximately 2 kg) and the only one-point contact between it and the actuator. Therefore, a mounting is designed and manufactured, which can turn the one-point contact of the actuator with the shoe, to a two-point one.



*Figure 4.6.* Close up of the actuator's mounting features.



*Figure 4.4.* The steel plate, before it was cut.

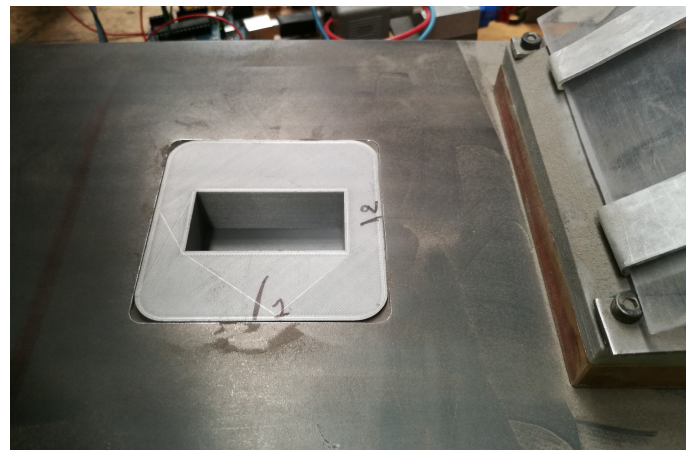


*Figure 4.5.* The die's and metal plate's top surfaces are adjacent.

The first version of this part was 3D printed in 75% fill PLA plastic, however, after a few fillings, the side boards were squished, and the contact part broke in half. It was obvious that the mounting receives rapid and very strong forces, and thus new alternatives were explored. In comparison to the alternative designs considered, the existing one was viewed as the best possible. Therefore, the same geometry was created in steel, Figure 4.7.

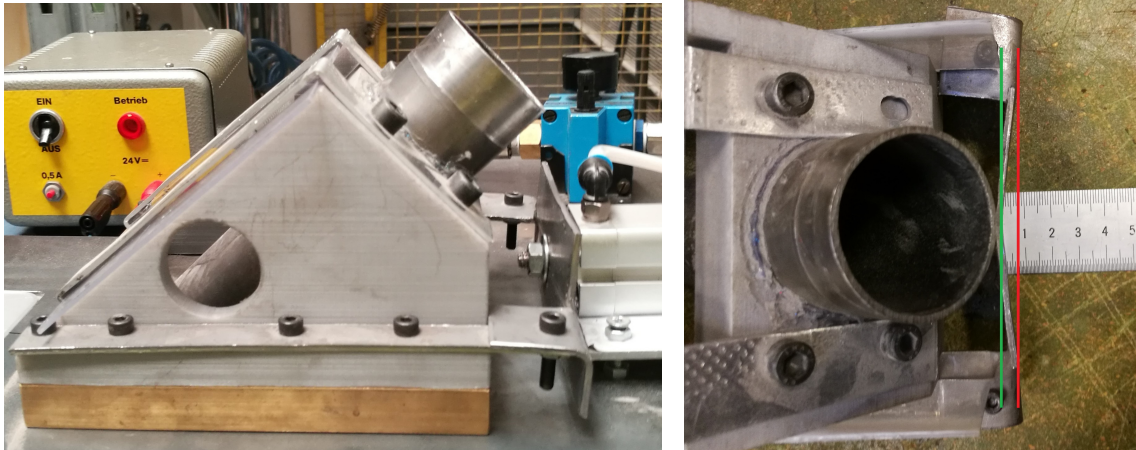


*Figure 4.7.* Left: the shoe mounting manufactured on its original form. Right: the mounting bended after some fillings.

The steel version of the shoe - actuator mounting prove to be significantly more durable. Only after many fillings, it started bending too. An idea at that point was to add a metal plate in the bended point, to add some more strength. That was not possible though, because the actuator's threads are only so long, and do not allow for thicker parts to be screwed on it. This, added to the difficulties of forming, were the reasons why the mounting was not re-manufactured from a thicker metal plate. In the end, the existing mounting was straightened and used again.

## 4.4 Parameters investigated

In order to fulfil the purpose of this study, distinct parameters in the process are varied. These parameters are presented summarily in Table 4.1 and in Figure 4.20. More information about them are presented in this Section.

*Table 4.1.* Settings of process parameters to be varied.

Parameter	Setting 1	Setting 2	Setting 3
Die geometry	circular	rectangular	rectangular with inlets
Shoe velocity	$\simeq 8.3 \text{ cm/s}$	$\simeq 10.7 \text{ cm/s}$	$\simeq 12.6 \text{ cm/s}$
Powder height	$\simeq 1 \text{ cm}$	filled shoe	—
Dwell time	$\simeq 4 \text{ ms}$	$\simeq 281 \text{ ms}$	$\simeq 388 \text{ ms}$

#### 4.4.1 Die geometry

For the experiments of this study 3 dies were initially designed and manufactured. A round die ( $50 \times 40 \text{ mm}$ ), a rectangular die (which can be used in two different orientations in comparison to the shoe filling direction,  $50 \times 25 \times 40 \text{ mm}$ ) and a rectangular die with inlets (which can be used in four different orientations,  $50 \times 25 \times 40 \text{ mm}$ ). The third, and most complex die, is designed with 2 inlets that are  $3/4$  of the die's height long, and are placed on the  $1/4$  and  $1/2$  of the die's length. The reason for that is that with results from one filling, the influence of two inlets depending on their position can be appraised simultaneously, by comparing density results of the left and right side.

Measuring density in the gamma densomat (see Subsection 4.6.4) in so tall parts (inner depth  $40 \text{ mm}$ ) prove to need around  $50 \text{ minutes}$  per point; hence, approximately  $8 \text{ hours}$  for measuring the density in 9 points of interest in the round die. Because of that, those initial die geometries were halved in height, which led to the measurement of the 9 points of the round die to need no more than  $40 \text{ minutes}$  in the densomat in total. The inner dimensions of those dies (basic dies) utilized can be seen in Figure 4.8, and their detailed sketches can be found in Appendix E.

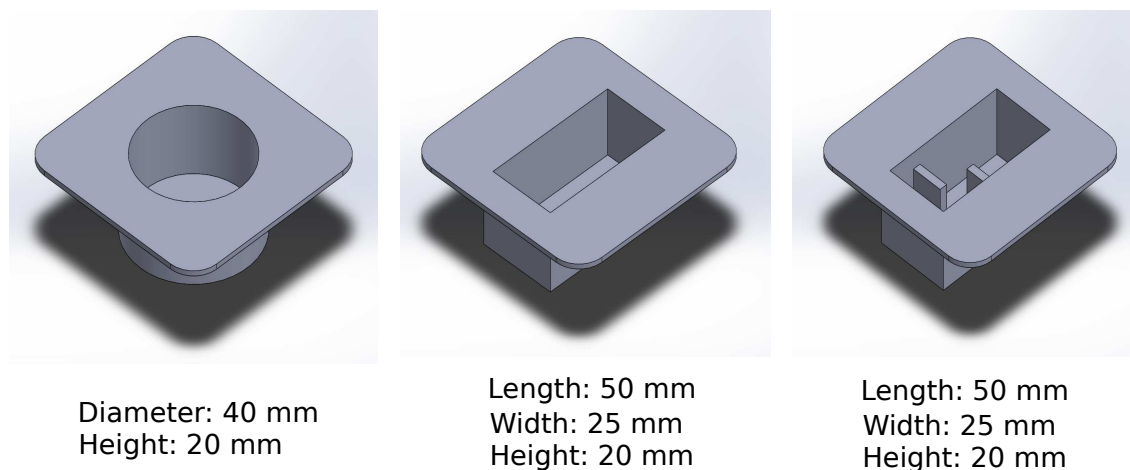


*Figure 4.8.* Inner dimensions of the three basic die geometries.

Furthermore, transparent dies were manufactured to be used in the high speed camera experiments (Figure 4.9). In those experiments, where the target is the observation of flow, deeper dies are considered more appropriate. The basic three die geometries were 3D printed transparent with the original dimensions ( $50 \times 40 \text{ mm}$ ,  $50 \times 25 \times 40 \text{ mm}$  and  $50 \times 25 \times 40 \text{ mm}$ ), so that there is enough depth for an observer to examine the powder flow inside them. However, the dies were milky white rather than clear after printing (see Appendix D for more details), but, thankfully, after a lot of grinding and a clear spray coating they became clear enough to facilitate their intended use.

In [19], Roudsary and Puri suggest the use of shallow dies (die width to depth ratio  $< 0.5$  for their rectangular dies) in filling studies, because their pressure profiles are significantly

less influenced by some process phenomena, as bridging and air build-up pressure inside the die, in comparison to deep dies. Nonetheless, differences in density from point to point are harder to detect in shallow dies as well as powder flow to observe, thus deep dies were employed in this study. More specifically, the basic dies utilized have a ratio of 1.25 width to height and 2.5 length to height, while the transparent ones have a 0.625 ratio of width to height and 1.25 length to height.

Furthermore, the same researchers in [18] state that deep dies allow for particle rearrangement and thus smoothed density. In the same article, they also argue that the ratio of particle size to die depth influences the density homogeneity, because the larger that ratio is, the less space for rearrangement the particles have. The particle-die ratios in their study were 0.1 and 0.01 for the BPM and Avicel powders respectively, in the 6.5 mm deep die utilized. In the present study, the particles have a 0.005 ratio with the basic

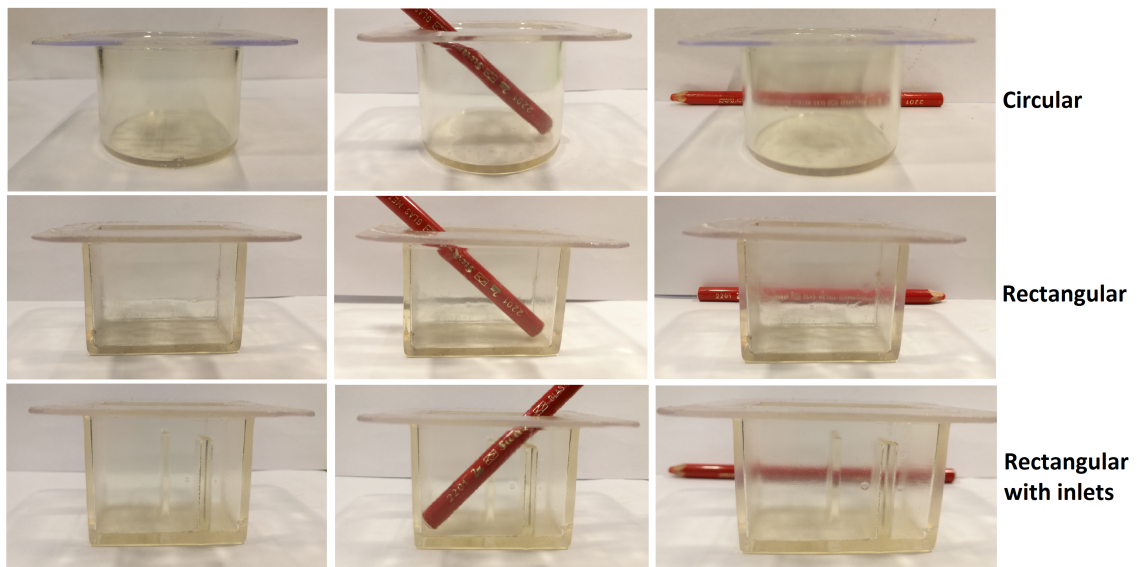


*Figure 4.9.* The three different transparent dies utilized.

dies' depth and 0.0025 ratio with the transparent dies'.

In the production line of Sintex A/S, there can be found dies deeper and shallower than the basic dies of this study, while transparent dies' height is a little bit taller than the industrial dies seen in Sintex.

#### 4.4.2 Shoe velocity

All die fillings performed, were monitored by a distance measuring sensor (Figure 4.11). The GP2Y0A41SK0F sensor used, is a product from SHARP, and it combines a position sensitive detector with an infrared emitting diode, it has a signal processing circuit, and it is connected to an ARDUINO board. The ARDUINO board is basically a micro-controller, that acts as an analogue to digital converter, a micro-processor and storage,

and is programmed in its own ARDUINO programming language. The ARDUINO scripts utilized can be found in Appendix A.

Time data alongside distance measurements from the distance sensor were written in a text file as output from ARDUINO, and were used as input in a MATLAB script, to obtain distance over time graphs. Those results are presented in Figure 4.12, and it is clear to see some accuracy issues. Because of that, some fitting, smoothing and averaging were applied so that the graphs on the right side of Figure 4.12 got acquired, which were used as speed input data for the numerical model in its initial stages.

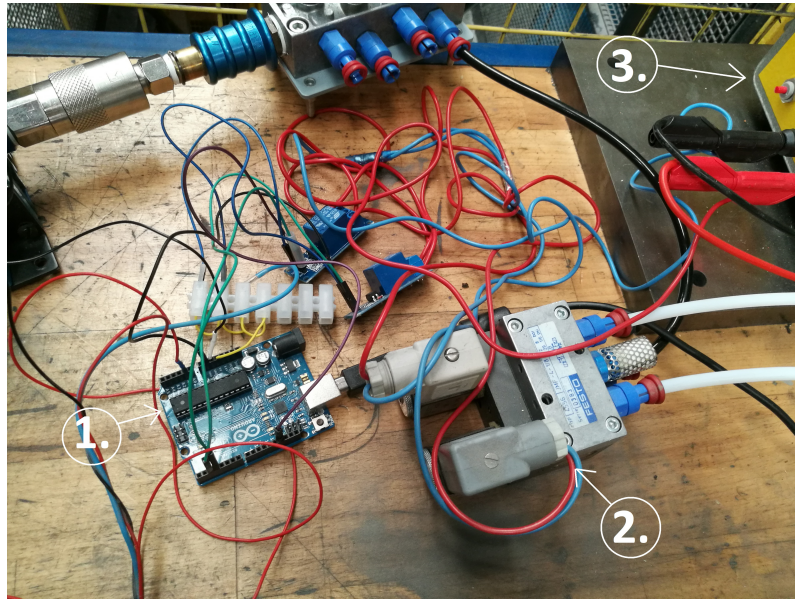


**Figure 4.10.** 1. ARDUINO board, 2. Double solenoid valve, 3. Power input.



**Figure 4.11.** The distance measuring sensor.

The ARDUINO is programmed to control a valve, whose output is used as input to the actuator, and thus controls the shoe movement. More precisely, a FESTO JMF-4-1/8 double solenoid valve is controlling the direction of air in the actuator, and thus whether the actuator moves outwards, inwards or stays still. The ARDUINO is directing the valve's input, and thus is indirectly controlling the shoe's movement.

The speed of the filling shoe though, is only controlled by inputting different air pressures (1-6 *bar*) to the valve, and thus to the actuator. This allows for some variation in shoe speeds, however the diversity was lower than expected. The highest pressure input of 6 *bar* yielded an average speed of 12.6 *cm/s*, the 4 *bar* pressure input 10.7 *cm/s*, and the lowest pressure input of 2 *bar* 8.3 *cm/s* (Figure 4.13).

ARDUINO's analogue to digital converter's sampling rate has a top limit, which means that the ARDUINO is not able to calculate signals of very high frequency. In addition to that, the distance sensor can require up to 25.2 *ms* to output a measurement. On top of that, the accuracy of the double solenoid valve could not be estimated or found. Those three reasons are the cause of some inconsistencies. For example, when ARDUINO script

dictated in which time point the air input in the actuator should be changed, so that it moves outwards, there was a delay of some *ms* needed from ARDUINO to actually output that command. When this command arrived in the valve, it was further delayed as the valve itself also needs some *ms* to accordingly change the actuator's air input. Finally, when the actuator, and thus the filling shoe did move outwards, the distance sensor due to its accuracy needed some time, to realize and output displacement data.

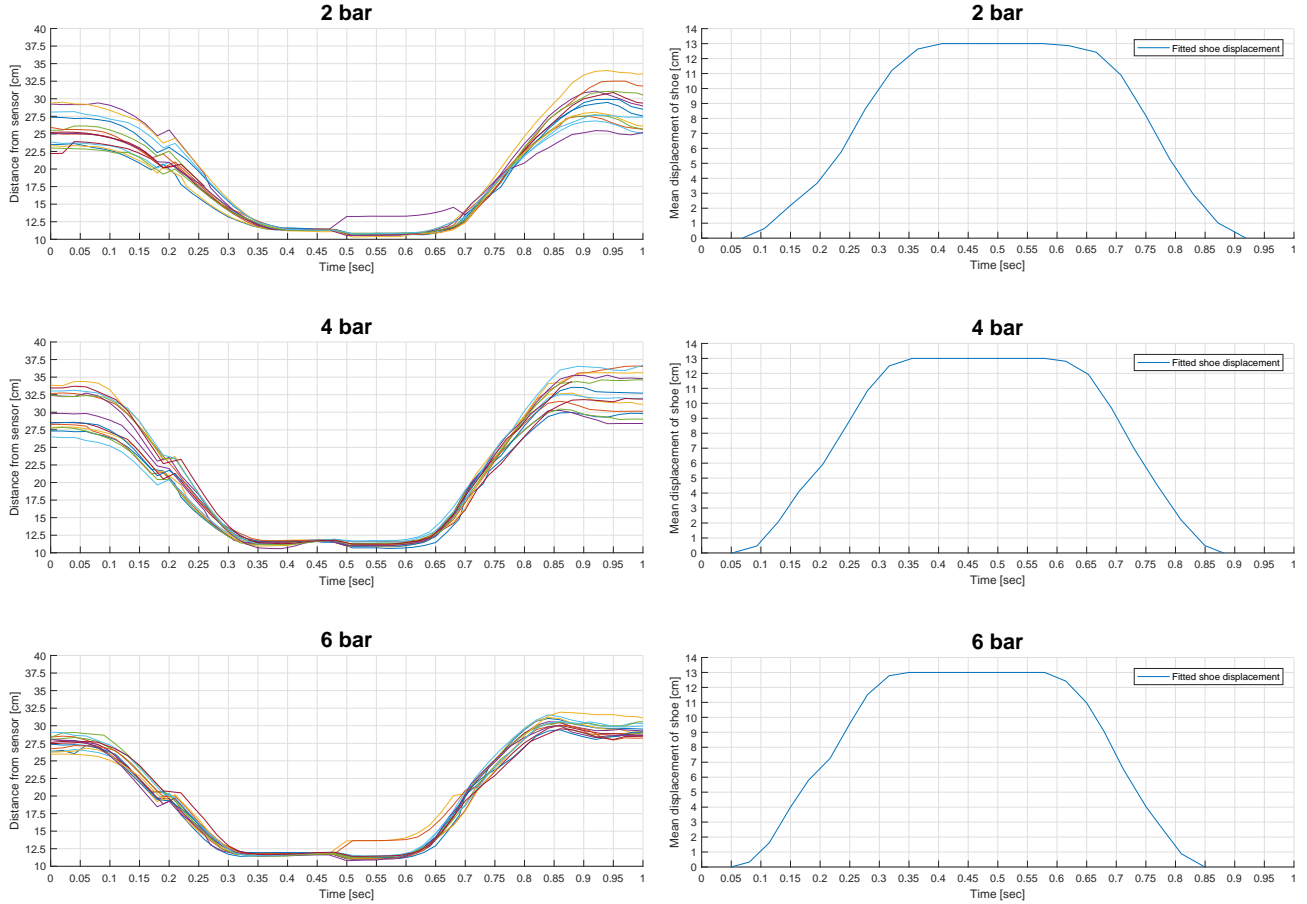


**Figure 4.12.** Distance over time graphs of the shoe movement when filling dies with different air inputs. Values from analysing the distance sensor results.

Later on, experiments with a high speed camera were conducted, with the target to capture the powder flow. The data obtained from those experiments were further analysed, to get more precise information about the shoe's velocity. Those results can be found in Figure 4.13. At this point it was realized that the displacement sensor was less accurate than expected, as its results are significantly different from the ones obtained by analysing the die filling videos from the high speed camera.

For instance, the sensor failed to portray how different the inward and outward speeds are. Thus, the sensor results were discarded, and the input regarding the shoe's speed in the numerical models was also quickly changed to the new and more accurate information. The displacement, distance and speed graphs presented in this section can be found in larger dimensions in Appendix D.

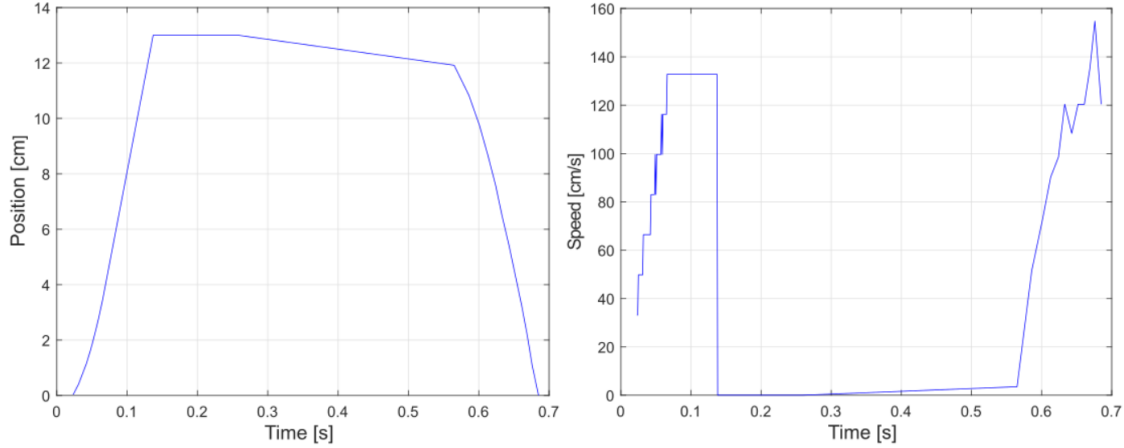


**Figure 4.13.** Distance over time and speed over time graphs of the shoe movement, from analysing the high speed camera results of the RB2 experiment (4 bar air input).

It is presumed that the reason why the displacement sensor gave so different results is that because it is a sensitive apparatus, the materials and lighting present in the die fillings were not the best match for its nature. Also, the sensor requires a processing time to give out results, which led to even more fluctuating output data when the higher shoe speeds were in use.

Furthermore, when it comes to the difference between the forward and backward speeds of the filling shoe, it should be mentioned that this is not the industrial reality. It only occurs in the experiments, because of the actuator, and it is not something that can be corrected. Those differences vary from  $-3 \text{ cm/s}$  to  $+1 \text{ cm/s}$ , and they average in  $-0.3 \text{ cm/s}$  difference from the outwards to the inwards speed.

#### 4.4.3 Powder height in the shoe

In the industrial environment, there is a powder supply system, constantly providing powder to the filling shoe, which is therefore considered full at all times. In an experimental set-up, ensuring that the filling shoe is fully filled in all repetitions is a little bit challenging, since the continuous powder flow can not be recreated easily. In addition to that, one of the most challenging parts of die filling process simulations is how to lower the computational time, which in most cases is enormous; i.e. in Guo's PhD work [32], there was a numerical model that took more than two months to complete. The main reason why the computational times of the die filling process are so high, is that calculations run for each powder particle involved, and not for the powder mass as a whole. This means that by lowering the amount of powder involved in the process, the computational times can significantly lower.



*Figure 4.14.* Powder in the filling shoe covering the brass plate.



*Figure 4.15.* Filling shoe filled with powder.

After considering those, it was decided that the majority of experiments, and thus simulations, would include significantly less amount of powder in comparison to the industrial process. It was agreed that the powder mass inside the filling shoe, would not fill the entire geometry, but that it would just cover the brass plate ( $\simeq 1$  cm height), as seen in Figure 4.14. This decision is based on the fact that the end goal is to include as less powder as possible in the process, but still enough powder to fill the dies. On top of that, some powder should be left inside the shoe after the die is filled, to ensure that the cascading powder, receives some downwards pressure, as in the industrial process.

It is not certain that this simplification will not affect the die filling results, and therefore experiments and simulations will also be explored with a filling shoe full of powder (Figure 4.15). This is expected to help in answering the question of whether or not the powder height in the filling shoe influences the results. This question has been of interest in the academic world, and researchers have investigated it, without conclusive results though. For example, Hjortsberg and Bergquist in [13], experimented with various powder heights in the shoe (from 2.5 up to 15 cm), and concluded that the density of the filled die is not affected by those different powder heights. On the other hand, Xie and Puri argued in [16], that a completely filled shoe might decrease the powder flow rate.

#### 4.4.4 Dwell time

The dwell time is an important parameter of the die filling process, as it gives extra time to the powder to fall out of the filling shoe and in the die. The moment when the double

solenoid valve should change the air input to the actuator, and thus indirectly control the dwell time, is defined in the ARDUINO script. The ARDUINO requires some processing time to output that command, and the valve requires some *ms* too, to accordingly alter the air flow. Thus, the dwell time defined in ARDUINO's script is slightly different than the one observed, because of necessary processing times. Furthermore, when the "move inwards" and "move outwards" commands to control the actuator, are very close in time, the system cannot keep up and the shoe never returns to its starting position. It is assumed that this is because of the valve's or ARDUINO's processing time. The lowest dwell time attained, before problems start arising, is 2 *ms* (RBBI experiments in Figure 4.20).

Moreover, what is defined in the scripts is the time points when the shoe should start moving outwards, and when inwards, but not the dwell time duration directly. Both the shoe outwards movement and the dwell time take place during the time frame that is defined between the command that initiates the outwards movement of the shoe, and the command that starts the next thing to be processed (the inwards movement of the shoe). Therefore, some fluctuation of the dwell time (from 1 to 14 *ms* in repetitions of the same experiment) can be seen, as they are affected by processing and response times of the shoe and the ARDUINO.



*Figure 4.16.* The densomat set up in Sintex A/S.

## 4.5 Experimental methodology summary

In this section the objectives and details of the two types of experiments conducted will be discussed, as well as the process of conducting them.

To start with, the first type of experiments has die fillings where the in points density of the powder mass is the main interest. The target is to see how do dwell time, shoe speed and powder height in the shoe affect the density distribution and the powder height in the die after filling. These experiments took place in Sintex A/S, as the densomat (Figure 4.16) is placed there and cannot be moved.

Subsequently, die fillings where the observation of the flow is of utmost importance are conducted. In those die fillings the objective is how the dwell time, shoe speed and powder height in the shoe influence the powder flow and deposition. These experiments took place in Aalborg University's lab, as the high speed camera utilized could not be loaned outside

of the university.

Both types of experiments can be greatly fruitful, as they can reveal information directly applicable to the industrial die filling process. By realizing how the filling process progresses, what influences it the most, and by identifying possible limits, a deeper understanding will be in obtained, which can lead to its better manipulation. All experiments are repeated (a minimum of) 3 times, to ensure minimum error interference; only exception being the RBB1 experiment, which in the density measuring experiments was conducted only once.

## 4.6 Density measuring experiments

The density distribution of the powder inside the die after filling can communicate information about the powder flow and deposition and is of interest. However, the resources for it are not available in this study, so instead a gamma ray densitometer is being utilized. It yields results about the powder average density in columns, through defining measuring points in 2D on the powder mass' surface.

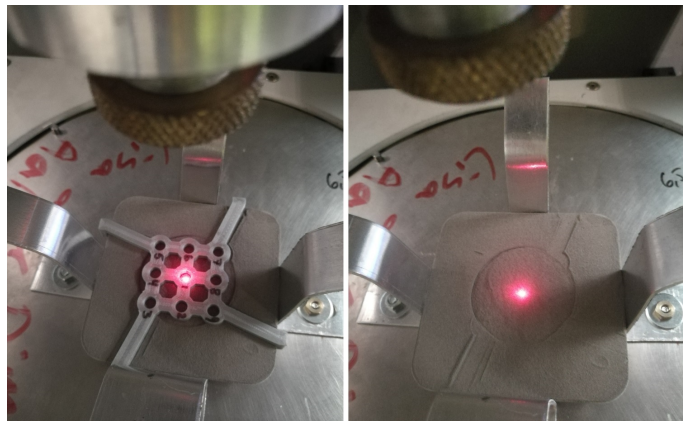


*Figure 4.17.* A filled die placed inside the densomat.

To start with, the points where the powder height and density measurements take place have to be defined. Measuring the exact same points in all the experiments conducted, requires that the die is always placed in exactly the same position in the densomat, and with the same orientation. Moreover, in some initial experiments it was observed that the die moves in the densomat when it is measuring, probably because of the rotational and translational movement of the densomat's stage, when it is changing point of measurement. To account for those, a type of mounting was manufactured. Four metal braces were mounted on a metal plate that was placed on the densomats' stage (Figure 4.16). Due to that mounting on the metal plate, the orientation, placement and immobility of the dies are ensured.

Furthermore, a way had to be found, to ensure that in both the densomat and in the powder height measurements, and throughout all experiments, the exact same points are gauged. The first guide for the measuring points designed and 3D printed (Figure 4.18 a)), was abandoned because its supports were overlapping with the densomat's supports (more on those can be found in Subsection 6.8.2. The second guide has a smarter design (see Figure 4.18 b)) as it securely attaches on top of the die even when in the densomat. However, its body is lying precisely on top of the die, in a way that in the points where

the die is over-filled the guide compresses the powder. Finally, the third measuring guide designed was able to overcome this problem, to provide more stable placement, and to function unmistakably. It can be seen in Figure 4.18 c), that it is equipped with more supports and all of them have props on them, ensuring that the guide is never in contact with the surface of the powder mass.

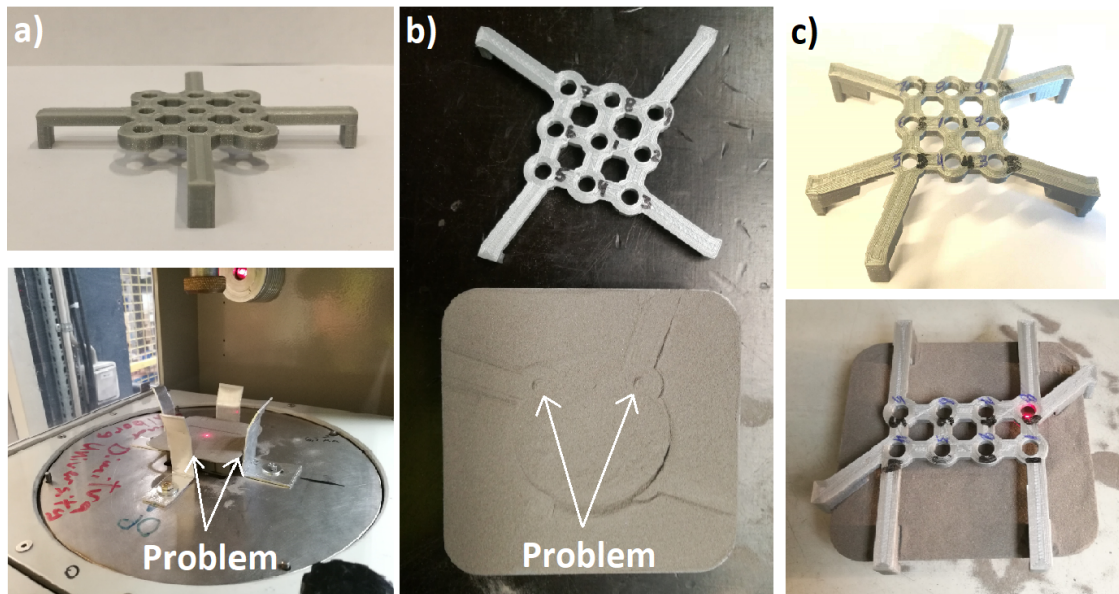


*Figure 4.18.* The three guides for measuring points designed, in timely order.

#### 4.6.1 Powder height in the die after filling

After a way is found, to measure precisely the same points in all experiments, the next step is to choose the best equipment to do the measurements. This is because, as discussed in Subsection 3.6.6, observations of the powder mass surface can reveal characteristics of both powder flow and deposition. On top of that, the measurements are utilized as input in the densomat. The various height measuring alternatives explored, can be seen summarily hereunder.

- **Image processing:** Image processing techniques are used on images of transparent dies filled with powder, which conclude on powder height in the die.  
**Problems:** This technique only grants the possibility to obtain the powder height in 2D, and it is impossible to tell where the identified peaks can be found in 3D. Furthermore, the dies used for the density measuring experiments were not transparent, thus this option was discarded.
- **3D surface scanning:** The complete 3D surface of the powder in the die can be

obtained by 3D surface scanning. This is of interesting not only for the powder height used as input for the densomat, but also as a validation criterion for the numerical model.

**Problems:** The experiments were performed at Sintex A/S, so even though Aalborg University has a brand new laser scanner, it could not be borrowed outside of the University. Furthermore, this laser scanner requires to be moved with controllable velocity over the part to be measured, which in turn requires a robot, conveyor or similar for the set-up.

- **Hand-held 3D scanner:** A hand-held 3D scanner with the intended use of scanning objects, saving the 3D files, and then 3D printing them was explored too. That was because given the fact that it has an accuracy of 1 *mm*, it could possibly output interesting information about the powder mass surface, specially on half full dies, where the height differences between points are large.

**Problems:** In filled dies the scanner did not output results that could be analysed. In half filled dies, because of the unavoidable poor lighting inside the die, added to the fact that the powder itself is dark, the supposed accuracy could not be reached too.

- **Proximitior sensor:** Proximity transducer systems output voltage, which is directly proportional to the distance between the system's probe tip and the observed conductive surface.

**Problems:** For this method to work, the surface of interest has to be magnetic. A small research yielded confusing results on weather the 430L steel is magnetic or not. Initially, the system's functionality was explored with a compacted part made of the STX2000 powder and it performed smoothly. However, when tested on the powder it did not provide output. Possibly the air between the powder particles is enough to minimize the mass' magnetism.

- **Micrometer:** In the first experimental die fillings, due to lack of necessary equipment and other alternatives, a digital electronic micrometer was utilized for the powder height measurements required (Figure 4.19 a)).

**Problems:** Micrometers are not applicable in measuring the height of the loose powder mass in the die, as the powder gets displaced during contact with them. Furthermore, the results from those first experiments are not published, as they were of introductory nature and for the researchers to get acquainted to the process.

What prove to be the needed solution to the powder height problem is a laser sensor. A ZS-LD350S sensor with an Omron ZS-LDC41 sensor controller were explored, which output measurements with 0.25  $\mu m$  accuracy for measuring distances between 215 and 485 *mm*. The sensor has to be mounted somewhere steady, and in the industrial environment there were not many alternatives, therefore, it was mounted under a shelf, see Figure 4.19 b).

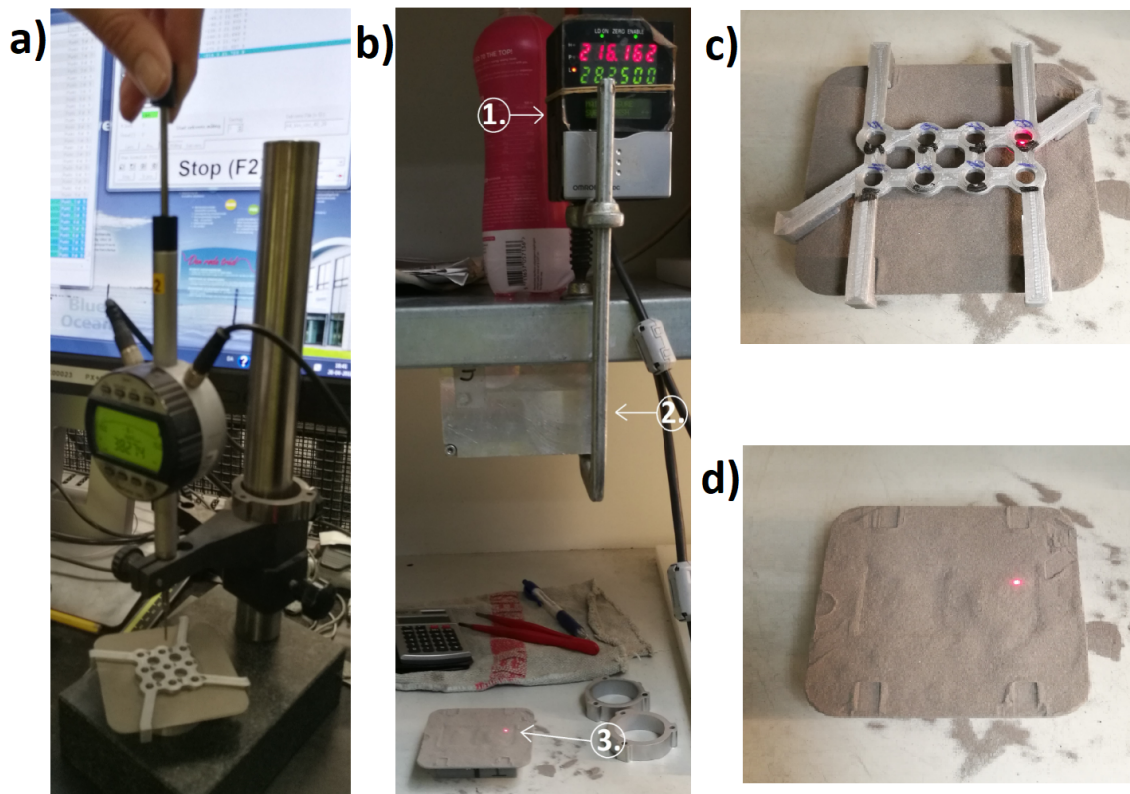


**Figure 4.19.** Powder height measurement with a) a micrometer and b) a laser, where: 1. Sensor controller, 2. Laser sensor, 3. Measurement point; c) and d) the utilized version of the measuring guide does not come in contact with the powder inside the cavity.

As mentioned in Section 4.3, the actuator transfers strong forces to the filling shoe, which results in the whole set-up receiving shocks, when the shoe reaches the end position of its each movement. This is the reason why the metal plate has been cut in half, and why so many mounting clamps are used on it. Even though those changes reduced the intensity of the shocks, they still exist, and they result in the creation of valleys and mountains on the powder surface after filling. Those mountains and valleys are no more than 1 *mm* tall, and thus they do not affect the overall image of the powder in dies, but when looking closely some surface details result from them solely and not from the filling.

#### 4.6.2 Sequence of density measuring experiments

Initial die fillings and density measuring experiments were conducted for the researchers to get acquainted to the process and the equipment. Right after, 12 die fillings were conducted. At that time, the laser sensor was not in hands, so the powder height was measured manually with a micrometer (see Figure 4.19 and Subsection 4.6.1). Therefore, when later on the laser sensor was obtained, to ensure as minimum human error as possible, these results were disregarded. There is no doubt that the manual way of measuring the powder height is not as accurate as a laser, nonetheless the measuring errors are not expected to exceed 1 *mm*, thus slightly affecting the densomat results.

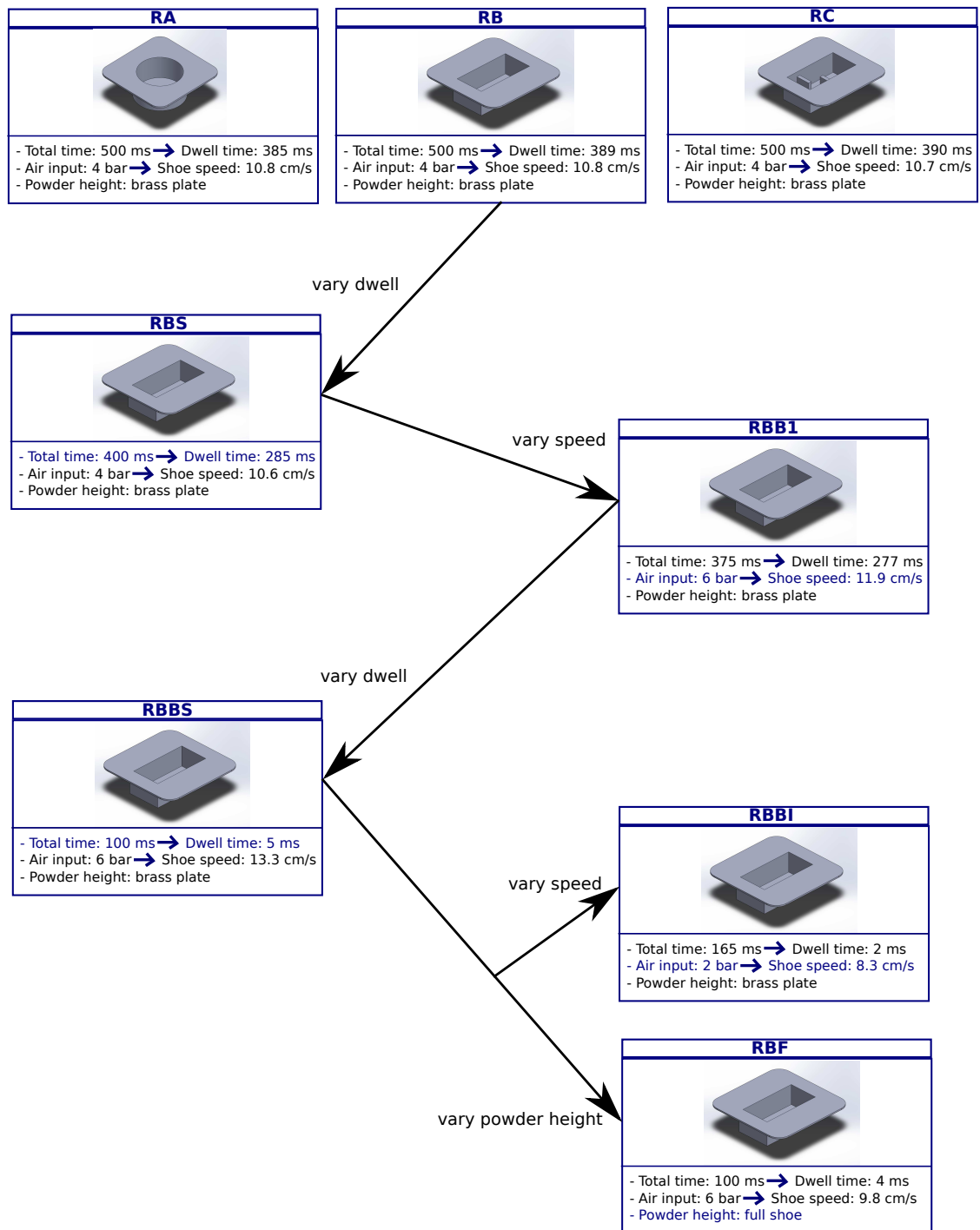


Figure 4.20. A tree diagram portraying the sets of parameters utilized in all the experiments conducted.

Seven of those experiments were die fillings with the same exact parameters set. By examining the density in points results, it was realized that they fluctuate somewhat; more than what is expected to be affected by human errors. Thus, the conclusion formed from this information comes to an agreement with what Hjortsberg and Bergquist stated in [13], that the powder behaves irregularly when packing, so even something as straight-forward as the density can vary from one experiment to another.

Summarizing the density measuring experiments presented in this report (where the powder height is measured by the laser sensor), the first three ones explore different die geometries with the medium shoe speed, the longest dwell time available, and the shoe filled with powder up to the brass plate level (see Table 4.1). Afterwards, the distinct effects of all the dwell times and shoe speeds attainable are investigated in one of the dies, by altering them one by one. In the end, an experiment with the shoe fully filled with powder is conducted. A diagram of the experiments conducted can be seen in Figure 4.20.

More analytically, to assess the effect of the die geometry on the powder density and density distribution, die fillings in the three different basic die geometries with exactly the same parameters set, are conducted (RA, RB and RC experiments in Figure 4.20). Further on, one die is chosen to be the one, where the rest of the parameters will be investigated on. The rectangular die is the chosen one, because it is a relatively simple geometry, which can however prove to be challenging, due to its corners.

Subsequently, with the RB experiments as base, the dwell time is lowered (RBS experiments) to evaluate its distinct effect on the the filling process, by comparing the RBS experimental results to the RB ones. Later on, and by following the same logic, experiments based on the RBS experiments are conducted, where the shoe speed is increased (RBB1 experiments). To evaluate the higher speed's distinct effect on the filling process, these results are compared to the RBS ones. Thereafter, experiments based on the RBB1 one are conducted, where the lowest attainable dwell time is utilized and investigated (RBBS experiments).

Finally, two different experiments are based on the RBBS ones. In the first, the lowest shoe speed and dwell time attainable are explored (RBB1 experiments). In the second, and final ones, the highest speed and lowest dwell times are implemented with a shoe filled with powder (RBF experiment), to assess whether the magnitude of the powder mass in the filling shoe influences the powder flow. It can be seen in Figure 4.20, that even though 6 *bar* pressure of air are input, the shoe speed attained is relatively low. Presumably this is because the weight of the powder in the fully filled shoe incommodes the actuator, as its output depends on the mass it has to push or pull.

### 4.6.3 Average density

Comparing average densities is not a very precise way to assess the success of a filling, however it can qualitatively deduce on similarities and differences between fillings. For example, in the industrial environment, weighting of the compacted parts is in use as a fast quality control.

Before each die filling repetition the empty die is weighted in an electronic scale with  $mg$  precision (Figure 4.21). After the filling and the in-points measurements of the density, the excess powder is swiped off of the dies' plane surface, and it is weighted (Figure 4.21). The difference of those two measurements equals to the mass of the powder inside the die. The formula that calculates density of mass and volume is  $\rho = m/V$ , where  $\rho$  is density,  $m$  mass, and  $V$  volume. For fully filled dies the powder volume is equal to the die volume (which is known), and thus calculating the average density is a straightforward calculation.



**Figure 4.21.** The scale used for measuring the average powder mass.

To calculate the average density of dies that are not filled, a calculation or an approximation of the volume they occupy has to be made. The powder masses inside the half full dies of the conducted experiments have complex 3D concave shapes, which constitutes volume calculations challenging. For those experiments where the cavities were not completely filled (RBBS and RBF as seen in Figure 4.20), more emphasis will be given on the powder mass surfaces instead.

After the RBS experiments were conducted with  $\simeq 258$   $ms$  dwell time and  $10.6$   $cm/s$  average shoe speed (can be seen in Figure 4.20, the target was to conduct experiments with the same dwell time and higher shoe speed. The shoe speed, as mentioned earlier, is only controlled indirectly, by altering the air input in the actuator. By changing the input from 4 to 6  $bar$ , the shoe speed was expected to increase noticeably. However, it only slightly rose in comparison to the speed of the RBS experiments ( $1.3$   $cm/s$  increase). This difference was not expected to influence the density results of the basic dies, and it was indeed witnessed from the densomat results; thus, no more repetitions of the RBB1 experiments were conducted for the density measuring type of experiments. On the other hand, since the dies utilized in the high speed camera experiments are significantly bigger, and the aim of the experiments is the flow and not the density, three repetitions of the RBB1 experiments were conducted there, to examine more thoroughly whether this small difference in the shoe speed can influence the powder flow or not.

#### 4.6.4 Density measurements in points of the powder mass

In those experiments, dies are filled with various combinations of different dwell times, shoe speeds and powder height inside the filling shoe; nonetheless, the process to obtain results after the fillings, is always the same. Initially, the die is placed under the laser sensor with a measuring guide placed on top of, which dictates the points where the powder height will be measured. When the powder height measuring is completed, it is used as input to the densomat, and the die is moved inside it (Figure 4.16). There, the same point measuring guide has been utilized, so that the sequence of the measuring points (consisting of their exact coordinates) has been saved, so that in every experiment the same points are measured. Finally, when material data are also assigned, the densomat will output the average density in the points.

### 4.7 Flow observation experiments

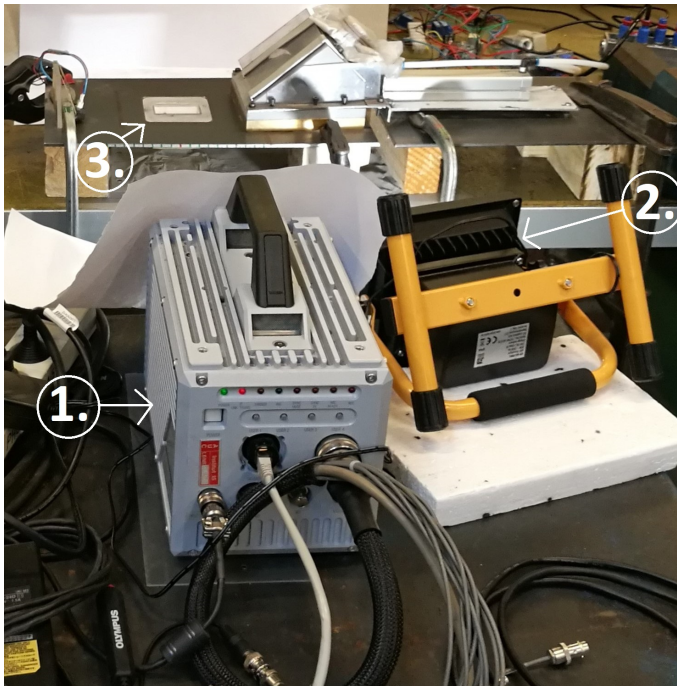


**Figure 4.22.** The experimental setup for the flow observation experiments. 1. High speed camera, 2. Light, 3. Die.

Experiments with a high speed camera and 1000 *frames/s* are conducted, to investigate the flow of the powder and its deposition in the die. The camera is a FAST-CAM SA5 model 775K-M1, and 23 of its recorded fillings will be discussed. In these experiments, the density distribution could not be evaluated, but the high frame rate of the camera allowed for a very close by investigation of the powder flow's progress.

The same parameter sets are investigated (see Figure 4.20), as in the density measuring experiments too, however, here, while the die is getting filled, the high speed camera is placed on the die's level, so that it is able to observe the powder flowing inside it (Figure 4.22). Furthermore, a white background is utilized and a strong lighting source, to aid the understanding of the powder flow. The filming is controlled through the PFV Photron FATSCAM Viewer Software, and the *.avi* files are subsequently saved and ready to be investigated, with the aim to deeper examine known information, and for new information to be identified.

As mentioned earlier, shoe speed data are to be derived from the high speed camera experiments too. To accommodate the collection of more precise data, rather than only the average shoe's speed, a ruler was fastened with a clamp on the top of the metal plate,

parallel to the shoe's movement (Figure 4.23). However, the camera has a limited depth of field, which is of course aimed to the die, and because the ruler is in different depth than the die, its marks are not distinguishable in the videos. A solution to that was found by marking lines every 1 *cm* on the metal plate's side, which can be discerned in the videos.



*Figure 4.23.* The initial setup for the experiments with the high speed camera.

Further on, a perspective issue arises though, which makes the 1 *cm* intervals look more distorted the further away they are from the centre of the image. Yet, this is a global problem, for which no solution has been found until now. Therefore, the distorted intervals problem is tried to be somewhat overcome with some calculations. In the end, the data collected are definitely more accurate than the distance measuring sensor's data, but objectively not very accurate.



*Figure 4.24.* The final setup for the experiments with the high speed camera.



# Experimental Results

# 5

In this Chapter the results of the conducted experiments will be presented and discussed upon. It should be noted though, that as concluded by Hjortsberg and Bergquistin in [13], caution should be given to the interpretation of specific die filling studies results in comparison to other studies, and to deducing on global conclusions. This is because due to the lack of an absolute understanding of the powder behaviour, the validity of results is limited to the experimental set-ups investigated at each study.

## 5.1 Powder flow observation

In this Section recordings from the experiments with the high speed camera will be analysed (Figure 5.1). In the beginning each experiment's die filling repetitions will be compared to each other, so that a general understanding of the repetitivity<sup>1</sup> of the process is understood. When this is established, different experiments will be compared to each other, to deduce on each parameter's influence on the powder flow, and thus filling process.

The first thing that was realized through the observation of the high speed camera recordings, is that when the actuator gets fully extracted, the shoe portrays vibrations, while it was assumed that it instantly stops. More specifically, at the furthest point of its forward movement, the shoe moves rapidly back and forth over a short distance for a short time a few times, mimicking the industrial vibration method. Most likely

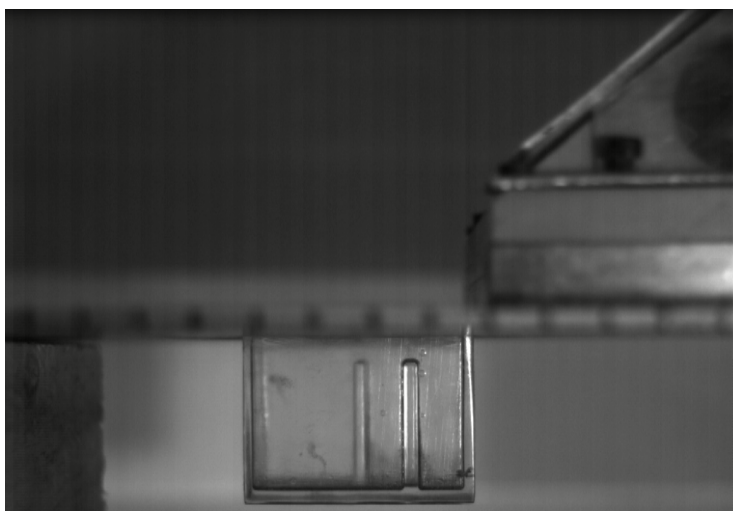


**Figure 5.1.** Capture of the shoe before it crosses the die from the high speed camera video. (RC2 experiment)

<sup>1</sup>Repetitivity is the ability of the developed system to yield the same results in more than one run.

that is because the mounting manufactured for the shoe-actuator joint, damps the force transferred more than previously understood. These vibrations might prove to be more influencing than small differences in shoe speeds or dwell times, as the powder inside the shoe gets strongly shaken, which presumably increases its flowability.

### 5.1.1 RA experiments

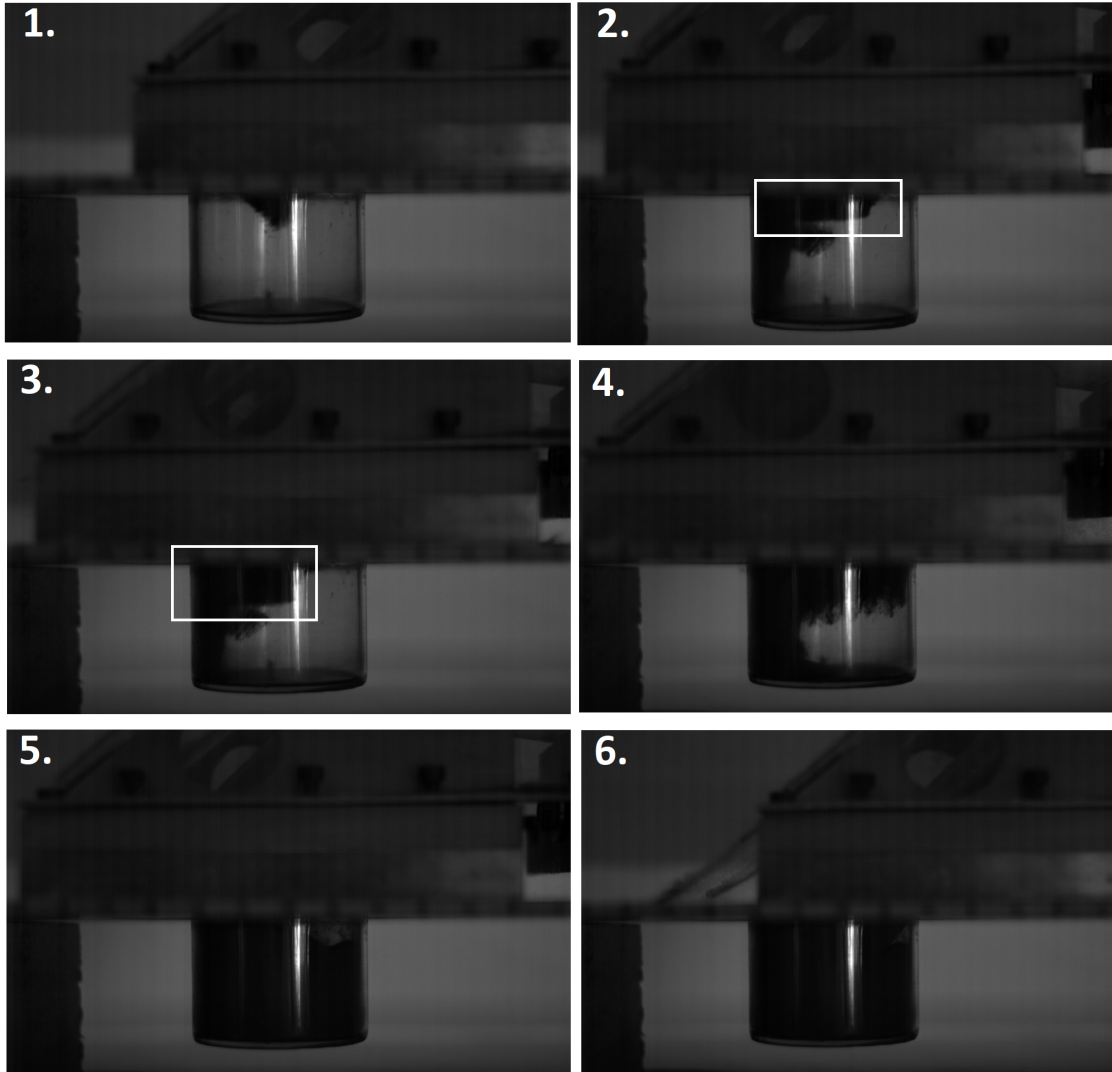


*Figure 5.2.* The filling process of the circular die. (RA3 experiment)

By investigating the RA experiments' videos, a few interesting remarks can be observed. To start with, the videos from the three RA die filling repetitions of the experiment are very similar to each other. In chronological order, when the shoe moves forward, the powder portrays nose flow, and thus, not much powder is supplied to the die (Figure 5.2 1.). The largest part of the powder mass flows in the die when the shoe is just above the die. When the shoe first reaches the end of its forward movement, it rapidly and evidently bounces back a few millimetres, which causes a part of the powder mass to detach from the rest of it inside the shoe, and fall in the die (Figure 5.2 2. and 3.). After that, there are a couple, less

powerful vibrations, however, in total, the vibrations clearly affect the flow. When they are all over, and the shoe stands still, the bulk flow distinguishably dominates (Figure 5.2 4.).

In that stage the flow rate is high, meaning that the die gets filled fast. Though, the bulk flow ceases soon, and the filling rate gets considerably lower. The die is not completely filled when the shoe starts its backwards movement, but the flow rate in-

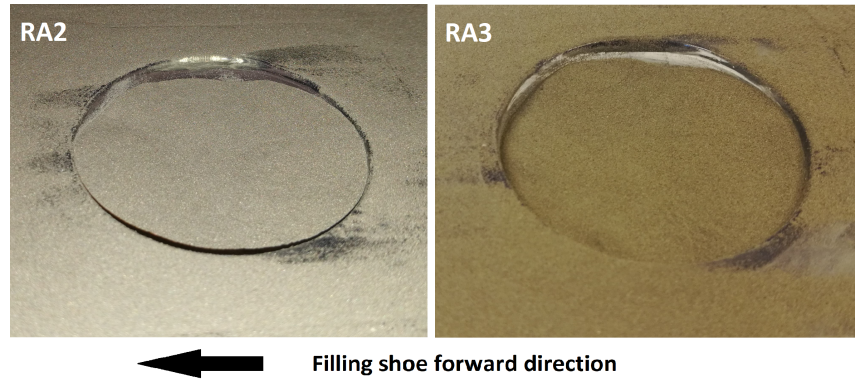


*Figure 5.3.* The filled dies of the RA2 and RA3 experiments.

creases again during its backward movement. The die's top right side (from the viewer's point of view) is not filled (Figure 5.2 5.), when the shoe is moving above the die (Figure 5.2 6.). Still, the die does not get completely filled in those experiments (Figure 5.3).

### 5.1.2 RB experiments

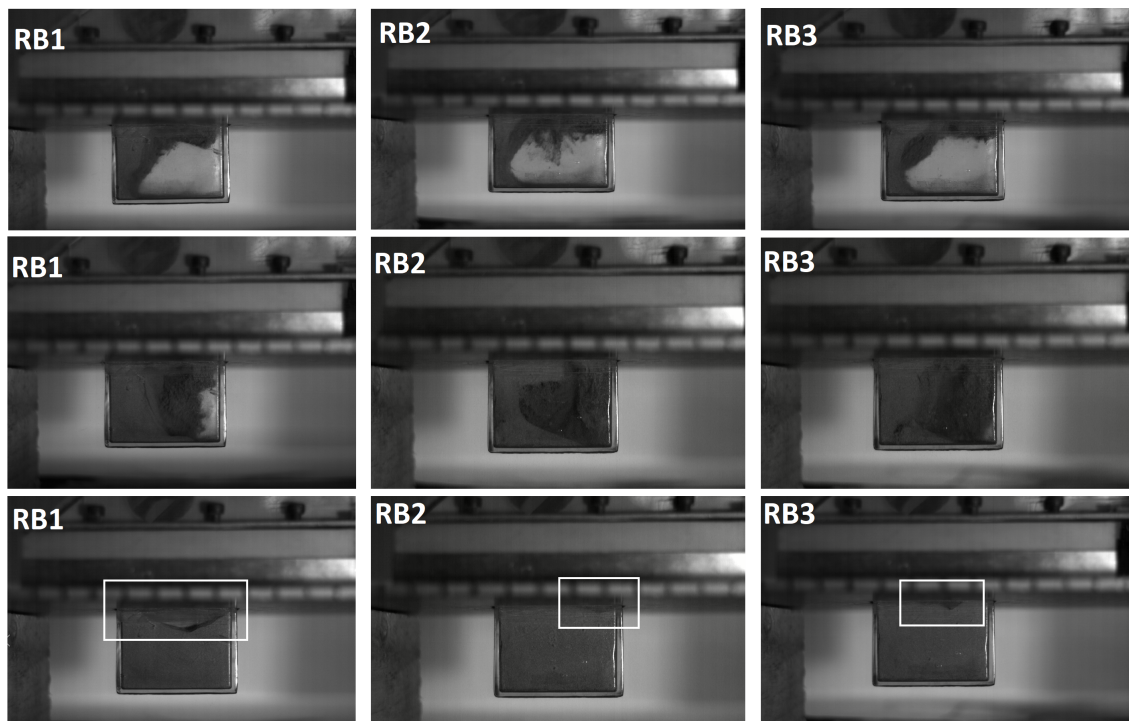


*Figure 5.4.* In the first and second lines, the straight flow of the RB1 experiment, and the more rotational ones of the RB2 and RB3 can be seen. In the third line the differently shaped lack of powder can be distinguished, just when the shoe starts moving backwards.

In the RB experiments some differences between its three repetitions conducted can be distinguished. Furthermore, in the RB experiments similarly to the RA experiments, the filling rate prominently decreases when the vibration effect stops and the shoe stands still, and it increases noticeably again when the shoe starts moving again. The vibration shocks seem to strongly influence the RB1 and RB3 repetitions, but less evidently the RB2 one. In the RB1 and RB3 fillings, the lack of powder is more eminent, and even though these powder lack voids initially portray triangles, they illustrate concave shapes towards the end of the filling (Figure 5.4). This empty space is unmistakably larger in the RB1, smaller in the RB3 and even smaller in the RB2 experiment. More precisely, in the RB2 experiment, this void is shaped like a triangle throughout the filling duration, and seems similar to the RA die fillings.

When it comes to flow rate, similarly to the RA experiments, the flow slows down when the shoe is still, and increases along the shoe's movement. However, in the RB1 repetition the flow rate decreases sooner than in the RB2 and RB3, and maybe that is the reason why it depicts the largest lack of powder. In all 3 experiments a rotational movement of the powder is evident (Figure 5.4) in different degrees. It is strongest in RB2, and slightly less evident in RB3, however, in the RB1 filling the powder flow trail would be better described as mainly straight or diagonal. Nonetheless, in all 3 fillings, nose flow is starts being evident while the shoe is approximately in the midpoint of its forward movement, and even though it seems to dominate the filling for the longest time interval, the bulk flow provides the largest part of the powder. Finally, in the end of the process, the die of the RB1 experiment seems to be noticeably less filled than the other two.

### 5.1.3 RC(2) experiments

All RC1(2), RC2(2) and RC3(2) portray the same straight or diagonal filling. The flow is similar among all three of them, and they depict lack of powder (voids) on the top right side. It is interesting to notice that the RC3(2) seems to receive the more smooth vibrations, in comparison to the RC1(2) and RC2(2), and has the largest lack of powder. Therefore, it is possible that the assumption that the vibrations increase the powder flowability are valid. Finally, in all 3 experiments, it is interesting to notice that the void gets translated before being filled (Figure 5.5), presumably due to the powder's rotational flow as it enters the die.

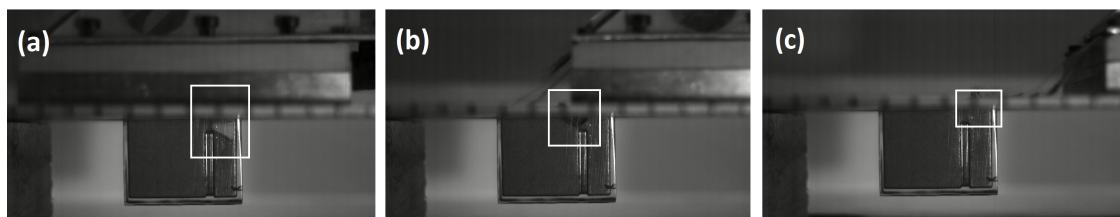


**Figure 5.5.** In the RC1(2) filling the lack of powder the moment when: (a) the shoe starts moving backwards, (b) the shoe is half-way to its starting position; (c) the shoe arrives in its starting position.

#### 5.1.4 RC(4) experiments

In those experiments, where the only difference with the RC(2) ones is the 180 degrees rotation of the die, there is some influence on the powder flow from the shoe vibrations. The bulk flow dominates in the process over the rotational, furthermore the three experiments share similar flows, and more specifically RC1(4) and RC2(4) appear identical. All repetitions portray lack of powder on the top right corner, shaped as triangle. The magnitude of the lack of powder though is different from experiment to experiment, more specifically the largest triangular void is seen in the RC2(4) experiment, a smaller one in the RC1(4), and the smallest in the RC3(4) (Figure 5.6). These voids, similarly to the RC(2) experiments first get translated and then filled.

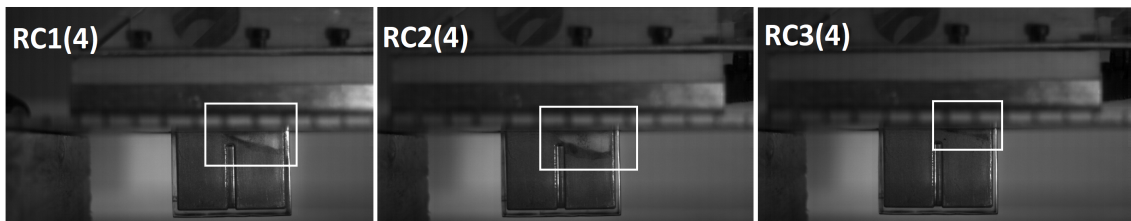


*Figure 5.6.* The voids of the RC1(4), RC2(4) and RC3(4) dies are similarly shaped, but different size.

#### Comparison of the RA, RB and RC experiments

By investigating the powder flow and deposition in the four different experiments, it is obvious that the inlets of the third die geometry (experiments RC(2) and RC(4)) influence the powder behaviour. Besides this observation, no big differences could be distinguished among the experiments.

#### 5.1.5 RBS experiments

The effect of the shoe's vibrations is seen in all three repetitions of the RBS experiment, and even though evident, it does not appear to be large. They also portray similar flow, as the bulk flow dominates, and the nose flow is less present. The powder's movement is rotational, which is supposedly created by the nose flow. Lack of powder is present in all these experiments on the top right side too, and the dies seem to be full while the filling



*Figure 5.7.* Filled dies from the RBS experiments.

shoe is still above the die. More specifically, in the RBS2 experiment, the void gets filled when the shoe starts moving backwards, in the RBS1 after the shoe has initiated its backwards movement, and, finally, in the RBS3 considerably later, when the shoe is in the middle of its backwards journey. Nonetheless, after the shoe returns in its starting positions, the dies look similarly filled with only a little bit of powder missing for a complete fill, and not distinct differences between them can be distinguished.

### Comparison of the RB and RBS experiments

Even though the bulk flow seems stronger (higher flow rate) in the initial stages of the powder transfer in the RB experiments than in the RBS ones, in the end the RB dies require more time to completely fill. That, added to the fact that the dwell time is the only difference between those experiments, signify that the around 30% higher dwell time in the RB experiments, did not contribute to the filling process.

#### 5.1.6 RBB1 experiments

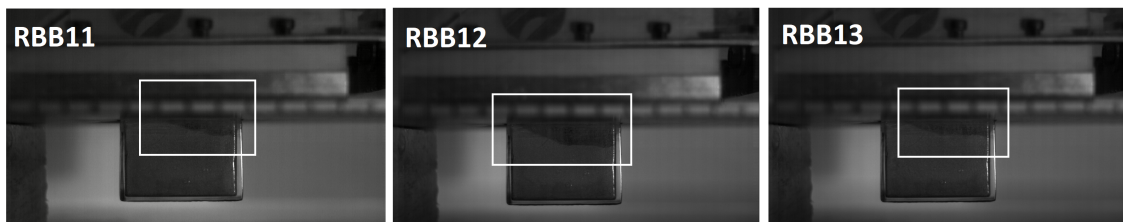


*Figure 5.8.* The lack of powder witnessed in the RBB1 experiments, just before the shoe starts moving backwards.

The influence of the shoe vibrations is not large on the RBB1 experiments. The bulk flow dominates the process, however rotational movement of the powder is also evident. When it comes to the lack of powder though, the RBB11, RBB12 and RBB13 experiments yield different results. The RBB11 experiment portrays the smallest void (top right corner), which is almost filled in the end of the filling. On the other hand, in the RBB13 repetition a larger lack of powder is distinguished, which is clearly not filled in the end of the process. The largest lack of powder is seen in the RBB12 experiment (Figure 5.8), and it is not filled in the end of the filling process.

### Comparison of the RBS and RBB1 experiments

The difference between the RBS and the RBB1 experiments, is that the latest has higher shoe speed. The results of the powder having less time to cascade in the die are obvious, as the dies in the RBB1 experiments are noticeably less filled than the dies in the RBS ones. Furthermore, in the RBB1 fillings a stronger rotational flow is observed, while the RBS ones are mainly dominated by bulk flow.

### 5.1.7 RBBS experiments

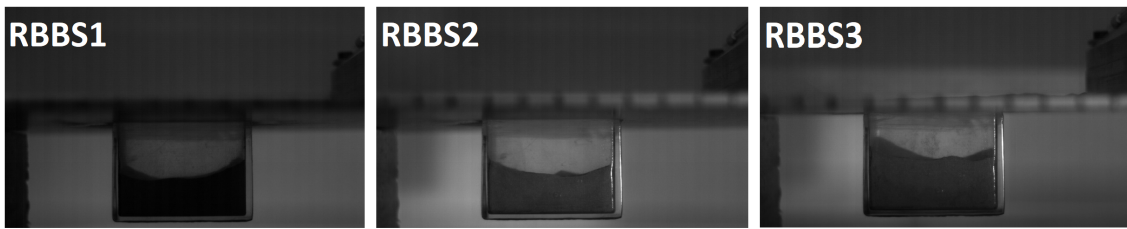


*Figure 5.9.* The filled dies of the RBBS experiments.

In the RBBS experiments the lowest dwell time attainable is employed, and when the filling shoe reaches the end of its forward movement, it momentarily starts its backward movement; thus, there are no shoe vibrations employed. Generally, in all three repetitions of this experiment the powder seems to have similar flow and deposition. The type of the flow cannot be clearly distinguished due to the involved speeds, nonetheless bulk flow appears to dominate the powder behaviour, and nose flow to be less present. Though, since there is not enough time for the bulk flow to take place, it is considered that the nose flow contributes to the powder fill significantly too. Because of the high shoe speed, the powder mass from the bulk flow can be seen entering the die, when the filling shoe is already moving backwards. Furthermore, it is noticed in all repetitions, that when the shoe is no longer above the die, the powder particles evidently rearrange.

The only distinguishable difference among the three repetitions is the different powder heights seen after filling (Figure 5.9). The edge of the powder mass of the RBBS1 experiment is similar to a half-circle or concave line, the RBBS2 experiment's mass outline resembles a straight line, and the RBBS3 one's a triangular or concave line. Finally, the die filled in the RBBS3 experiment seems noticeably more filled than the RBBS1 and RBBS2.

#### Comparison of the RBB1 and RBBS experiments

In the RBB1 experiments it is clear that the extra time of the dwell time allows for bulk flow to occur for longer time, which supplies a large amount of powder in the cavity. On top of that, the light effect of the shoe vibrations in the RBB1

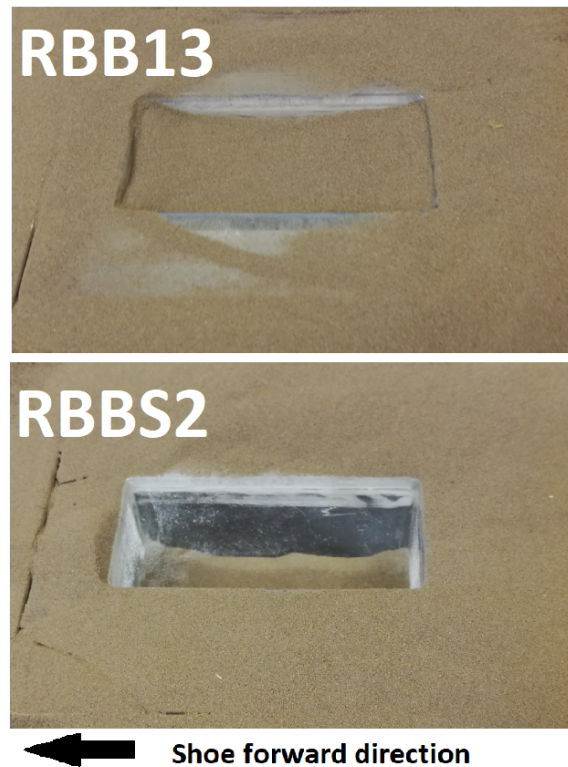


*Figure 5.10.* The filled dies of the RBB13 and RBBS2 experiments.

experiments is considered to assist the powder flow and transfer; while in the RBBS experiments no shoe vibrations are present. Concluding, the lower dwell time significantly affects the die fill process, which is evident in Figure 5.10, where the amount of powder in the die after filling is clearly larger for the RBB1 experiments.

### 5.1.8 RBBI experiments

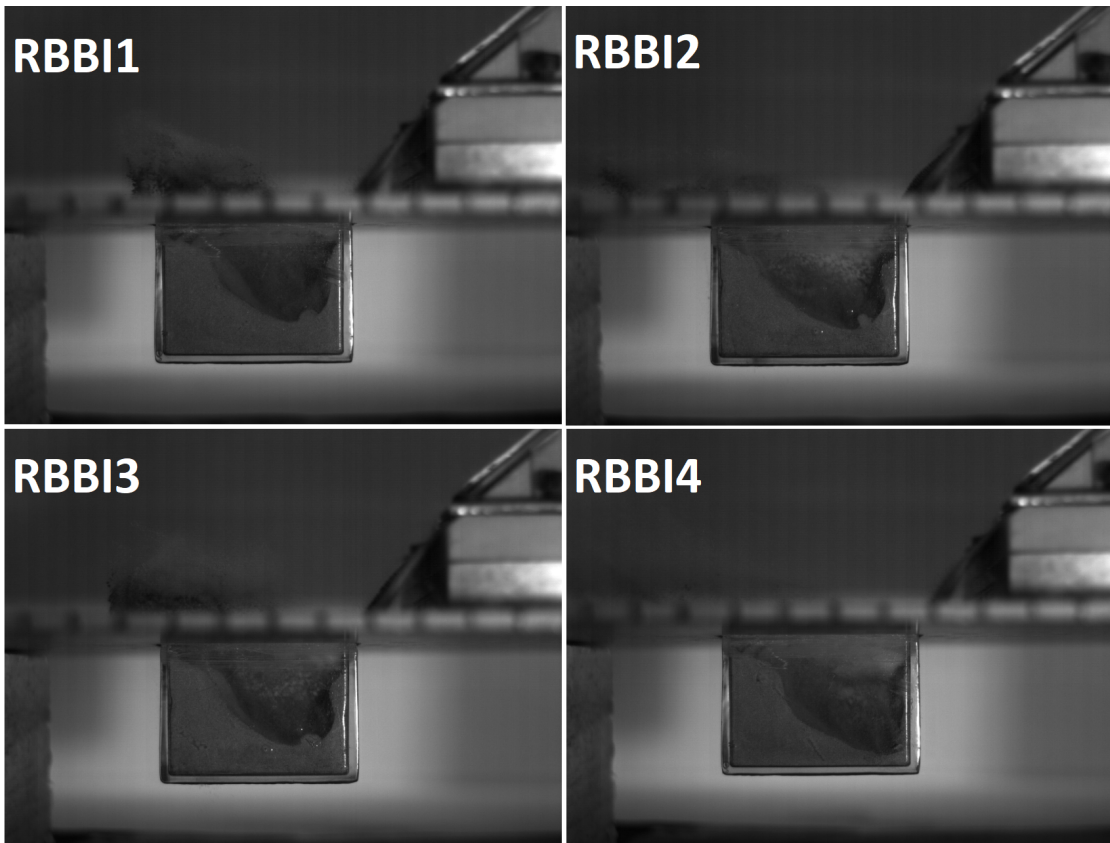


*Figure 5.11.* The four different repetitions of the RBBI experiment.

In all four RBBI experiments the powder flow evolves in a similar way, only difference being that the powder flow in the RBB14 repetition does not appear to be as rotational, as in the other three experiments (Figure 5.11). Until the filling shoe reaches the end of its forward movement, only a small amount of powder can be seen cascading in the die. However, when the shoe begins its backwards movement the flow rate increases noticeably, and the bulk flow dominates. At the point when the shoe is on the middle of its backward movement, the flow rate reaches its peak. Similarly to the RBBS experiments, here there is powder rearrangement following the departure of the shoe from above the die. Furthermore, the powder mass in the RBB14 repetition is noticeably smaller than the other three, though the other three experiments have very similar results, and more specifically the RBB12 and RBB13 ones look identical.

### Comparison of the RBBS and RBBI experiments

The RBBI and RBBS die filings are evidently different, as the RBBS experiments take place in shorter time frame and result in less filled dies. Shoe vibrations are absent in both experimental sets, as the (relatively) low dwell times do not allow for them, and in the RBBS experiments it is difficult to distinguish details about the powder flow.

#### 5.1.9 RBF experiments

In the RBF experiments the filling shoe does not travel the whole 130 *mm* it is expected to, presumably, because of the combination of low filling shoe speed (consequence of the filled shoe) and low total time of the filling (see Figure 4.20). Nonetheless, the nose flow dominates the filling, and only a small amount of powder ends up in the die. Powder particles detach from the powder mass that is inside the shoe, and flow in the cavity, when the shoe finishes its (short) forward movement. When the filling is complete, powder rearrangement takes place less evidently here than in the RBBS and RBBI experiments. In the end of the process RBF2 and RBF3 repetitions are very similar, but the RBF1 seems to have less powder than these (Figure 5.12).



*Figure 5.12.* The filled dies of the three RBF experiments.

### Comparison of the RBBS and RBF experiments

In the RBBS experiments the bulk flow is more evident than in the RBF ones, which comes in terms with the theory studied, where it was mentioned that bulk flow usually dominates in fillings where high shoe speeds are implemented (Subsection 3.2.2). Moreover, the powder mass in the RBF experiments appears to be larger than in the RBBS ones. This can be a result of the lower shoe speed and/or the larger powder mass in the shoe aiding the powder's downfall. Finally, the powder mass outline of the RBF experiments resemble concave-like lines, while the RBBS ones appear to be more straight.

## 5.2 Density measurements in points of the powder mass

To start with, it should be reminded that, because the densomat did not allow for large dies to be measured, the dies used in these experiments, are smaller (half the

height) than the dies utilized in the flow observation experiments. Moreover, the density values output from the densomat, are slightly influenced by the die's bottom. Density measurements were conducted on empty dies too, to be able to gauge that influence, and thus account for it. In the results presented, the die bottom's effect on the density results has been subtracted.

As earlier mentioned, density measurements are conducted on points of the powder masses inside the dies after filling. 8 points are investigated in the rectangular dies, and 9 in the circular one, to give an overview of the density distribution. There is no doubt that measuring the density in more points would more accurately communicate information regarding the powder's behaviour; however, these strategically placed points are expected to suffice in providing qualitative information about it, for example by identifying trends. Measurements of density in more points were not conducted, as they would constitute the density measuring process exceptionally time consuming.

The density results of the measurements on the above-mentioned points are input into a MATLAB script, and graphs to visualize the results are generated. In addition to the density results, minimum and maximum values are input, to be used as the limits of the colour levels portrayed. These graphs do not accurately represent the results, as the measuring area of a point in the densomat is considerably smaller than the point measurements represented in the graphs. Nonetheless, they can very directly communicate information regarding the results. The density result of the RBBI1 experiment can be seen in Figure 5.13, alongside the filling shoe's direction, and the colour levels of the colour map utilized.

Initially, the minimum and maximum values input in the MATLAB script to define the colourmap's colour levels in the graphs are the minimum and maximum density values of the repetitions of the specific experiment at hands (local minimum and maximum). For instance, in Figure 5.13 (a) the graph of the RBBI1 experiment is portrayed, with

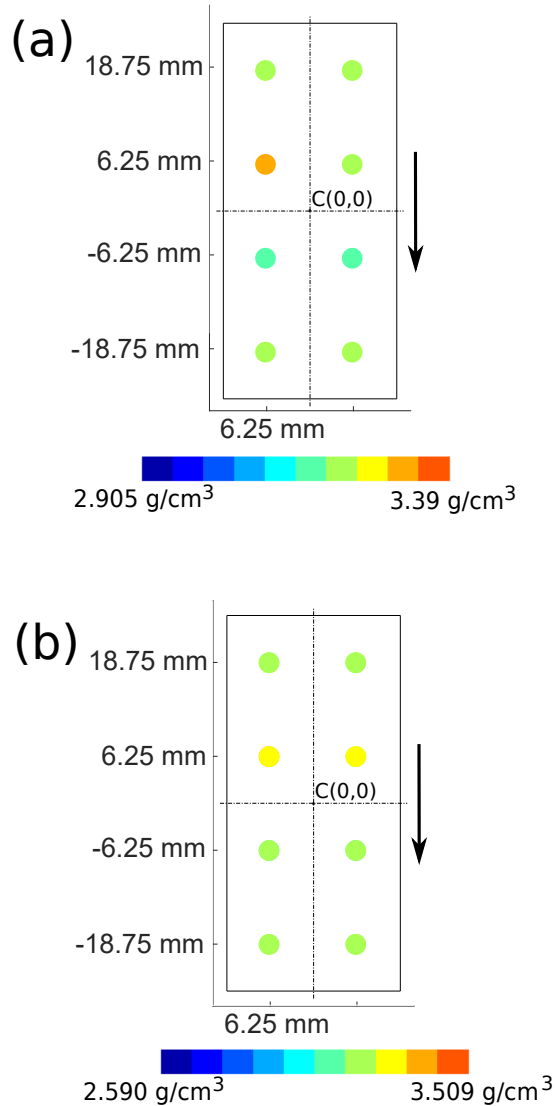


**Figure 5.13.** Results from the RBBI1 experiment, and the colourmap utilized. The arrow signifies the shoe's forward movement direction.

dark blue representing the minimum density value of the RBBI1, RBBI2 and RBBI3 experiments, and dark red the maximum density respectively. Later on, the minimum and maximum values of the density results of all the experiments conducted in this study (global minimum and maximum) are implemented in the MATLAB script, so that different experiments can be compared to each other. For instance, Figure 5.13 (b) portrays the density results of the RBBI1 experiment, but the colour levels are fitted to the global minimum and maximum measured densities; and for this reason the graphs appears to be different than the Figure 5.13 (a). With the implementation of the global minimum and maximum values in the colourmap, Figure 5.13 (b) can be compared to other examples (e.g. to RBBS2).

### 5.2.1 Comparison among repetitions

As mentioned in Subsection 4.6.2, Hjortsberg and Bergquist stated in [13] that powders deposit randomly, because of the inter-particle friction. Graphs with the use of local limits are created, to assist in the understanding of the powder's irregular deposition, by comparing density results between repetitions of the same experiment. Hjortsberg and Bergquist's statement is verified by the graphs studied, as it is seen that for the majority of the experiments, there are apparent variations between their repetitions (Figure 5.14). Moreover, no global trends or distinct inconsistencies could be identified.

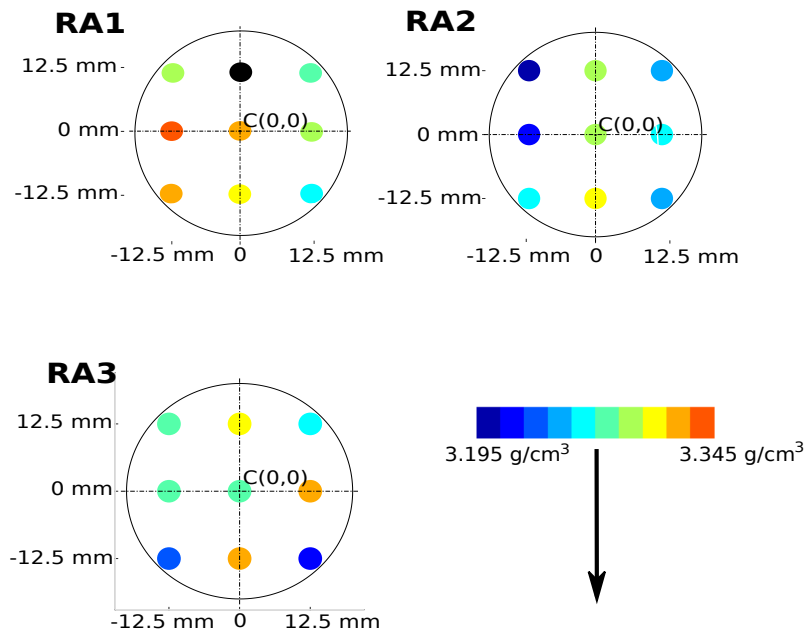


**Figure 5.14.** Results from the RA experiments. The arrow signifies the shoe's forward movement direction.

Nonetheless, in the RBBS and RBBI experiments some tendencies can be distinguished. More specifically, in the RBBS experiments it can be discerned that the part of the die the shoe crosses second is less dense than the one it crosses first (Figure 5.15). It has been discussed by Xie and Puri in [16] (see Subsection 3.2.5) that differences between the density of the left and right sides of the dies are not anticipated, however, the part of the die that the shoe crosses first is expected to be more dense than the second one. Therefore, the results from the RBBS experiments are unexpected. The RBBS experiments involve the lowest dwell time and higher shoe speed explored, and it was seen in the high speed

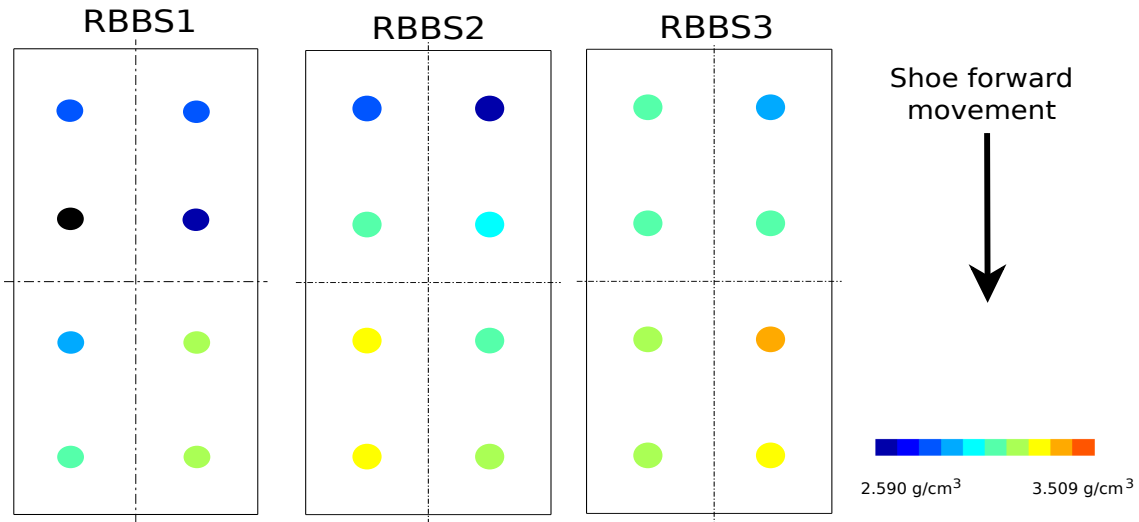


*Figure 5.15.* Density in points results of the RBBS experiments.

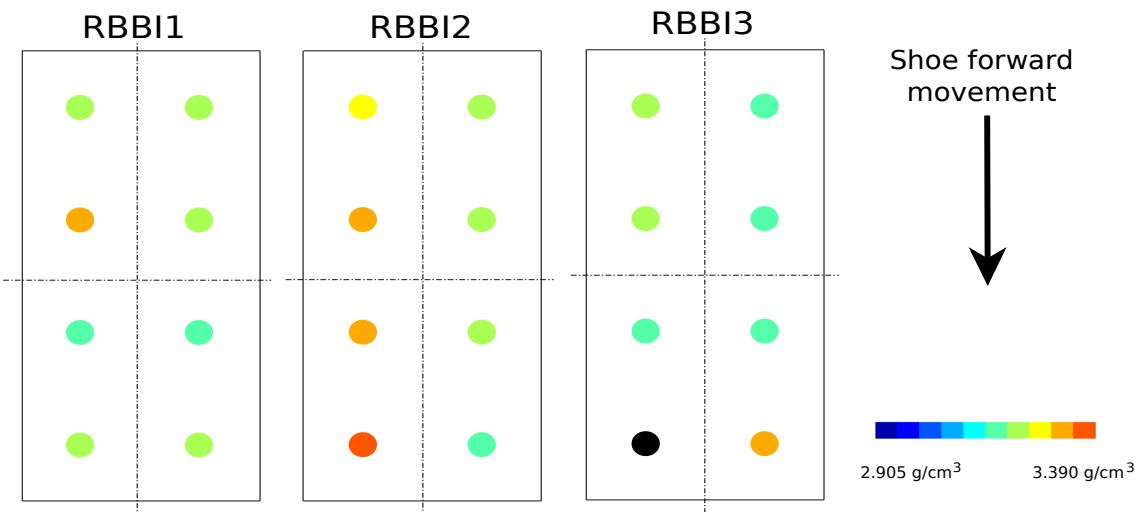


*Figure 5.16.* Density in points results of the RBBI experiments.

camera videos, that the powder flow and deposition take place and progress very intermittently. These instabilities are presumably the reason why unexpected results are yielded.

Further on, in the RBBI experiments a trend can also be identified. As seen in Figure 5.16, the density of the powder is higher in the left side than in the right one. This is also unexpected, because as mentioned above, there should not be density differences between the left and right sides of the powder mass, and a possible cause for this has not been found.

### 5.2.2 Comparison among experiments

In this section, the density results of the conducted die filling experiments will be presented and compared to each other, following the sequence introduced in Figure 4.20. However, the RA experiments will not be considered, as because to the fact that the die has a eminently different geometry, it can not be compared with other experiments. Further on, since the different repetitions of the experiments do not portray any similar trends, the utilization of average in point density graphs cannot be made, as all their irregularities will vanish. Therefore, the process of comparing different experiments has all repetitions of one experiment investigated in contradiction to the repetitions of another experiment.

After examining the 6 graphs of the in point density results of the RB and RC experiments, the effect that the inlets of the RC experiments have on the density can not be clearly distinguished (Figure 5.17). However, it can be seen that the measured points after the inlets (according to the shoe's forward movement) portray higher density in comparison to the ones before the inlets.

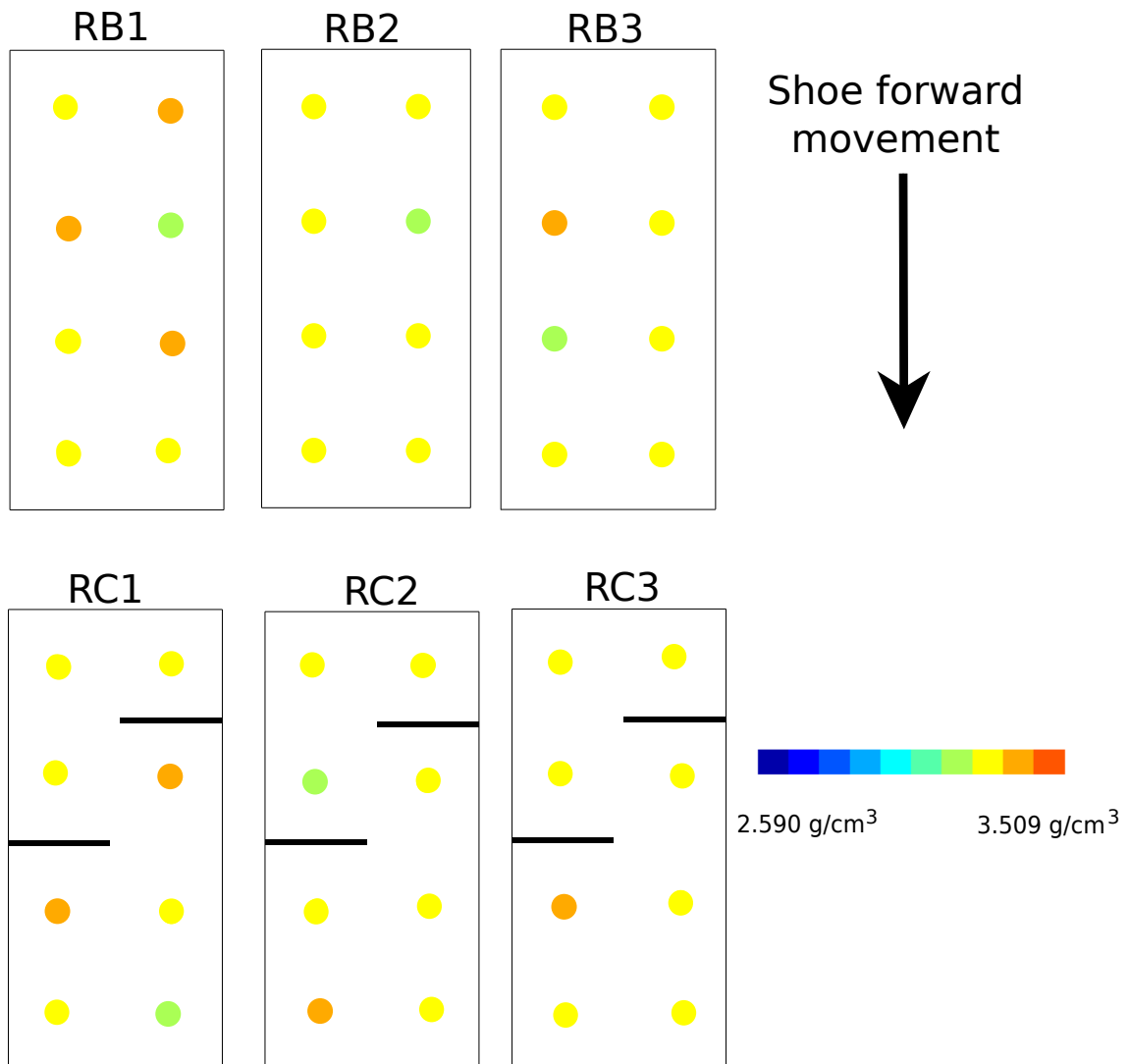


*Figure 5.17.* Density in points results of the RB and RC experiments.

When comparing the RB and RBS experiments, even though the RBS results were expected to show lower densities than the RB ones because of the decreased dwell time, this was not seen.

Similarly, between the RBS and RBB1 experiments there are no distinguishable differences, apart from the fact that the density in the RBS appears to be slightly lower than in the RBB1 one (Figure 5.18).

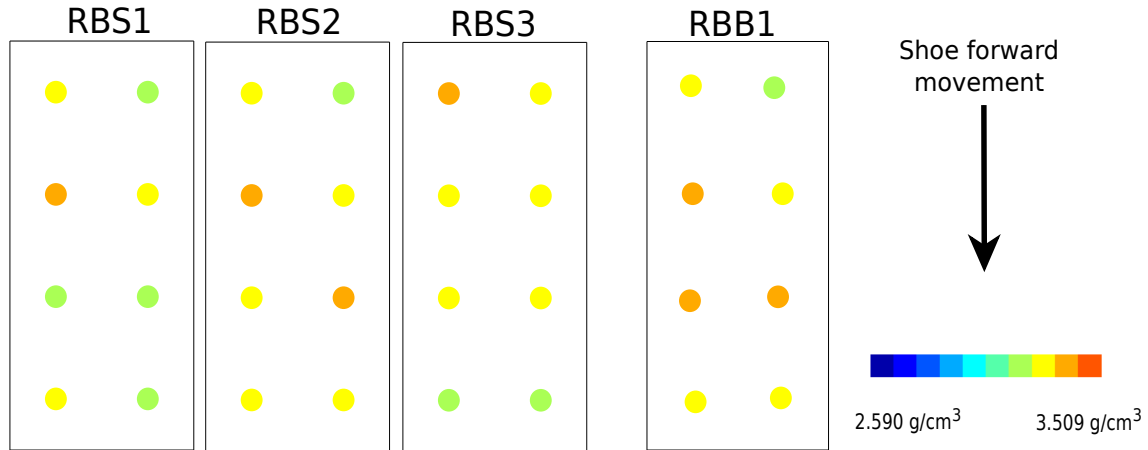


*Figure 5.18.* Density in points results of the RBS and RBB1 experiments.

On the other hand, the density difference between the RBB1 and the RBBS experiments is more evident, as the RBB1 experiment seems to be considerably more dense than the RBBS ones, specifically in the back side of the dies. This is expected, as it has been generally witnessed that the RBBS experiments seemed to push the limits of the filling process.

Moreover, in the investigation of the results of the RBBS and RBBI experiments, it is seen that in the RBBI experiments, the dies were more densely filled.

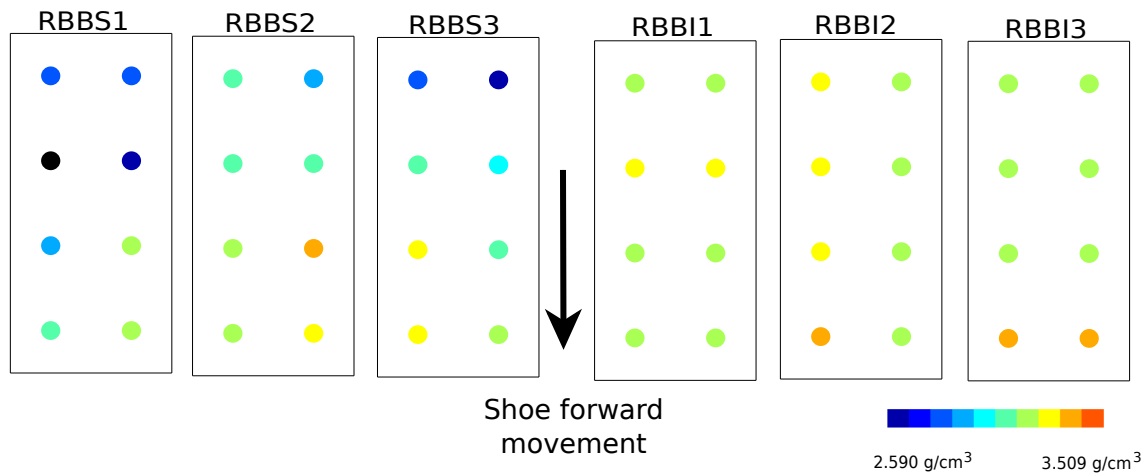


*Figure 5.19.* Density in points results of the RBBS and RBBI experiments. Shoe direction and colour level limits as in Figure 5.18.

Finally, in the comparison of the RBF and RBBS experiments, no distinct differences can be acknowledged, apart from the fact that the powder in the RBBS dies appears to be slightly less dense than in the RBF ones.

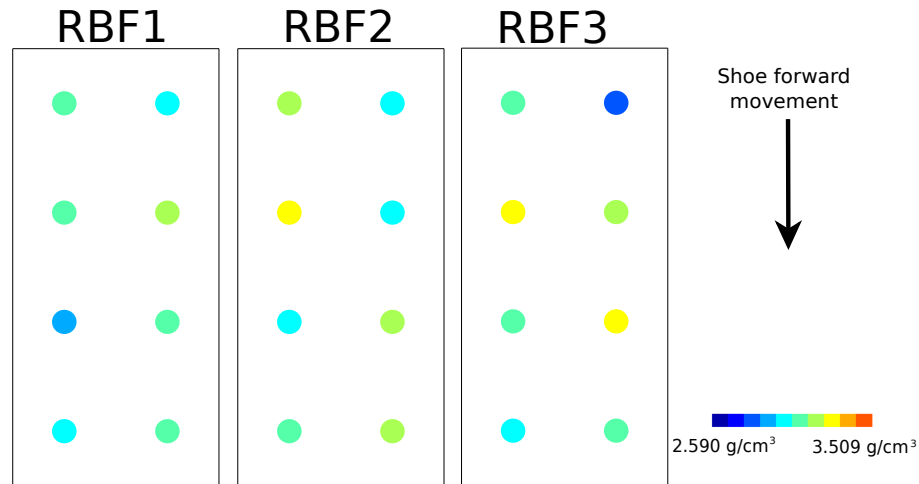


*Figure 5.20.* Density in points results of the RBF experiments, to be compared with the RBBS experiments results of Figure 5.19.

The comparisons of the in point densities between experiments have been inconclusive. It was expected that some trends would be understood, however no distinct features can be identified between the repetitions, and thus between the experiments too.

### 5.3 Average density

In this section the average density results will be introduced and investigated. The methodology followed can be found in Subsection 4.6.3.

#### 5.3.1 Comparison among repetitions

When comparing the repetitions of each experiment to each other, it is clearly seen, that for the majority of the experiments there are no big differences. In Table 5.1, the results can be found summarized. Furthermore, the difference between the maximum and minimum values in each experiment are calculated.

*Table 5.1.* Average density results of the die filling experiments. Density measured in:  $g/cm^3$ .

***	RA	RB	RBS	RBB1	RBBI
Rep. 1	3.415	3.635	3.384	3.483	3.152
Rep. 2	3.432	3.394	3.453	—	3.119
Rep. 3	3.475	3.407	3.459	—	2.987
M-m	0.060	0.042	0.075	—	0.174

The biggest variation between repetitions is found in the RBBI experiments, where the difference between the maximum and minimum values portrayed is  $0.174 g/cm^3$ , and no

rationale for this has been found. As seen in Subsection 3.6.5 no average density results are calculated for the RBBS and RBF experiments, as the shape of the powder mass inside the die after filling is too arbitrary for its volume to be calculated.

### 5.3.2 Comparison among experiments

In this Subsection, the results and comparisons between experiments will be performed. The average densities of each experiment's repetitions are averaged, and these results can be seen summarised in Table 5.2.

#### Comparison of the RA, RB and RC experiments

As mentioned in Subsection 3.2.4, a rule of thumb is that the more challenging the die geometry is, the harder it is to be filled; which has been verified by the experimental data in hands. The average density of the fillings of the round die ( $3.441 \text{ g/cm}^3$ ) is larger in comparison to the density of the rectangular die ( $3.388 \text{ g/cm}^3$ ) (Table 5.2). This is possibly, because the rectangular die's corners hinder the powder flow, as it is more challenging for it to be deposited there. Furthermore, the rectangular die yields larger average density than the rectangular one with inlets ( $3.369 \text{ g/cm}^3$ ). This difference was both expected (see Subsection 3.2.4) and witnessed in the experiments, where it was seen that the inlets interfere with the powder flow.

**Table 5.2.** Settings and average density results of the experiments conducted.

Experiment	Die geometry	Shoe velocity	Powder height	Dwell time	Average density
<b>RA</b>	circular	$10.8 \text{ cm/s}$	$\simeq 1 \text{ cm}$	$385 \text{ ms}$	$3.441 \text{ g/cm}^3$
<b>RB</b>	rectangular	$10.8 \text{ cm/s}$	$\simeq 1 \text{ cm}$	$389 \text{ ms}$	$3.388 \text{ g/cm}^3$
<b>RC</b>	rectangular with inlets	$10.7 \text{ cm/s}$	$\simeq 1 \text{ cm}$	$390 \text{ ms}$	$3.369 \text{ g/cm}^3$
<b>RBS</b>	rectangular	$10.6 \text{ cm/s}$	$\simeq 1 \text{ cm}$	$285 \text{ ms}$	$3.432 \text{ g/cm}^3$
<b>RBB1</b>	rectangular	$11.9 \text{ cm/s}$	$\simeq 1 \text{ cm}$	$277 \text{ ms}$	$3.483 \text{ g/cm}^3$
<b>RBBS</b>	rectangular	$13.3 \text{ cm/s}$	$\simeq 1 \text{ cm}$	$5 \text{ ms}$	—
<b>RBBI</b>	rectangular	$8.3 \text{ cm/s}$	$\simeq 1 \text{ cm}$	$2 \text{ ms}$	$3.083 \text{ g/cm}^3$
<b>RBF</b>	rectangular	$9.8 \text{ cm/s}$	full	$4 \text{ ms}$	—

#### Comparison of the RB and RBS experiments

By comparing the RBS and the RB experiments' average density results, it is understood that this small difference in the dwell time ( $104 \text{ ms}$ , see Figure 4.20) apparently assisted the die filling process, as the RBS experiments portrayed a little bit larger average density ( $3.432 \text{ g/cm}^3$ ) than the RB ones. This is against expectations, as larger dwell times are expected to assist the powder flow. It is assumed that the  $104 \text{ ms}$  is maybe such a small difference, that the results are not affected by it, and the difference in the results is reasoned by the powder's irregular behaviour or by random errors that went unnoticed.

**Comparison of the RBS and RBB1 experiments**

In like manner, the results from the RBB1 experiment showed slightly higher average density ( $3.483 \text{ g/cm}^3$ ) than the RBS experiment, which was unexpected too, and also seen in the density in point results. Here again, the assumption for why this happens, is that the parameters' differences between the two experiments are so poor, that they are negligible, and the different densities are incidental. Moreover, perhaps the slightly higher shoe speed in the RBB1 experiments, results in more intense vibrations of the shoe, and thus increased powder flow rate. Still, the results are only slightly different, and because of that only one repetition of the RBB1 experiment was conducted, as it was decided to prioritize experiments with larger variations in their parameters settings.

**Comparison of the RBB1 and RBBI experiments**

Both the dwell time and the filling shoe speed are significantly varied between those two experiments, so conclusions about effects of them can not be made independently.

The average density of the RBBI experiments ( $3.083 \text{ g/cm}^3$ ) is lower than the one of the RBB1 experiment. The total time of the filling is almost halved from the first to latter, which is most possibly the reason for the density difference between them. The shorter time frame during which the powder can cascade in the cavity is evident in the average density results; however, it can not be distinguished if the lower dwell time or the higher shoe speed contribute the most to the densities' difference.



# Numerical Simulations

---

# 6

In this chapter the reason why simulations are employed will be talked upon, and details about their setting up will be given.

## 6.1 Purpose

The purpose of simulating the die filling process is to understand it better. The user can control both relevant time and dimensions, so that the observations and analyses of relevant parameters and variables are assisted. Furthermore, experimenting with different parameters and variables (such as die geometries and shoe velocities) is of interest, as results that would require days with the traditional "trial and error" method can be yielded in a matter of hours. Naturally there are also drawbacks halting an even wider spread of the filling process simulations. In [33] there can be found three main deficiencies of the die compaction process simulations, which can be drawbacks of the filling process simulations inductively too. In some cases the models' abilities do not meet the manufacturers' needs, and also very often a specialist is required to operate and modify the models. Finally, simulations of this nature are very costly. Cante et. al. in [34] also talk about the limitations of the implementation of powder filling simulations in an industrial context. They argue that it is practically impossible to include the actual number of particles involved in the process in a numerical model. Thus, a study should be conducted, to specify the model's intended use, upon which the minimum number of discrete elements for which the model converges towards the same result, should be determined. Moreover, for the models to be solved in realistic computational time, accuracy regarding parameters such as resolution of the contacts between particles, is bound to be limited.

## 6.2 Introductory information

The numerical models developed in this project are composed and post-processed in LS-PrePost. The finite element simulation program used for running the simulations is LS-DYNA. The simulations are calculated on an external cluster of computers (due to the long computational times incorporated), which is accessed through a basic LINUX

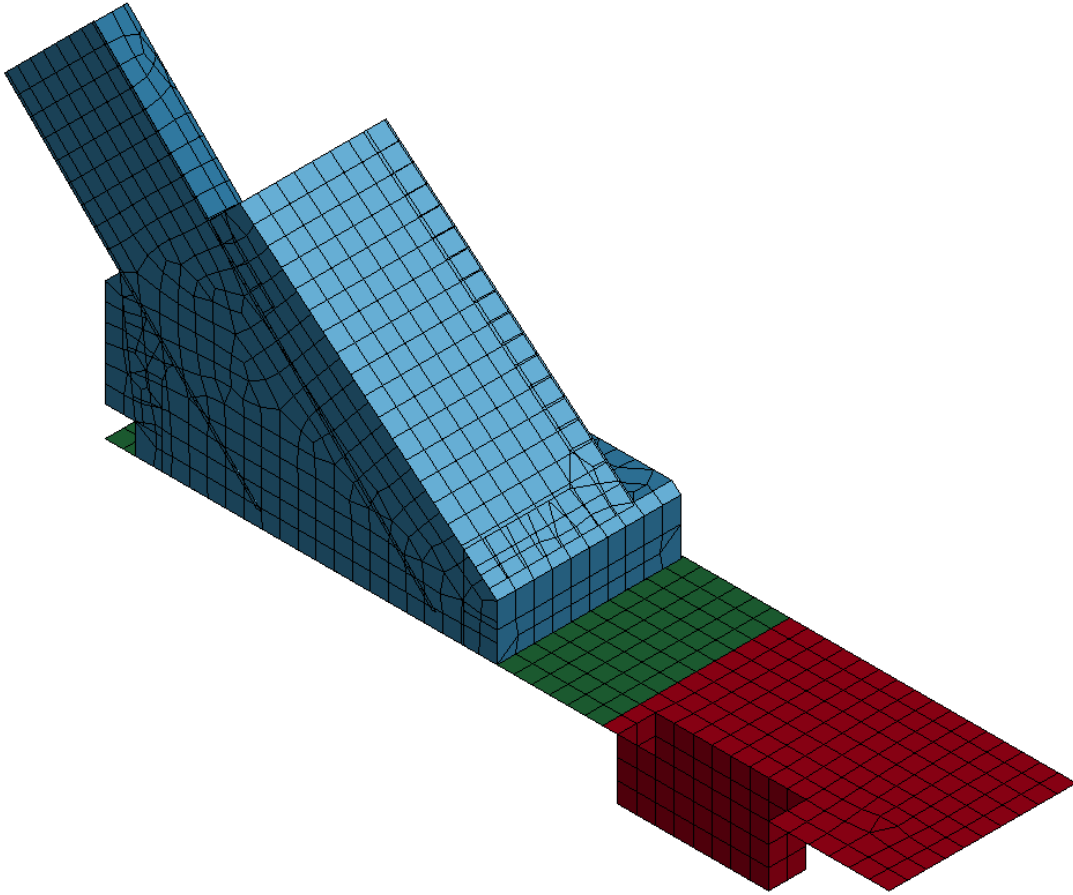


*Figure 6.1.* The geometry of the symmetric numerical model.

terminal. Livermore Software Technology Company (LSTC) is the company that provides LS-PrePost as a GUI used for pre- and post- processing, as well as LS-DYNA.

All the geometries utilized (see Figure 6.1) are imported to or constructed in LS-PrePost and saved as individual files. Afterwards, they are included in a master keyword file, and the required keyword cards are set. The master keyword file can be edited in LS-PrePost or by a simple text editor. Keyword manager is a window of LS-PrePost, which includes various branches responsible for communicating information to the solver. Each one of its branches includes various keyword cards, each one of them being responsible for one specific thing and being set up with the required input information by the user.

Even though measuring units are not specified in LS-PrePost in the process of building the models, a consistent system of units has to be followed. The unit scheme used here measures length in millimetres, time in seconds, mass in tonnes and force in Newtons (scheme (b), as seen in page 10.2 of [35]).

The keyword file of the numerical model developed can be found in Appendix F.

### 6.3 3D simulations

Depending on the scope of each study, different demands are set about the simulation results the researchers would like to analyse. For example Guo, Wu and Thornton in [36] were interested in studying segregation phenomena during die filling. They asserted that segregation is a 2D phenomenon, and thus they develop 2D numerical models. Without having to deal with the more complex and computationally time consuming 3D models, those models sufficed, and the researchers reached their target. Respectively, Bierwisch et. al. in [12] developed 3D models, because they wanted to study the powder settlement in dies, while accounting for particle rearrangements, which can not be achieved fully with 2D simulations.

In this study the target is to deepen on the powder deposition characteristics, mechanisms and behaviour. All those are three-dimensional variables, thus developing 3D numerical models is of interest.

#### 6.3.1 Inclusion of air in die filling simulations

Researchers have studied the powder filling process with the inclusion of air ([21], [37], [31], [36], [32], [22]), because they argue that the presence of air is influential in the filling process, as it can get trapped in the die when the filling shoe is above it and perturb the particles' movement.

Bierwisch et. al. in [12] argue that the presence of air affects more substantially fillings of deep and narrow cavities with small and light grains. Moreover, in [22], Wu and Cocks elaborate on the significance of the inclusion of the air in the numerical models, and they indicate four important effects it has on the filling process.

Summarily, those are, that trapped air inside the die creates a pressure built up which opposes powder flow, and a pressure gradient is created during powder deposition which also hinders powder flow. Furthermore, air provides a lubricant effect to the particles, which assists their movement relevant to each

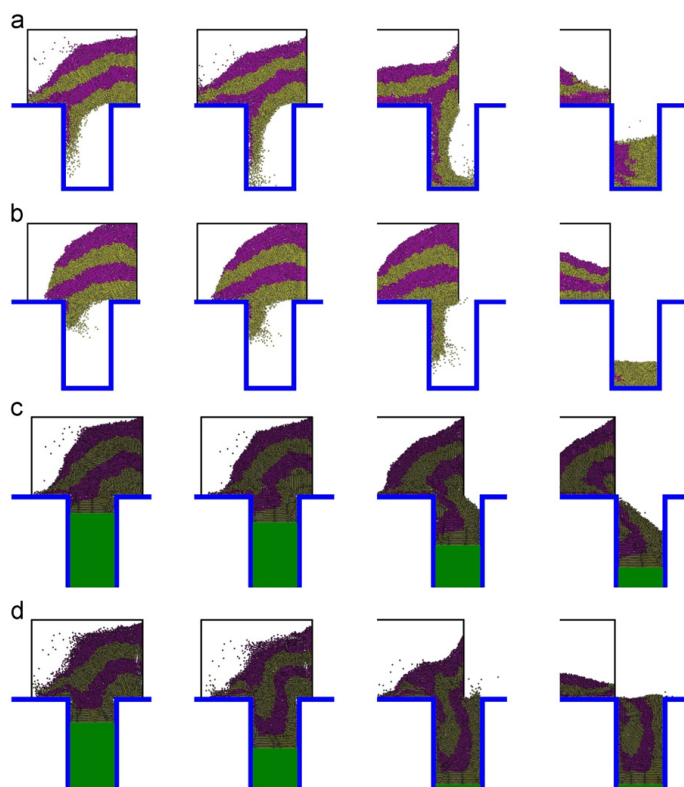


**Figure 6.2.** Powder flow observation during (a) gravity filling in a vacuum, (b) gravity filling in air, (c) suction filling with a punch velocity of 100  $mm/s$  and (d) suction filling with a punch velocity of 276  $mm/s$ . Source: [31].

other, and finally the drag force created by air leaving the die, also disrupt the powder flow, and can even lead to light particles being pushed upwards, rather than flow downwards.

On the other hand, Guo, Wu and Thornton in [36], showed that for heavy particles (density  $7800 \text{ kg/m}^3$ ), the powder flows in the die as the filling is conducted in vacuum. They argue that it is because when the powder mass is so 'heavy', the air influences only to a minor degree the process.

## 6.4 Simulation methods

In the section the most popular methods employed to simulate filling processes are mentioned, and more detailed information is given in regards to the simulation method used in this report.

As seen in the literature, computer simulations of the filling process most commonly employ the Discrete Element Method (DEM). The DEM is chosen over alternatives such as Smooth Particle Hydrodynamics (SPH) and Computational Fluid Dynamics (CFD) methods, because it proves to be easier and more direct to simulate the nature of many, small, independent particles (the metal powder) as discrete elements, rather than as continuum media (discretized fluid volume).

Numerical models developed can be found, that describe experiments accurately and have been validated in a plethora of points. Including the presence of air in a numerical model, grants the ability to visualize and analyse the filling process with greater precision and accuracy, as it reflects the reality more precisely. The most commonly seen solution to this is the utilization of the coupled DEM/CFD method.

### 6.4.1 The Discrete Element Method

A short introduction to the DEM, as well as relevant notions and essential keyword cards utilized, are outlined here.

The DEM is the numerical technique utilized to describe the powder particles in this project, as it is broadly accepted as the best method for this type of problems. It is widely used for simulations of liquids and solutions, granular matter and powder, because each solid particle is represented as a discrete element. That constitutes DEM as a costly method, as large numbers of calculations are required.

Initially, a confined space is created, which will serve as the case where the Discrete Element Spheres (DES) will be generated in. In the "Disc Sphere Generation" tab of the "Mesh" menu, the percentage of the closed volume that should be filled with the DES, as well as the minimum and maximum radius of the spheres are required as input. When the model runs, LS-DYNA will create the required spheres. The steps of powder creation is seen in figure 6.3.

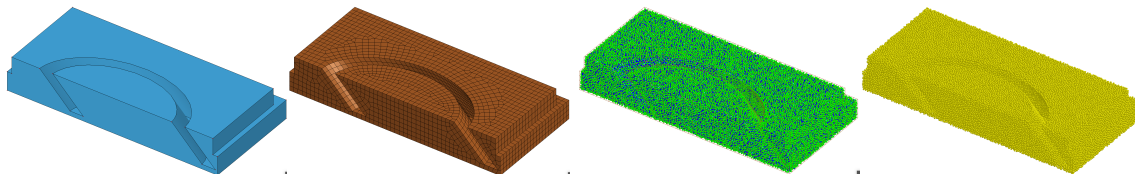


**Figure 6.3.** Discrete elements sphere generation. *Step 1:* Import geometry to Ls-Prepost, *Step 2:* Mesh the geometry, *Step 3:* Generate discrete sphere elements in the meshed volume, *Step 4:* Delete the meshed volume and define the generated discrete elements.

Some of the necessary keyword cards are the `*DEFINE_DE_TO_SURFACE_COUPLING`, which is used to establish non-tied coupling interfaces between the spheres and the other parts. The `*DEFINE_DE_ACTIVE_REGION` and `*DEFINE_BOX` cards are incorporated, to define a volume in space, which serves as the region of interest for the DES. This means that any sphere leaving this domain will stop being considered in feature DES searching, and will also be disabled in the contact algorithm.

### 6.4.2 Friction

In many studies the friction coefficients, and how they affect the filling process, have been a topic of interest. Even though many studies are on the same topic, they have different variables, parameters or scope, so the friction input values they use differ significantly from one to another.

In [9] Tsunazawa et. al. discuss that since the die filling models include a very large number of spheres, the number of their interactions is so large, that the particle-particle friction coefficient is more influencing than the particle-wall one. Bierwisch et. al. in [23] explored models with different variables, i.e. rolling friction coefficients ( $\mu_r$ ), Coulomb friction coefficients ( $\mu$ ), and cohesive energy densities ( $w$ ). They let powder fall out of a slit and form a heap on the ground, which then they compared to experimental results. In Figure 6.4 the difference of lowering the fitted  $\mu$  from 1 to 0.3, and the fitted

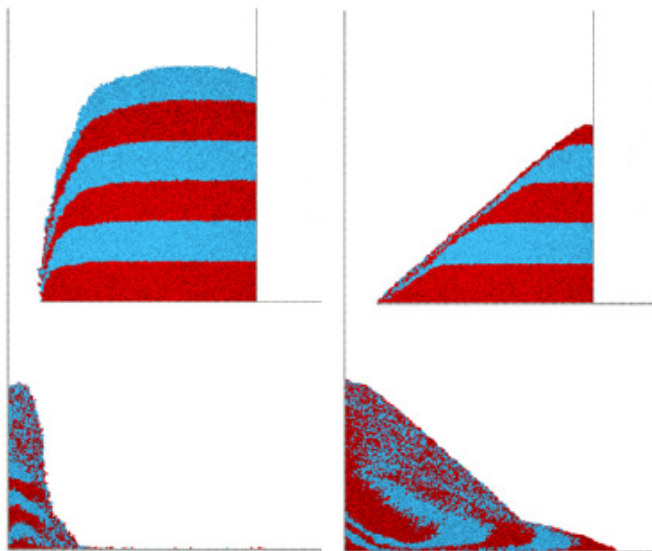


**Figure 6.4.** Powder flowing from a slit and forms a heap, with different friction coefficients. Left:  $\mu=1$ ,  $w=0.01$ ; Right:  $\mu=0.3$ ,  $w=0$ . Adapted from [23].

$w$  from 0.01 to 0 can be seen. The powder is significantly less cohesive in the second case, thus it can more easily detach from the bulk and flow through the slit. When it falls on

the ground it forms a heap, rather than a pillar-looking mass of powder, as in the first case. Furthermore, in [12] they argue that the angle of repose is a gauge of the static properties of powders.

In [12], Bierwisch et. al. understood that a realistic value for the Young's modulus  $E$ , obligates an exceptionally small time-step, which in turn enlarges the calculation time. Therefore, to avoid that, they experimented with lower  $E$  values, down to four orders of magnitude smaller than in reality. By analysing the results, they saw that as long as  $E$  is at least  $10^7 Pa$ , the results are not essentially affected. Moreover, they studied the effect of the particle size and geometry. By incorporating different size particles in their simulations, they found out that particles up to 10 times larger than the original ones can adequately portray density features, as well as flow and filling characteristics, in the cavity dimensions tested. As long as the enlarged particles' diameters are not comparable to the cavity dimensions, the models were considered functional and realistic, and only some exaggeration in the surface densification depth was observed. Furthermore, they concluded that a model where each powder particle is represented by a cluster of discrete spheres, performs slightly better than the single sphere model, as it represents the singularities of the particle geometries better. Moreover, they prove that the multi-sphere model increases the computation time by a factor of ten; nonetheless, they suggest that it should be chosen in DEM studies which focus on macroscopic flow observation.

In [22], Wu and Cocks also studied the effect of the particle geometries in die filling simulations, by employing disks and polyhedral particles in their models. They explain that the geometry of the particles is one of the parameters defining how the air will escape between them, and thus influences the filling process, the flow rate and the final density in the die. This is why they modelled different particle contacts for the distinct particles geometries. Furthermore, they analysed the effects of the incorporated frictions on the results of the simulations by systematically varying their values. They found out that the particle-particle friction coefficient highly affects the flow process and the density distribution, i.e. high coefficients can assist particles to create bridges, which in turn can reduce the average density. On the other hand, it was argued that the die wall friction has a minimal influence on the flow.

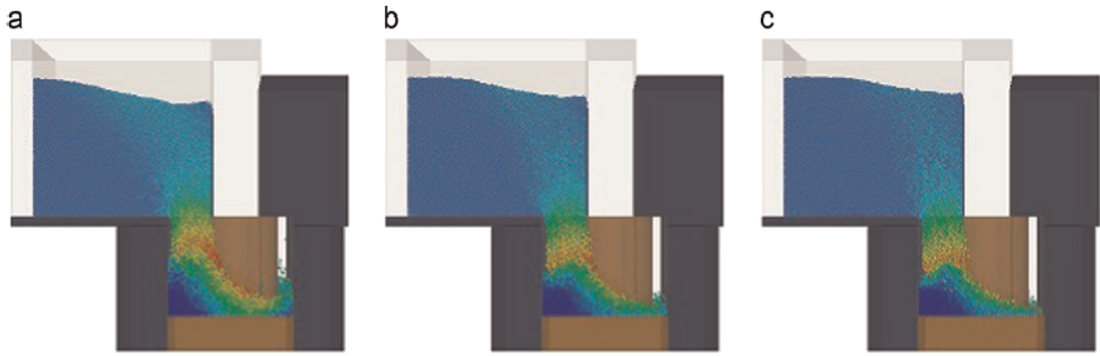


**Figure 6.5.** The die filling process develops differently, for different friction values. (a)  $\mu_{particle} = 0.3$ ,  $\mu_{wall} = 0.3$  (b)  $\mu_{particle} = 0.3$ ,  $\mu_{wall} = 0.1$  (c)  $\mu_{particle} = 0.3$ ,  $\mu_{wall} = 0.5$ . Source: [9].

## 6.5 Description of the model

The numerical model excluding ICFD, consist of 4 part. Two planes, a filling shoe, and the powder, which can be seen in figure 6.6.

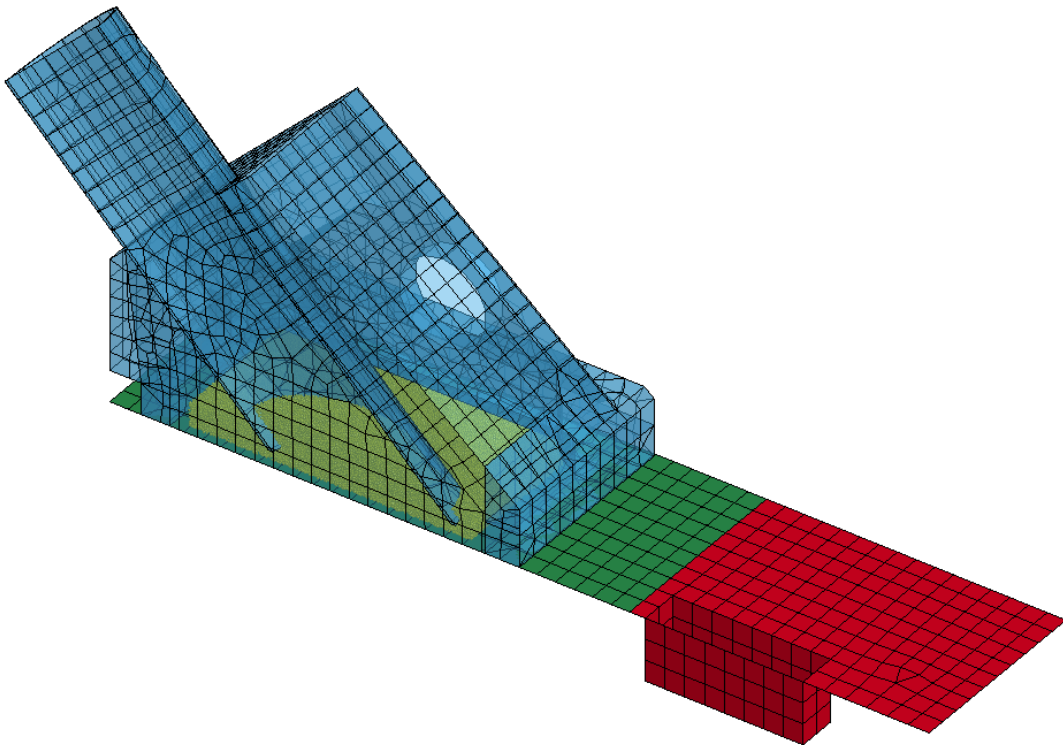


**Figure 6.6.** Numerical simulation. Red: Die plane, Green: Sliding plane, Yellow: Powder, and Blue: Filling shoe.

### Mutual considerations for die plane, sliding plane and filling shoe

The geometries of the planes and shoe is created in Solid Works and imported as a .step file to Ls-Prepost. For a seamless change of the die geometry, the geometry in Solid Works

are placed and oriented as the numerical set-up in Ls-Dyna, with the mutual centre of the dies defined. After importing the geometry in Ls-Prepost, the auto-mesher function is used, with mixed auto-computed mesh size. The mesh is included in the keyword file with \*NODE and \*ELEMENT\_SHELL. In general, a fine mesh can improve the quality of a model, but it comes with an increase in computational cost. For this reason, the minimum required element size for the model to converge should be chosen. The required mesh size is dependent on the purpose of the specific part. In this project, the interest is in the flow and deposition of the powder, and merely a realistic behaviour between the guiding parts and the powder particles are considered sufficient. Through the model iterations, no observations suggest that the coarse mesh size is insufficient for the purpose of this part, and therefore no further investigation is done. This decision is supported by the previous mentioned observation by Wu and Cocks [22], being that the particle-wall interaction effect is negligible compared to the particle-particle interaction effect, when the particles are small relative to the die opening. Equivalent considerations and observations are done in relations to the element formulation and material card, which is set to default (Belytschko-Tsay) and rigid (with steel properties) respectively.

The mutual section keyword card can be seen in keyword card 6.1.

```

1 *SECTION_SHELL_TITLE
2 Shell
3 $#   secid      elform      shrf      nip      propt    qr/irid    icomp    setyp
4       1          2          1.0       5         1.0       0          0         1
5 $#   t1         t2         t3         t4        nloc     marea     idof     edgset
6       1.0       1.0       1.0       1.0       0.0       0.0       0.0       0

```

**Keyword Card 6.1.** Section keyword card used for die plane, sliding plane and filling shoe

Two material cards are defined, as these are used for setting up specific part constraints as well. Both planes are fully constrained during simulation, so this card defines constraints in all translations and rotations, specified by 7 in the keyword card 6.2.

```

1 *MAT_RIGID_TITLE
2 rigid_fully_constrained
3 $#   mid      ro      e      pr      n      couple      m      alias
4       1  7.850E-9  210000.0  0.3     0.0     0.0         0.0
5 $#   cmo      con1     con2
6       1.0       7         7
7 $#lco or a1     a2     a3     v1     v2     v3
8       0.0     0.0     0.0     0.0     0.0     0.0

```

**Keyword Card 6.2.** Material card used for die plane and sliding plane, steel properties and fully constrained.

The filling shoe is allowed to travel in the x-direction when it is moving over the planes and filling the die. Therefore it is constraint in all rotation and all translation except x, defined by the card 6.3

---

```

1 *MAT_RIGID_TITLE
2 rigid_y,z&rot_constrained
3 $#      mid      ro      e      pr      n      couple      m      alias
4          1  7.850E-9  210000.0  0.3      0.0      0.0      0.0
5 $#      cmo      con1     con2
6          1.0      5        7
7 $#lco or a1     a2      a3      v1      v2      v3
8          0.0      0.0      0.0      0.0      0.0      0.0

```

**Keyword Card 6.3.** Material card used for the filling shoe, steel properties and constrained in y z traslation and all rotation.

Each part and its part specific keywords will be presented in the following subsections.

### 6.5.1 Die plane

The purpose of this part is to include the die geometry and elude powder from falling.

The geometry of the die in the die plane is one of the parameters of interest, so the shape and depth of the die is changed specific to the die of interest. However the input for the keyword is held constant. The die plane with a 12.5x50x20mm rectangular die can be seen in figure 6.7.

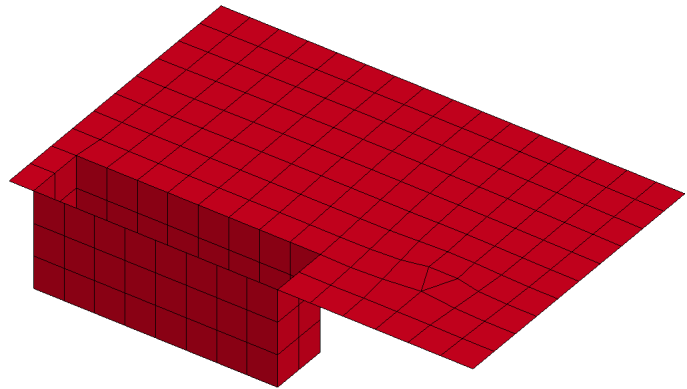


**Figure 6.7.** Die plane, here with a rectangular die.

The die plane part is defined by the part keyword card in 6.4 specifying part id, and which section and material card that are related to the part.

```

1 *PART
2 $#                                     title
3 die_plane
4 $#      pid      secid      mid      eosid      hgid      grav      adpopt      tmid
5          1        1        1        0        0        0        0        0

```

**Keyword Card 6.4.** Part keyword card for die plane.

### 6.5.2 Sliding plane

The purpose of this part is to elude powder from falling prior to and during die filling. The geometry is constant between experiments. The sliding plane can be seen in figure 6.8.

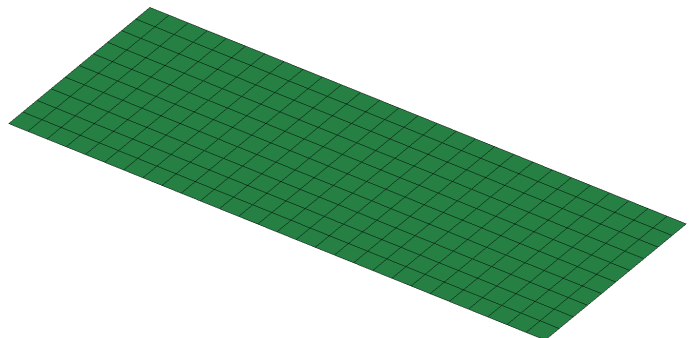


**Figure 6.8.** Sliding plane.

Initially, the sliding plane and the die plane was a single plane, see figure 6.9, but for reducing the computational cost, it was split in order to dissolve the powders contact to the sliding plane when the filling shoe has returned from filling the die, thereby letting the powder fall outside the active region.

*Other things investigated include redefining of the DES active region during simulation, but this proved unsuccessful.*

The sliding plane is defined by the part keyword card in 6.5 specifying part id, and which section and material card that are related to the part.

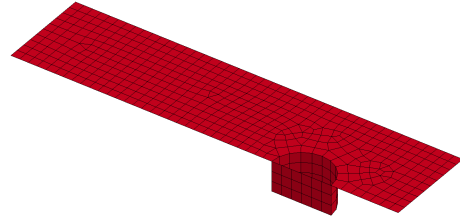


**Figure 6.9.** Initial plane which was split into die plane and sliding plane, here with a circular die.

1	*PART								
2	\$#								title
3	sliding_plane								
4	\$#	pid	secid	mid	eosid	hgid	grav	adpopt	tmid
5		3	1	1	0	0	0	0	0

**Keyword Card 6.5.** Part keyword card for sliding plane.

### 6.5.3 Filling shoe

The purpose of the filling shoe is to confine the powder and transport it across the planes to the die cavity, with acceleration and velocities obtained from experiments.

The geometry is constant between experiments. The sliding plane can be seen in figure 6.10. Initially, the tube in the filling shoe was in a distance of  $5mm$  from the sliding plane, however in the final model, the tube is raised to  $10mm$  above the plane. This was done due to additional packing of particles at the tube end, hindering of flow, due to the increased size of the particles. This is presented in the iteration overview in Appendix B. This increase of clearance between tube and plane does

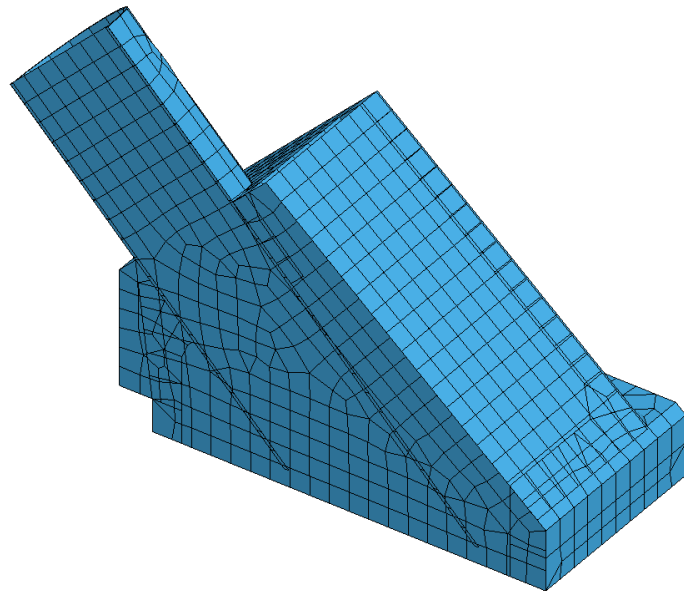


**Figure 6.10.** Filling Shoe.

not correspond to the experimental data, but is still within the actual production setup limit, ranging from  $5$  to  $10mm$ . The filling shoe is defined by the part keyword card in 6.6 specifying part id, and which section and material card that are related to the part.

```

1 *PART
2 $#                               title
3 filling_shoe
4 $#   pid   secid   mid   eosid   hgid   grav   adpopt   tmid
5     2     1     1     0     0     0     0     0

```

**Keyword Card 6.6.** Part keyword card for filling shoe.

For specifying the movement of the filling shoe, a motion is prescribed by a load curve which is a separately defined curve holding the values of the displacement. The values are imported from the experimental results to the curve card by the "Load XYData" function in Ls-Prepost. The prescribed motion is specified as displacement and can be seen in keyword card 6.7, while an reduced example of a curve holding displacement data for 6 bars and minimum cycle time is seen in keyword card 6.8.

```

1 *BOUNDARY_PRESCRIBED_MOTION_RIGID_ID
2 $#   id                               heading
3 shoe_movement
4 $#   pid   dof   vad   lcid   sf   vid   death   birth
5     2     1     2     1     0   0     8.0     0.0

```

**Keyword Card 6.7.** Prescribed motion keyword card for filling shoe displacement in x.

```

1 *DEFINE_CURVE_TITLE
2 shoe_displacement
3 $#   lcid   sidr   sfa   sfo   offa   offo   dattyp   lcint
4     1     0     1.0  10.0  0.0   0.0   0     0
5 $#
6     a1     o1
7     0.001  0.0
8     0.043  2.363636
9     0.08   7.090909
10    0.131  13.0
11    0.136  13.0
12    0.205  5.909091
13    0.23   1.181818

```

**Keyword Card 6.8.** Example of define curve keyword card for holding time and displacement values from experiments. *The scale factor (SFO) is used for converting from cm to mm.*

#### 6.5.4 Powder

The powder is the part in focus. The part can be seen in figure 6.8, note that the powder is already settled when it is included in the die filling model. This is done through an initial model, settling model, presented in section 6.5.7.

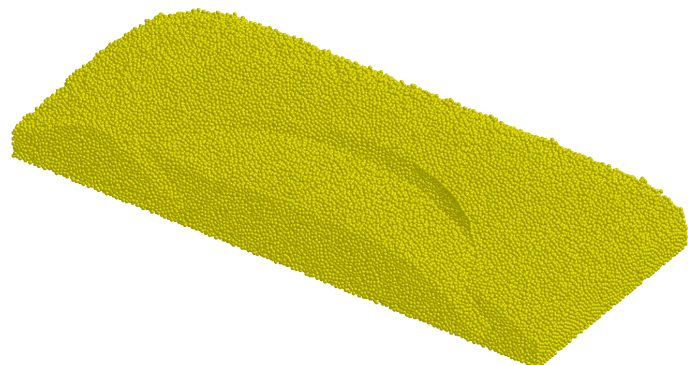


**Figure 6.11.** Powder.

The powder particles are modelled with an radius of  $0.32\text{ mm}$  contra  $0.075\text{ mm}$  in reality. This is a big enlargement of the particles. Reduced particle size have been attempted, but without success as seen in Appendix B.

From the presented literature, it is observed that the interaction between the particles are the most influencing parameter of the process. As seen in the iteration overview, Appendix B, models with different particle-particle properties have been conducted for the DES contact.

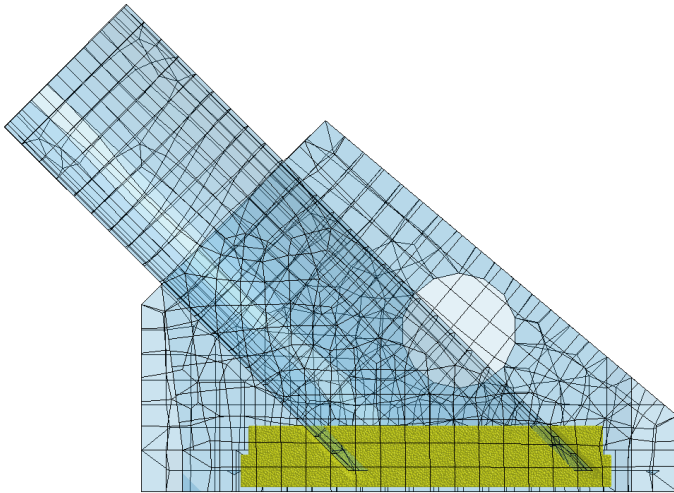


**Figure 6.12.** Final powder height, 15 mm from plane, before settling.

The number of discrete elements are directly influencing the computational cost for the simulation as previously described, so the objective is to reduce the amount within an realistic range. The final powder height in figure 6.12 is the one closest to the experimental data, and is set at  $15\text{mm}$ , but with a minimum distance to the shoe mesh of  $1\text{mm}$  in order to avoid initial penetration between the shoe and powder part.

The powder part is defined by the part keyword card in 6.9 specifying part id, and which section and material card that are related to the part.

1	*PART								
2	\$#								title
3	powder								
4	\$#	pid	secid	mid	eosid	hgid	grav	adpopt	tmid
5		4	2	4	0	0	0	0	0

**Keyword Card 6.9.** Part keyword card for powder.

The section card for the powder can be seen in card 6.10, the element formulation is left default as this is ignored due to the powder being defined as discrete elements [38].

```

1 *SECTION_SOLID_TITLE
2 solid_des
3 $#   secid   elform   aet
4         2       2       0

```

**Keyword Card 6.10.** Section keyword card for powder.

Different material cards have been investigated, presented in the iteration overview. In general, the literature study show that 4 different material cards are the ones regularly used for DEM models. These are \*MAT\_RIGID, \*MAT\_RIGID\_DISCRETE, \*MAT\_SOIL\_AND\_FOAM, and \*MAT\_POWDER, where the first 3 have been tested in this project. The last card, \*MAT\_POWDER, requires extensive input parameters, and is mostly used for simulation of powder compaction. As this is outside the objective of this project, only the other and less complex material models are considered for limiting the computational cost. The difference between \*MAT\_RIGID and \*MAT\_RIGID\_DISCRETE is, that \*MAT\_RIGID\_DISCRETE allows a part to be discretized into multiple disjoint pieces. Each piece will thereby behave as an independent rigid body. The inertia properties for each discrete element are determined directly from the finite element discretization [39]. The advantage of using a rigid material model over fx. the \*MAT\_SOIL\_AND\_FOAM is the computational cost of the simulation, however it is with the cost of material properties such as deformability. Initially the powder material was specified by \*MAT\_SOIL\_AND\_FOAM, which was the recommendation from a contact in Luleå University, but simulations have shown that for the purpose of this project, the material card \*MAT\_RIGID\_DISCRETE is sufficient. The final material card can be seen in 6.11.

```

1 *MAT_RIGID_DISCRETE_TITLE
2 rigid_DE
3 $#   mid      ro      e      pr
4         4  7.750E-9  205000.0  0.28

```

**Keyword Card 6.11.** Material keyword card for powder.

As presented in section 6.4.1, it is possible to define an active region of discrete elements. Reaching beyond this region the elements are no longer considered, and will be excluded from all algorithms. This is an efficient tool for limiting the computational cost of the simulation. The keyword card activating the active region is can be seen in card 6.12, with the region defined by the box in card 6.13.

```

1 *DEFINE_DE_ACTIVE_REGION
2 $#   id      type      xm      ym      zm
3         1       1       0.0     0.0     0.0

```

**Keyword Card 6.12.** Active region keyword card the discrete elements (powder).

```

1 *DEFINE_BOX_TITLE
2 de_active_box
3 $# boxid      xmn      xmx      ymn      ymx      zmn      zmx
4           1      -10.0    270.0   -10.0    72.0    -41.0    150.0

```

**Keyword Card 6.13.** Box keyword card defining the box for the active region.

The coupling between powder particles are defined by keyword card 6.14. Multiple simulations with different particle-particle coupling parameters have been conducted as can be seen in the iteration overview Appendix B. The reason for the focus of the particle-particle interaction is the observations through the literature study, ex. previous mentioned observation of particle-particle contact have the greatest influence on the process, by Wu and Cocks [22]. Furthermore a paper by Chu et. al [40] from 2107, deduces that scaling of particles, coarse graining, can be done, to a reasonable extent, and should be conducted without changing model parameters, but states that *"There are current no general agreements for the scaling or coarse-graining of particle-particle interaction forces and different scaling may be necessary for different situation."*

```

1 *CONTROL_DISCRETE_ELEMENT
2 $# ndamp      tdamp      fric      fricr      normk      sheark      cap      mxnsc
3           0.25     0.25     0.15     0.05     0.0       0.0       0       0

```

**Keyword Card 6.14.** Control keyword card for the interaction between the powder particles.

The keyword cards defining the powder-surface coupling can be seen in card 6.15, for the powder to die plane, to filling shoe, and to sliding plane, respectively. Note the death time of 0.225 for the coupling of powder to both the filling shoe and sliding plane. These couplings are ceased for letting the powder particles fall out of the active region, limiting computational cost in the last part of the simulation where settling of the powder in the die is achieved. The specific time of death is changes depending on the when the shoe is free of the die opening, to secure that the powder left in the die after filling is not influenced.

```

1 *DEFINE_DE_TO_SURFACE_COUPLING
2 $# slave      master      stype      mtype
3           4         1         3         1
4 $# frics      fricd      damp      bsort      lcvx      lcvy      lcvz      wearc
5           0.15     0.15     0.4       10        0         0         0         1.5
6 $# w1        w2        w3        w4        w5        w6        w7        w8
7 *DEFINE_DE_TO_SURFACE_COUPLING
8 $# slave      master      stype      mtype
9           4         2         3         1
10 $# frics     fricd     damp     bsort     lcvx     lcvy     lcvz     wearc
11           0.15     0.15     0.4     10        0         0         0         1.5
12 $# w1        w2        w3        w4        w5        w6        w7        w8
13 $# sfp       sft       unused   unused   unused   cid_rcf   bt       dt
14           1.0     1.0             0         0.0     0.225
15 *DEFINE_DE_TO_SURFACE_COUPLING
16 $# slave      master      stype      mtype
17           4         3         3         1

```

18	\$#	frics	fricd	damp	bsort	lcvx	lcvy	lcvz	wearc
19		0.15	0.15	0.4	10	0	0	0	1.5
20	\$#	w1	w2	w3	w4	w5	w6	w7	w8
21	\$#	sfp	sft	unused	unused	unused	cid_rcf	bt	dt
22		1.0	1.0				0	0.0	0.225

**Keyword Card 6.15.** Coupling keyword card for the powder to the die plane, filling shoe, and sliding plane respectively. *The death time (dt) is changed depending on the shoe displacement, here RBBS*

### 6.5.5 Gravity

Gravity is included in the system by the keyword card 6.16 prescribing a load in z direction equivalent to the curve defined in 6.17.

1	*LOAD_BODY_Z							
2	\$#	lcid	sf	lcidrr	xc	yc	zc	cid
3		5	1.0	0	0.0	0.0	0.0	0

**Keyword Card 6.16.** Load keyword card in z for including gravity

1	*DEFINE_CURVE_TITLE								
2	gravity								
3	\$#	lcid	sidr	sfa	sfo	offa	offo	dattyp	lcint
4		5	0	1.0	1.0	0.0	0.0	0	0
5	\$#	a1		o1					
6		0.0		9810.0					
7		100.0		9810.0					

**Keyword Card 6.17.** Curve keyword card for gravity loads.

### 6.5.6 Additional keywords cards

The input of the additional keyword cards controlling timestep, termination and outputs can be found in the full keyword in Appendix F.

The time step, \*CONTROL\_TIME\_STEP, is left default, and is thereby determined by LS-DYNA. The upper limit is set equivalent to the output of D3 plots.

The termination time, \*CONTROL\_TERMINATION, is changed depending on the time of the filling shoe displacement, additional 0.25 sec are added to secure that powder in the die is settled.

The D3 plots, \*DATABASE\_BINARY\_D3PLOT, is with output time following an curve, \*DEFINE\_CURVE, which is changed depending on the filling shoe displacement, so that before and during die filling, a D3 plot is outputted in the intervals of 0.02 sec, while when the shoe is retracting and free of the die, the output is every 0.1 sec.

Additional keywords for output includes \*CONTROL\_OUTPUT, \*DATABASE\_ELOUT, \*DATABASE\_GLSTAT, \*DATABASE\_NODOUT, \*DATABASE\_BINARY\_DEMFOR.

### 6.5.7 Additional models

#### Model for DE creation and settling

For limiting the simulation time, the discrete element spheres are initially created and a single model is run for letting the powder settle in the shoe. The simulation time is set to 1 sec. The model is identical to the one already described, except that no displacement is prescribed the feeding shoe. From the simulation a .dynain file is written, containing the coordinates of each individual settled powder particle, ready for import in the experimental model.

#### Model for testing

A model with a thin box was used in a small extent to investigate different parameters, ex. seen in the iteration overview Appendix B. However the primary use of this model has been in the setting up of the coupled ICFD model.

#### Full model

A full model has been used for testing if the half sliced model is able to sufficiently mimic a full model.

Observations and average density results suggest that the half model can be used instead of the full one. Average density for full model RBBS model is  $3.808 \text{ g/cm}^3$  with CPU time of 291 hr, while the half is  $3.794 \text{ g/cm}^3$  with CPU time of 130 hr.

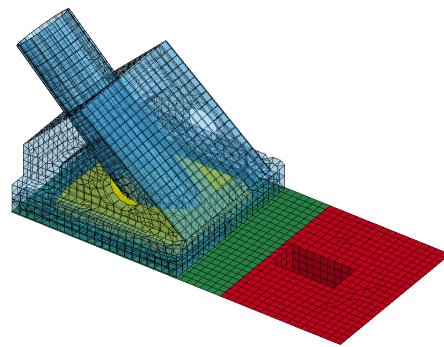


*Figure 6.13.* Full model.

## 6.6 The computational fluid dynamics method

The CFD method is employed to achieve the inclusion of air, as the presence of air is considered influencing on the quality of the simulation results. The LS-DYNA ICFD solver is an incompressible CFD solver based on the Finite Element Method, and it uses an implicit time-stepping and solution method. [41]

The first step for representing the air with the CFD method is to create a closed volume, inside which the fluid or gas of interest will be generated. Each one

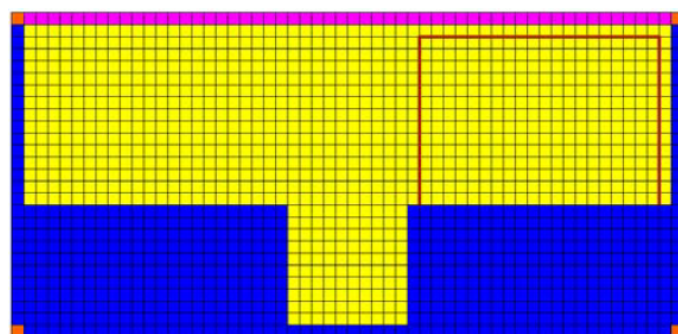


*Figure 6.14.* A schematic diagram of computational fluid cells and boundary conditions (discerned by different colours). Source: [32].

of this volume's surfaces may serve as a different type of boundary (free-slip, continuous gas outflow, etc.). Thus, each surface that will be attributed different features, must be meshed (by shell elements) as a distinct part (see Figure 6.14). Those surfaces must also be meshed with an adequate accuracy, because the volume's 3D mesh derives from those surfaces' meshes. It is of high importance to make sure that there are no duplicate nodes, as well as all that the boundaries are connected.

The structural meshes of those surfaces have thereafter to be converted to ICFD surface meshes, which can be done either in a text editor or in LS-PrePost. The ICFD solver uses the \*MESH\_ family of keywords to define the fluid mesh; more specifically, the \*MESH\_VOLUME keyword card defines the volume that will be meshed, based on the defined surface meshes. Other cards from the \*MESH branch of the Keyword manager tree can be used to assist in the creation of the mesh (e.g. refinements) (for more information see [42]).

Various options for the Incompressible Fluid solver (ICFD) can be found in the \*ICFD branch of the Keyword manager tree cards. There, among others, boundary conditions can be specified, initial conditions set, as well as database output and solver preferences can be determined. The fluid properties are associated with the fluid volume through the \*ICFD\_PART\_VOL card. Furthermore, the \*ICFD\_MAT, \*ICFD\_PART and \*ICFD\_SECTION cards that are required, can be found there too.

### 6.6.1 Implementation of the coupled method

As discussed in [37] and [32], here similarly the fluid cells are set in the range of 1.6 times the particle diameter. In [27] it is suggested that, in order to adequately simulate the behaviour of the air bubbles created in the powder mass, the fluid cells should be smaller than the macroscopic motion of those bubbles, and still larger than the particle size.

The nature of the boundaries set is something of high importance also, as each different choice delivers various attributes and features to the model. In [36] Guo, Wu and Thorton adopted a simplification, they ignored the interaction of the air with the walls of the shoe.

#### The coupled DEM/CFD method

One of the filling model presented in this report is developed as a coupled DEM/CFD model, as it combines characteristics and features from both methods for better results.

In models incorporating the coupled DEM/CFD method, the metal powder particles are described as discrete spheres by the DEM, and the filling process takes place inside a continuum media (that has been assigned air characteristics) with the use of the CFD method.

The \*ICFD\_CONTROL\_DEM\_COUPLING card which is nested in the \*ICFD branch of the Keyword manager is responsible for the coupling of the DEM and CFD methods, and thus should be activated.

## 6.7 Model description - ICFD

The air is included in the model as an incompressible fluid using the ICFD solver in Ls-Dyna, presented in 6.6. The air volume included in the model can be seen in figure 6.15.

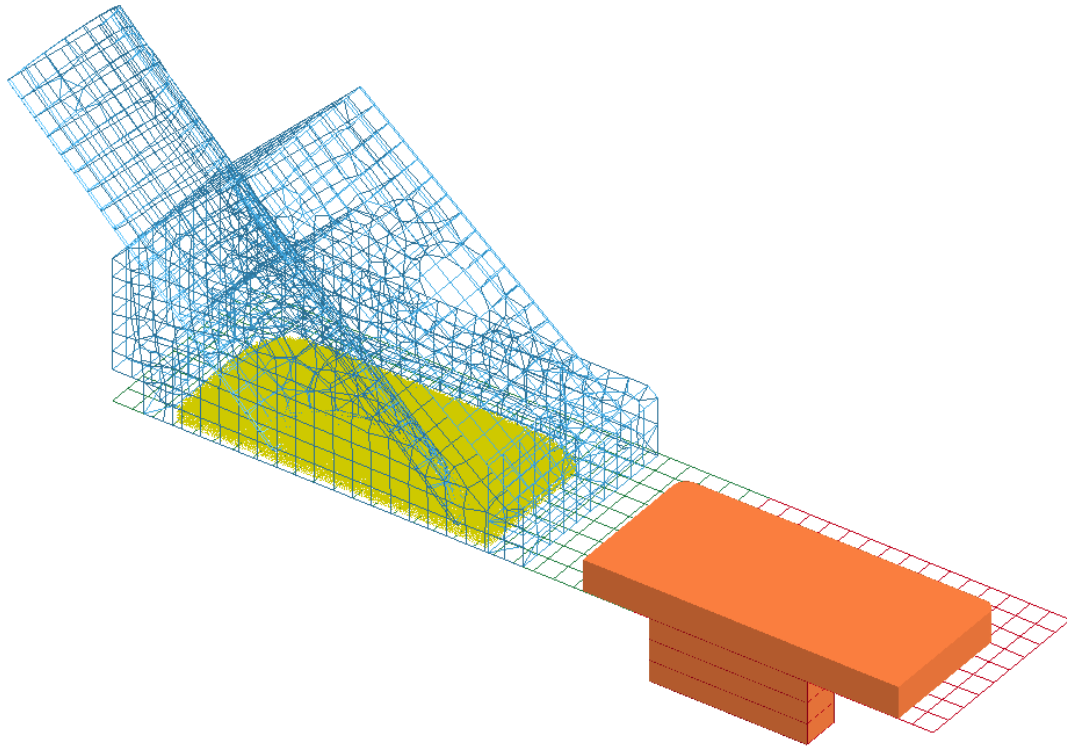


*Figure 6.15.* Orange: Air (fluid volume) included in the model.

This coupled model is build by 3 keyword files:

- ICFDmodel.k

This is the primary keyword file, and must be the one defined at simulation initialization. It includes the other keyword files with the card `*INCLUDE`. Furthermore it contains the keyword cards for the ICFD.

- ICFDmesh.k

This keyword file contains the ICFD mesh of the fluid volume.

- Model.k

The keyword file contains the model for the mechanical solver, identical to the one presented in 6.5. *The Model.k will not be elaborated further in this section.*

The ICFDmodel.k and the ICFDmesh.k will be presented in the following subsections.

### 6.7.1 The ICFD Mesh

For meshing of the fluid volume, the geometry of the air volume for the die in the specific simulation is imported to ls-prepost as a .step file from Solid Works.

The geometry for the final volume is defined by the die and shoe geometry up to the top of the brass plate as seen in 6.16.

After importing the geometry, automesh is used for creating a triangular mesh. It must be noted that the fluid volume for the ICFD solver in Ls-Dyna must be defined by a tetrahedron mesh. Furthermore, surfaces with different boundaries (e.g. freeslip, nonslip) must have individual mesh.

Different mesh sizes have been applied through the iterations, but a mesh size of 1mm is chosen for the final model (*because it is close to the suggestion presented in section 6.6.1, from [27], and because it is not causing error terminating*). After meshing, duplicate nodes are found and merged with the duplicate node tool in Ls-Prepost, as any duplicate point will cause immediate error termination. This must be done prior to the next step, as doing it after will result in Ls-Prepost crashing.

The next step is to convert the mesh into a mesh for the implicit solver with the MSMesh tool, which is simply converting the elements to the keyword cards \*MESH\_SURFACE\_NODE and \*MESH\_SURFACE\_ELEMENT for the file ICFDmesh.k. It should be noted that no node, element and part id number should be the same as the ones defined in the file Model.k. The different part id's confining the fluid volume can be seen in figure 6.17.

### 6.7.2 The ICFD model

The keyword file ICFDmodel.k is including the other two keyword files with the keyword card 6.18.

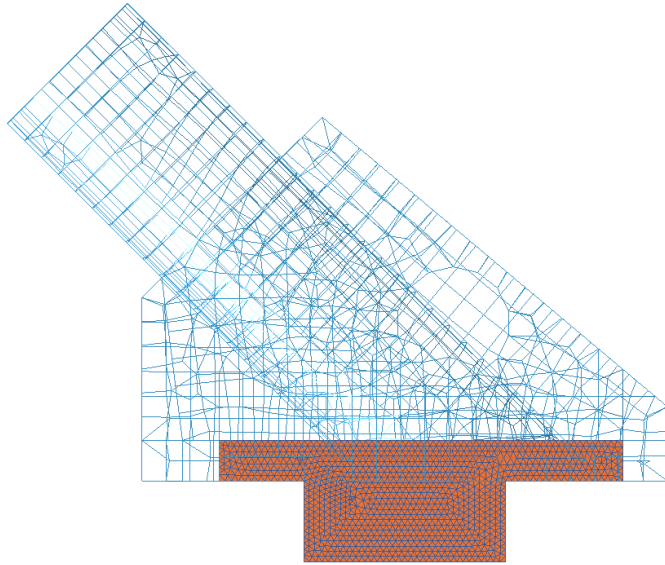


**Figure 6.16.** Air volume height in shoe.

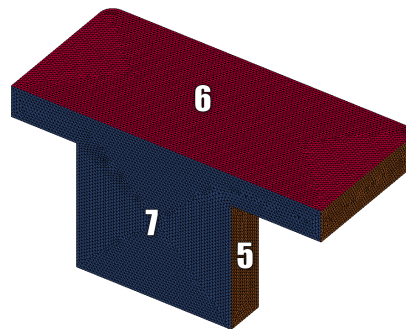


**Figure 6.17.** 3 parts confining the air volume included in the model, here for 40 mm rectangular die. Non-visible surfaces are belonging to part 5

```

1 *INCLUDE
2 $#
3 ICFDmesh.k
4 *INCLUDE
5 $#
6 Model.k

```

**Keyword Card 6.18.** Include keyword card for including the fluid volume mesh and the model for the mechanical solver.

Furthermore the file is containing the ICFD keyword cards, which will presented here. The different surfaces shown in figure 6.17 are defined by keyword card 6.19.

```

1 *ICFD_PART_TITLE
2 wall
3 $#   pid   secid   mid
4     5     5     6
5 *ICFD_PART_TITLE
6 outlet
7 $#   pid   secid   mid
8     6     5     6
9 *ICFD_PART_TITLE
10 symmetry
11 $#   pid   secid   mid
12    7     5     6

```

**Keyword Card 6.19.** Part keyword card for the fluid surfaces.

The card for section id (secid 5) must be defined by \*ICFD\_SECTION, but has no function in the current Ls-Dyna version.

The input for the material card 6.20 is set to incompressible (flg = 1), and the flow density (ro) and dynamic viscosity (vis) properties is for atmospheric air for 20 deg C [43].

```

1 *ICFD_MAT_TITLE
2 Air
3 $#   mid   flg   ro   vis   st
4     6     1 1.204E-12 1.821E-11 0.0

```

**Keyword Card 6.20.** Material keyword card for fluid (air).

For prescribing the fluid boundary condition the keyword card 6.21 is defined. Surface 5 is acting along the surface of the die plane and brass plate, and should have wall boundary, and is therefore prescribed a nonslip boundary condition. Surface 6 is acting like an outlet for the air, therefore a 0 pressure condition is defined. The 0 pressure is prescribed in the boundary condition through a load curve (lcid 6), which is a curve of 0 to all time, defined by \*DEFINE\_CURVE. Surface 7 is the symmetry plane, and for this the free slip boundary condition should be the prescribed [44].

```

1 *ICFD_BOUNDARY_NONSLIP
2 $#   pid

```

```

3      5
4 *ICFD_BOUNDARY_PRESCRIBED_PRE
5 $#   pid      lcid      sf      death      birth
6      6        6        1.0    1.000E28    0.0
7 *ICFD_BOUNDARY_FREESLIP
8 $#   pid
9      7

```

**Keyword Card 6.21.** Boundary keyword card for the 3 difference surface meshes.

The volume is defined by the cards in keyword card 6.22. Both are necessary in an ICFD model.

```

1 *ICFD_PART_VOL
2 $#   pid      secid      mid
3      1        5        6
4 $#   spid1     spid2     spid3     spid4     spid5     spid6     spid7     spid8
5      5        6        7        0        0        0        0        0
6 *MESH_VOLUME
7 $#   volid
8      1
9 $#   pid1     pid2     pid3     pid4     pid5     pid6     pid7     pid8
10     5        6        7        0        0        0        0        0

```

**Keyword Card 6.22.** Fluid volume defining keyword cards.

The coupling between the fluid and the powder is prescribed with card 6.23, defining a two way coupling (ctype 0), so the powder is influenced by the fluid, and the other way around.

```

1 *ICFD_CONTROL_DEM_COUPLING
2 $#   ctype     bt      dt      sf
3      0        0.0    1.000E28    1.0

```

**Keyword Card 6.23.** Coupling keyword card for the coupling between the fluid (air) and the discrete elements (powder).

Finally, the \*ICFD\_CONTROL\_TIME is used for prescribing simulation time of the fluid problem. The rest is left as default, letting the solver compute the timestep.

## 6.8 Validation of the numerical models

In this section, the results from the numerical model will be presented.

A selection of the experiments have been reproduced by the numerical model. These experiments are RB, RC, RBBI, RBBS, and RBBS including air (ICFD). For more information, see Figure 4.20.

In the validation, a presentation of the flow with the 40 mm deep dies is included, together with density in points and average density of the 20 mm deep dies.

### 6.8.1 Powder flow

In this section the flow obtained in the model will be compared to the flow obtained from the high speed camera at multiple time points from the beginning of the shoe's movement. The first time point of comparison will be at the first time step that powder is visual in the die (in the model). The intervals of comparison are set at 0.04 s and limited to the time when powder flow from the shoe is present. The last time point of comparison in each experiment is after the die filling, when the powder has settled. The repetition of each experiment used for this comparison is based on the image quality and best fit for the model.

For the RB and RC in figure 6.18 and 6.19 respectively, it is seen that until 0.26 s the flow appear similar, but after this point, bigger differences are present. More specifically the powder mass in the simulations is noticeably less than in the experiments. Presumably, it is more difficult for the bigger particles in the simulations to move underneath the tube, and because they get packed in this clearance between the tube and the plate, they do not flow as freely as the experimental ones.

The final packing of the powder in the dies after filling, seems similar between experiments and simulations for the RBBS experiments in figure 6.21, but oppositely curved for the RBBI ones in figure 6.20.

Finally, when investigating the influence of including air in figure 6.22 in the simulations it is seen that not distinguishable differences are portrayed, as both the powder flow and deposition between these two simulations are very alike. It is assumed, that the effect of the air is only a little bit influential because of the big powder particles involved. As discussed earlier the larger and heavier the particles are, the less affected they get from the presence of air, as it is more difficult for it to affect their movement.

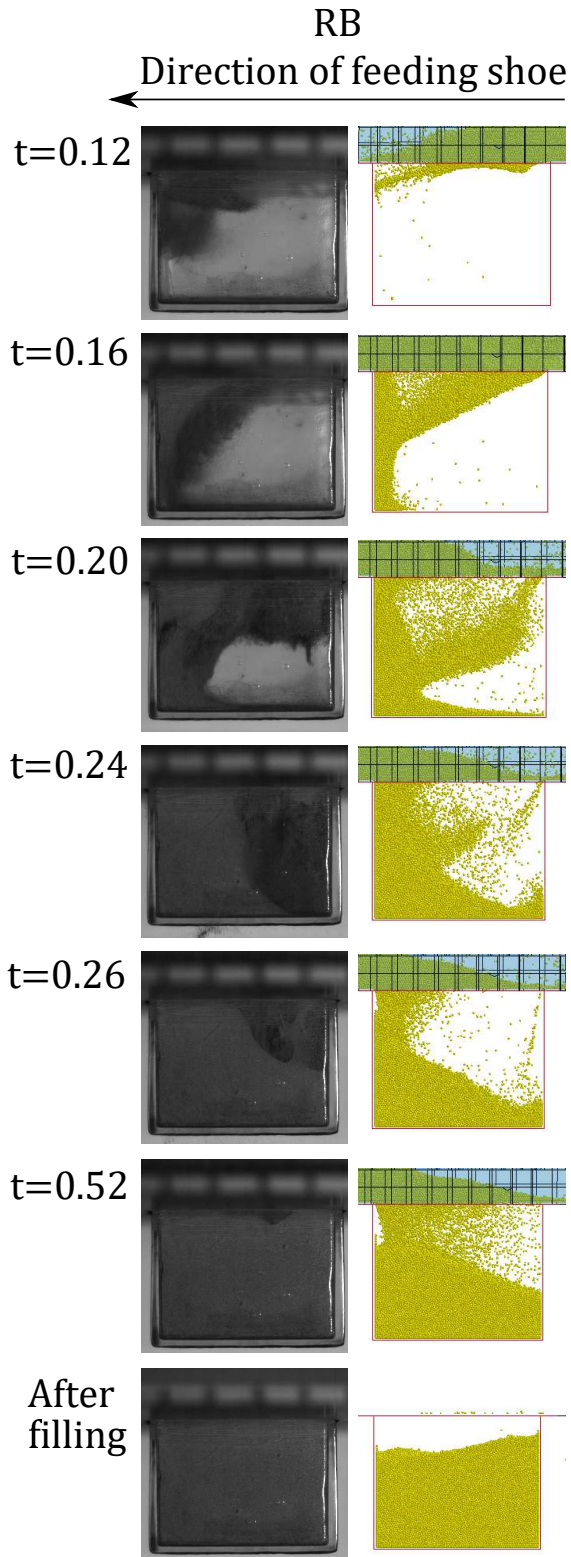


*Figure 6.18.* Powder flow for RB at different time for shoe displacement, left is from high speed camera while right is the final model.

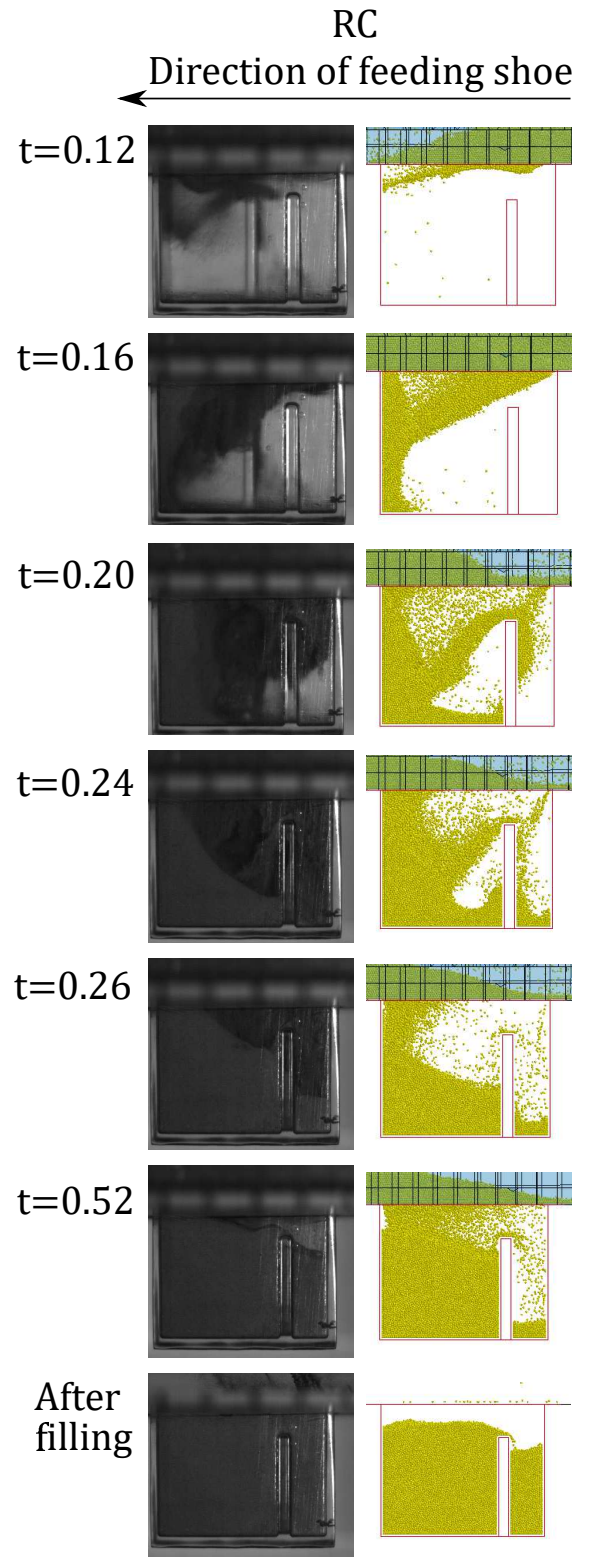


*Figure 6.19.* Powder flow for RC at different time for shoe displacement, left is from high speed camera (3rd repetition) while right is the results from the final model.

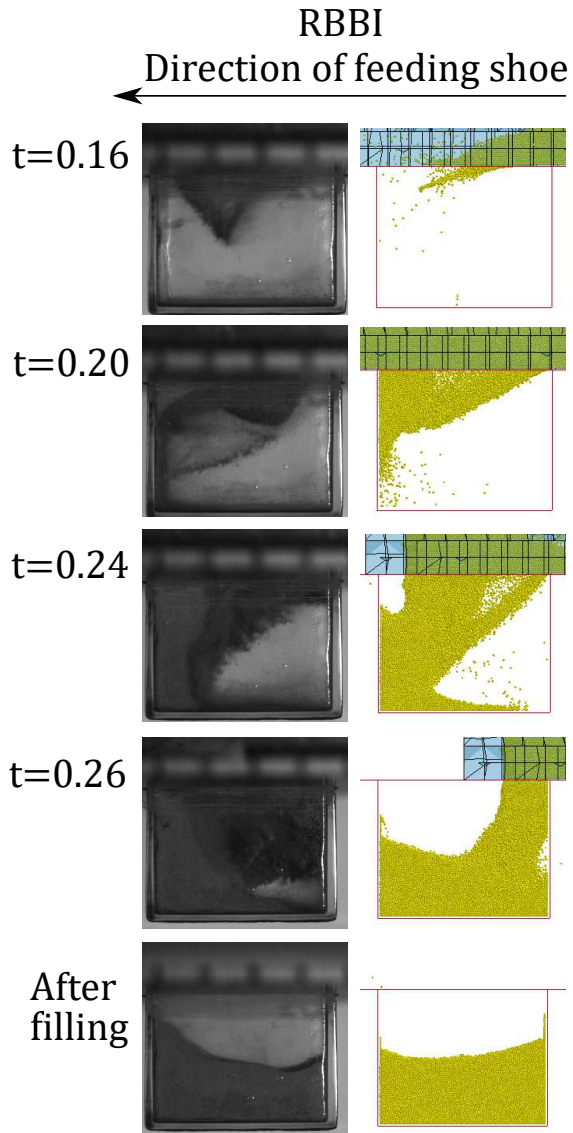


*Figure 6.20.* Powder flow for RBBI at different time for shoe displacement, left is from high speed camera (2nd repetition) while right is the results from the final model.

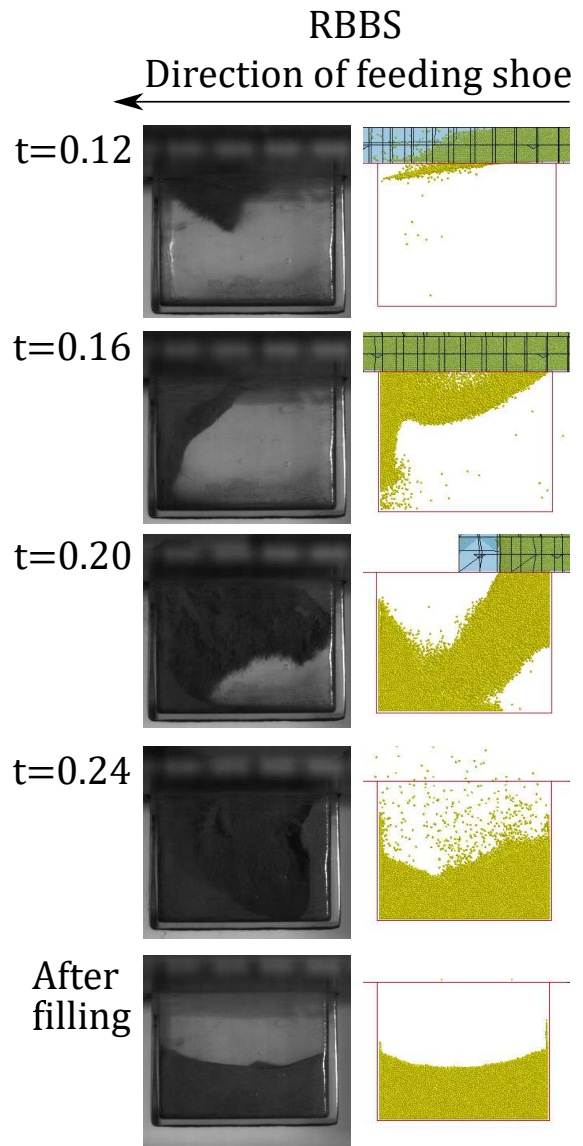


*Figure 6.21.* Powder flow for RBBS at different time for shoe displacement, left is from high speed camera (2nd repetition) while right is the results from the final model.

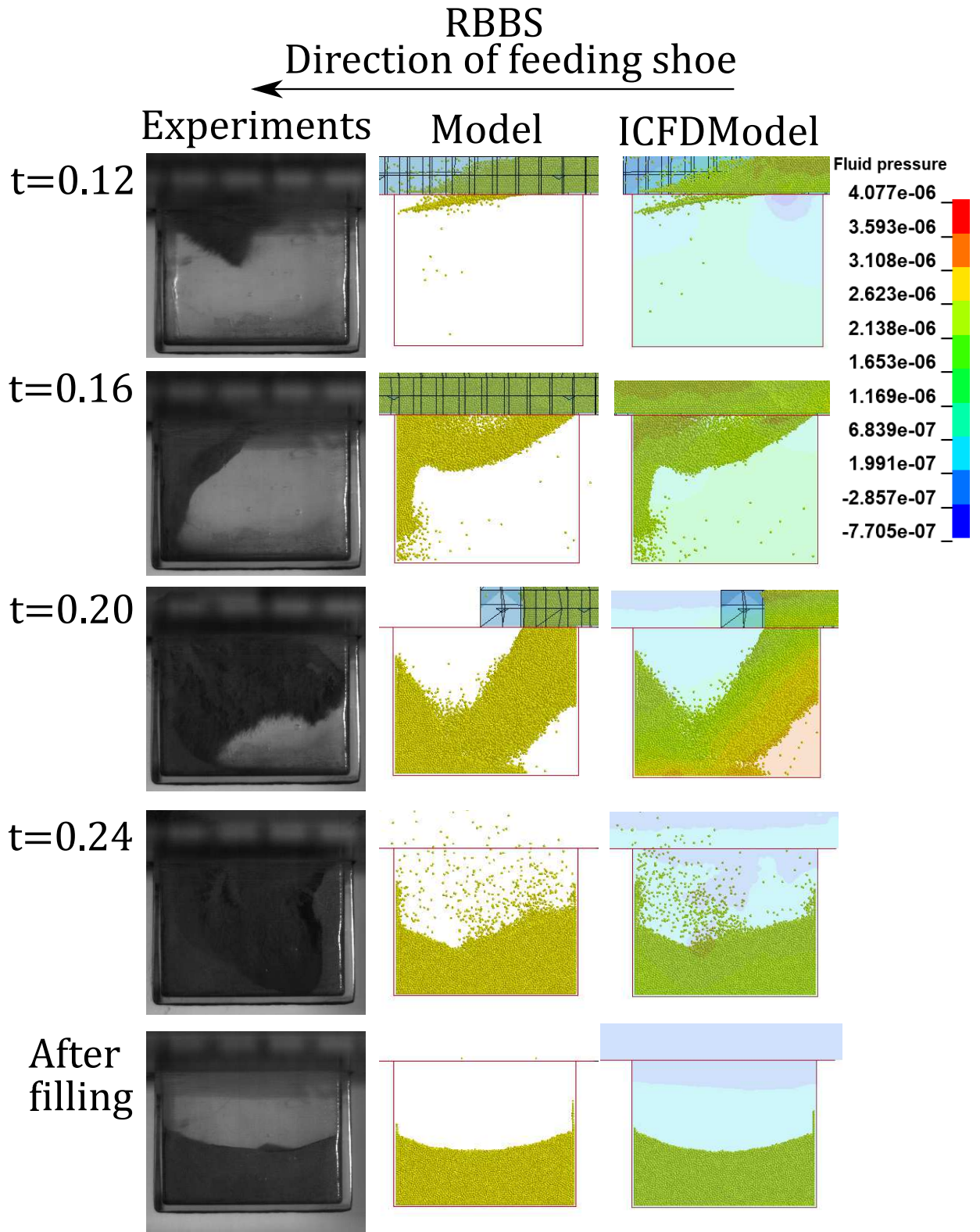


**Figure 6.22.** Powder flow for RBBS at different time for shoe displacement, left is from high speed camera (2nd repetition), middle is the model with no ICFD, and right is the results from the model including ICFD (with fluid pressure indicated. *Unit:  $N/mm^2$* ).

### 6.8.2 Density in points

Because no clear trend is observed in the experimental results presented in Section 6.8.2, a direct comparison to the simulation results is considered of less interest. Instead, the tendencies observed in the numerical simulations are presented, in a similar manner with a "point" density. The density is calculated in a rectangular volume, of  $6 \times 6 \times$  (difference from the bottom of the die to the  $z$  coordinate of the highest placed particle in the area of interest)  $mm$ , with the same centrum as for the experiments. Even though no specifications of the measuring area for the densomat could be obtained,  $6 \times 6 \text{ mm}$  is assumed to be considerable larger than this. This enlargement of the measurement area is done in order to reduce the error of accidentally measuring in a point that is not general to the neighbouring area, also considering the enlargement of the powder particles, which makes the risk even greater. However, despite the enlargement of the area of interest, the results are still non general due to the partial data focus. This is also the case for the results from the experimental results, which may contribute to the randomness between repetitions.

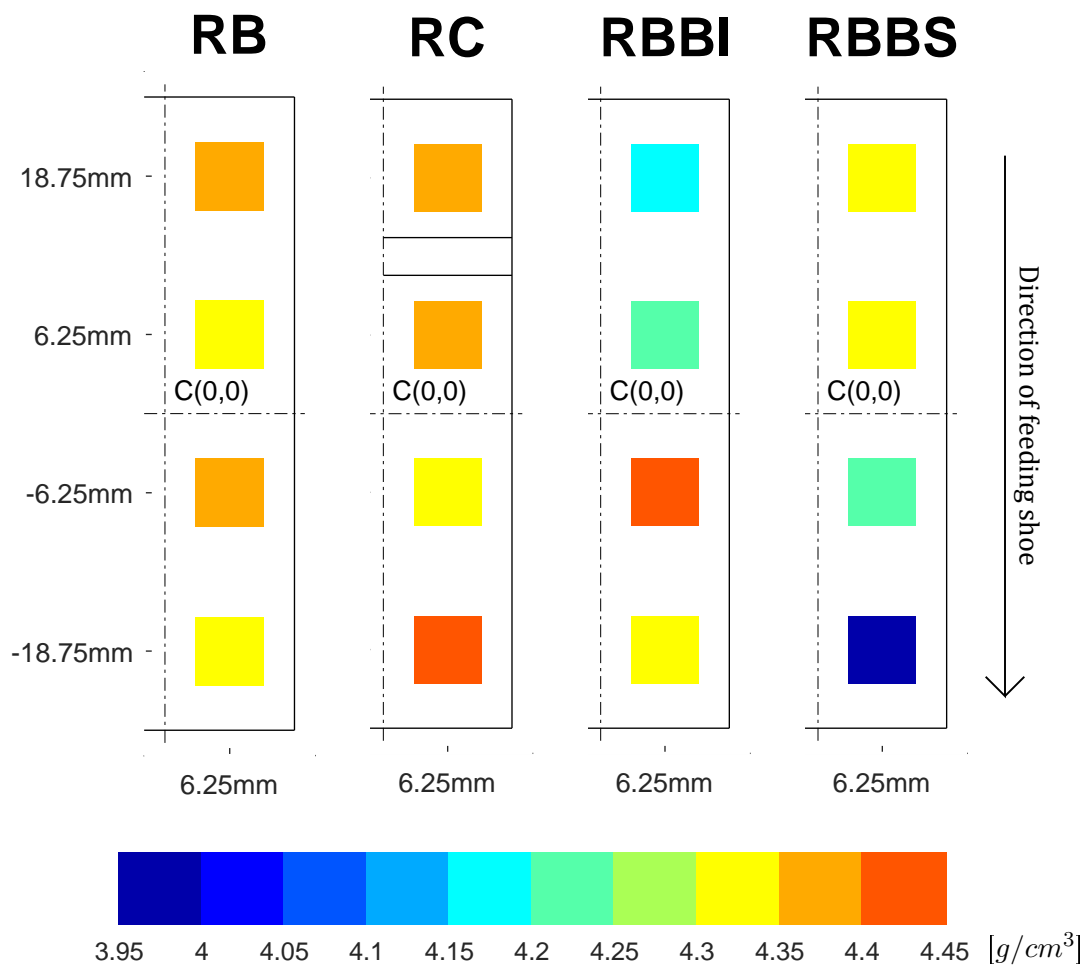


**Figure 6.23.** Density in "points" results from the numerical model, with the half-sliced dies.

From the density in points seen in figure 6.23, we see results opposite to the experimental ones, as the pull back side for RBBS has a higher density, agreeing with the discussions by Xie and Puri in [16]. However, RBBI is showing the contrary which is unexpected. RB and RC have more equally distributed density.

### 6.8.3 Average density

The average density from the numerical simulation, is measured in dies of  $20\text{mm}$  depth for comparison with the experimental data. In contrast to the  $40\text{mm}$  dies used in for the flow results in section 6.8.1, a near to complete filling is observed for the  $20\text{mm}$  dies (except for RBBS, as the case for the experimental results), so in order to compare with the experimental results, the whole die volume is used for calculating the average die density. The average density of the  $20\text{mm}$  deep dies is given in table 6.8.3.

Experiment	Experimental Result [g/cm <sup>3</sup> ]	Model Result [g/cm <sup>3</sup> ]
RB	3.388	3.791
RC	3.369	3.667
RBBI	3.136	3.525

**Table 6.1.** Average density results for the RB, RC and RBBI experiment, from experiment and from the numerical model.

It is clear from the average densities in the table, that the average density is higher in the model than in the experiments. This is expected to be caused by the enlarged particle size, however, the trend of the average density between experiments is similar. As in the experiments, RBBI, where the dwell time is low, has the lowest density. This is due to the shorter time where the powder bed is above the die, and therefore the powder has less time to cascade in the die cavity. Furthermore, less pressure is applied from the powder above, which results in less reorganising (compaction) of the powder which is already in the die.

## 6.9 Computational cost

The computational cost of the simulations in this project have been of great interest, in order to be able to investigate the different parameters of interest. Efforts have been made in order to lower this, which includes initial model for powder settling in the feeding shoe, where the powder particle placement is outputted and reused in the different models. Also coupling deaths are introduced, in order to allow the left over particles to fall outside the active region, while making sure, that the powder in the die has time to settle. An overview of the computational cost for the initial model together with the models presented in the validation section 6.8 (only for 40 mm dies) is given in table 6.2.

Experiment	No. particles	Sim. time	CPU time	No. CPU/elapsed real time
Original	92522	2.2 s	1696 hr	56/31 hr
RB	183169	0.85 s	316 hr	22/14 hr
RC	183169	0.85 s	304 hr	22/14 hr
RBBI	183169	0.7 s	279 hr	22/14 hr
RBBS	183169	0.6 s	137 hr	22/6 hr
RBBS (ICFD)	183169	0.6 s	355 hr	22/27 hr

*Table 6.2.* Overview of computational cost of the models.

In order to further lower the computational cost of running a simulation, various ideas is yet to be explored. To start with, in [21] they found that the flow results were very similar between a full 3D and a thin-sliced 3D model of the die filling process. They used the DEM/CFD method, and concluded that models with the 1/5th of the width of the original model, save up a lot of computational time, and can adequately communicate accurate results. They also found that for a specific shoe speed, the filling in air is very much alike the filling in vacuum, since there is enough time for the air to escape the die before the latest is completely filled. Guo showed in [32] that a 2D model and a thin-sliced model (see Figure 6.24) imitated the powder behaviour in the middle of a fully 3D model. In addition to that, he argued that even though irregular particles are generally more realistic than the spheric ones, because their inter-particle contact model is much more complicated, their use highly increases the computational time. The largest simulation ran in that study, needed more than two months to finish.

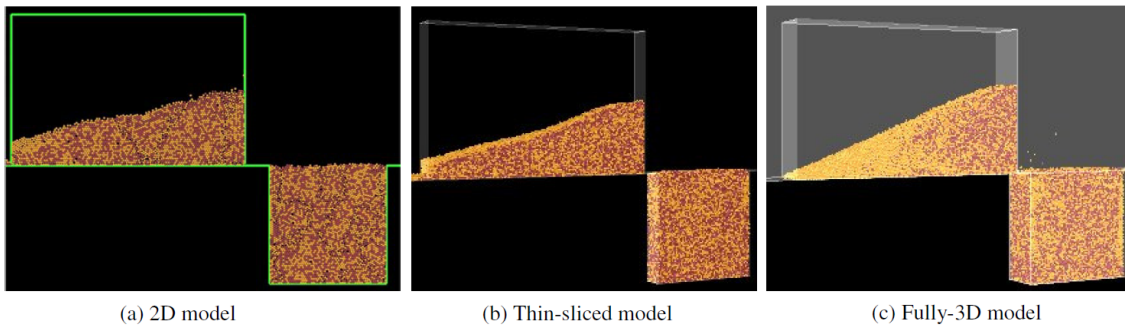


*Figure 6.24.* The final packing of powder in a die from 3 different models. Adapted from: [32].

Bierwisch et. al. used larger grains in their simulations than the experimental ones, because they understood that this is the only way to overcome computing power and memory limitations. In [23] they studied deeply the influence of lowering the die dimensions in the simulations, in order to bring down the computational time. They concluded that for their study, as long as the die width was 5 times the particles diameter, there was no influence on the simulation results.

# Conclusive Remarks

# 7

---

In this Chapter the findings of this study will be discussed, with the intention of achieving a further understanding of the die filling process.

## 7.1 Reflections on the experimental results

A summarized understanding of the experimental results will be presented in this Section, along with their impact on the so far knowledge regarding the die filling process.

To start with, the target of this research is to understand the powder behaviour, and utilize the gained knowledge towards the benefit of the PM industry. Die filling experiments are conducted with varying parameters, in an effort to assess their distinct and accumulated influence on the process. It is seen that variations between repetitions of the same experiment are evident in all experiments conducted. The human error involved could not be appraised, thus some of these variations should be contributed to it. The powder's irregular behaviour when packing is most certainly also one of the more -if not the most- important reasons why these inconsistencies appear so frequently.

When examining the high speed camera results, where die fillings are monitored by a high speed camera, even though the aim was to gain knowledge about the powder flow, other unexpected important information were also gained. Initially, the realization that the filling shoe portrays vibrations, is a highly influencing discovery on the understanding of all the experimental results. Shoe vibrations have been studied by various researchers, and have proven to be beneficial for the die filling process. Because of this, initially it was of interest to this study to investigate them. However, this was utopian as no vibrations could be implemented on the shoe's movement. Because of the experimental set-up developed though, shoe vibrations unexpectedly appeared and prove to be highly influential on the powder flow. This is because every time the shoe fiercely reached the end of its journey, the powder mass inside it was shaken and big blocks of powder were seen cascading in the die.

Furthermore, it was observed that the biggest part of the powder enters the die during the later parts of the shoe's forward movement, and in the later ones of the backwards. More

specifically, in the majority of data in hands, the flow rate was considerably increased after the shoe passed the midpoint of its forward movement, and similarly when it passed the midpoint of its backward movement. It is presumed that this occurs, because when the shoe's acceleration causes the powder to gather on its back side (during forward acceleration), it is difficult for the powder particles to detach from this mass and start flowing in the cavity.

Moreover, in the experiments that involve longer dwell times, it can be clearly distinguished that the flow rate of the powder significantly decreases over time. In the experiments where the longest dwell times were explored, and after a point in time when the shoe was immobile above the die, the flow rate portrayed was the lowest witnessed. It is understood that even though nose flow is present in all the die fillings conducted, the biggest part of the powder is supplied in the die through bulk flow. The rotational flow observed in many experiments, is most probably an aftermath of the nose flow, and seemed to impede the powder's uniform deposition, as it displaced it.

The dwell time and the shoe speed are considered highly influential, in opposite manners. It is generally observed that higher shoe speeds and/or lower dwell times jeopardize the powder flow, deposition and density. No concrete results are yielded about the effect of the powder height in the shoe. This is due to the fact that in those experiments the shoe did not travel the full distance that it was supposed to.

The experiments where the density in points of the powder mass inside the dies was measured were expected to be the most fruitful ones, as they are the only ones that directly communicate information about the filling process result, the density. However, not many things could be deduced by analysing their data, as no packing tendencies could be distinguished. Nonetheless, one of the things that was deduced by examining this information, is that by solely increasing the shoe speed (RBBI to RBBS experiments) the density in points decreases. Moreover, higher shoe speeds in addition to lower dwell times resulted in poorer density in most parts of the die. Thus, the distinct influence of the dwell time can not be discerned. Lastly, when the shoe gets filled with powder and its speed is decreased, even though it does not travel the full the distance, the density in the dies is a little bit higher. No reasoning why this occurs can be speculated.

Lastly, when analysing the average density results, the first important observation regards the influence of the die geometry on the filling process. The studied theory was verified, as it was witnessed that the rectangular die portrayed a lower average density than the circular one, and respectively, the rectangular one with inlets lower than the rectangular. No conclusive remarks can be deduced for the dwell time influence or shoe speed.

## 7.2 Reflections on the simulations

A lack of input data, necessitated the utilization of engineered guesses and the trial and error method. In the time span of this study, these methods prove to be insufficient in

generating the desired results.

More specifically, even though the simulated powder flow of some developed models portrays acceptably accurately the experimentally observed flow for the first half of the filling process, in the second part of the simulations that changes, and a considerable lack of powder is evident in the simulations. Even though, some experimentally observed tendencies are portrayed in the numerical results also, they are not reliable enough to constitute the model realistic. Finally, in some of the numerical models developed, the shape of the powder mass inside the die after the filling, accurately portrays the experimental reality. Summarizing, none of the numerical models developed accurately describes the experimental process of the die filling.

The conclusions of this study provide indeed information about the powder behaviour, and the assessment of the involved parameters' influence has been rewarding. Nonetheless, there are a lot more blanks to be filled about the interesting evolution of the powder flow during filling.

### **7.3 Industrial applications and future work**

Even though the conclusions of this study are not directly applicable to the industrial process, it is aspired that they will inspire other researchers to deepen in the understanding of the die filling process, and maybe even serve as a basis, for future works.

More specifically, vibrations should be further studied, so that they can be more controlled and understood when applied in industrial levels. Moreover, the effect of the filling shoe's acceleration on the powder mass inside the die is of interest, as it directly influences the flow rate. Perhaps higher shoe speeds with smaller accelerations can assist the flow rate and aid the bulk flow, which would lead to dies getting filled faster. Finally, looking deeper into the dwell times can prove beneficial, as it appears to be that up to a point they significantly contribute to the filling process, but not that significantly later in time.



## Bibliography

---

- [1] Sintex A/S. Company site. [www.sintex.com](http://www.sintex.com).
- [2] P. K. Samal and J. W. Newkirk, editors. *ASM Handbook Volume 7, Powder Metallurgy*. ASM International, 2015. ISBN: 978-1-62708-089-3.
- [3] [https://commons.wikimedia.org/wiki/File:Iron\\_pillar\\_of\\_Delhi.jpg](https://commons.wikimedia.org/wiki/File:Iron_pillar_of_Delhi.jpg), 21/03/18.
- [4] D. Apelian. *Encyclopedia of Materials: Science and Technology*. Elsevier, second edition, 2001. ISBN: 0-08-0431526, pp. 6761-6768.
- [5] G. Dowson and D. Whittaker. *Powder metallurgy - the process and its products*, 2008.
- [6] A. Ruys, O. Gingu, G. Sima, and S. Maleksaeedi. *Handbook of Manufacturing Engineering and Technology*. 2015.
- [7] C. Nguyen Van, S. Sistla, and S. van Kempen. A comparative study of different sintering models for al<sub>2</sub>o<sub>3</sub>. 124:301–312, 02 2016.
- [8] Globe Metal. [globemetal.com](http://globemetal.com).
- [9] Y. Tsunazawa, Y. Shigeto, C. Tokoro, and M. Sakai. Numerical simulation of industrial die filling using the discrete element method. *Chemical Engineering Science*, 138:791–809, December 2015.
- [10] P. Brewin, O. Coube, P. Doremus, and J. H. Tweed, editors. *Modelling of Powder Die Compaction*. Engineering Materials and Processes. Springer London, 2008.
- [11] S. Burch. Measurement of density variations in compacted parts using x-ray computerised tomography. *Metal Powder Report*, 57(2):24,26–24,28, 2002.
- [12] C. Bierwisch, T. Kraft, H. Riedel, and M. Moseler. Die filling optimization using three-dimensional discrete element modeling. *Powder Technology*, 196:169–179, 2009.
- [13] E. Hjortsberg and B. Bergquist. Filling induced density variations in pm compacts. *Powder Metallurgy*, 45(2):146–153, 2002.

- [14] C.-Y. Wu and A.C.F. Cocks. Flow behaviour of powders during die filling. *Powder Metallurgy*, 47(2):127–136, March 2004.
- [15] D. Alexouli. Simulation of powder filling and research of the involved parameters, 2018.
- [16] X. Xie and V. M. Puri. Uniformity of powder die filling using a feed shoe: A review. *Particulate Science and Technology*, 24(4):411–426, 2006.
- [17] S. S. Roudsari and V. M. Puri. Uniformity differentiation analysis. part 1: Powder deposition characteristics in rectangular shallow die using feed shoe with circular cross section. *Particulate Science and Technology*, March 2010.
- [18] S. S. Roudsari and V. M. Puri. Uniformity differentiation analysis of powder deposition characteristics in circular and rectangular shallow dies using feed shoe with square cross-section. *Particulate Science and Technology*, 29(3):260–271, April 2011.
- [19] S. S. Roudsari and V. M. Puri. Uniformity differentiation analysis. part 2: Powder deposition characteristics in circular shallow die using feed shoe with circular cross section. *Particulate Science and Technology*, March 2010.
- [20] O. Coube, A. C. F. Cocks, and C-Y. Wu. Experimental and numerical study of die filling, powder transfer and die compaction. *Powder Metallurgy*, 48(1):68–76, 2005.
- [21] Y. Guo, C.-Y. Wu, K.D. Kafui, and C. Thornton. 3d dem/cfd analysis of size-induced segregation during die filling. *Powder Technology*, June 2010.
- [22] C-Y. Wu and A. C. F. Cocks. Numerical and experimental investigations of the flow of powder into a confined space. *Mechanics of Materials*, 38(4):304–324, 2006.
- [23] C. Bierwisch, T. Kraft, H. Riedel, and M. Moseler. Three-dimensional discrete element models for the granular statics and dynamics of powders in cavity filling. *Journal of the Mechanics and Physics of Solids*, 57(1):10–31, 2009.
- [24] D. Aole, M. K. Jain, and M. Bruhis. New characterization methods for powder die fill process for producing powder metallurgical components. *Powder Technology*, 232, 2012.
- [25] P. S. Dhanoa and V. M. Puri. Deposition of particulate materials into confined spaces - new tester development and experimental results. *KONA Powder and Particle Journal*, 1998.
- [26] X. Xie. Uniformity of simultaneous powder deposition in multiple dies; measurement and modelling. *Ph.D. Thesis; Pennsylvania State University, Agricultural and Biological Engineering Dept.*, 2006.

- [27] Y. Guo, K. D. Kafui, C-Y. Wu, C. Thornton, and J. P. K. Seville. A coupled dem/cfd analysis of the effect of air on powder flow during die filling. *AIChE Journal*, 55(1):49–62, January 2009.
- [28] G. Schlieper. Principles of gamma ray densitometry. *Metal Powder Report*, 55(12):20–23, 2000.
- [29] J. H. Tweed, S. F. Burch, A. C. F. Cocks, M. Eriksson, R. Maassen, P. Brewin, W. Markeli, L. C. R. Schneider, F. Snijkers, and W. Vandermeulen. Pm modelling workshop: Validation data for modelling of powder compaction: Guidelines and an example from the european dienet project. In *European Congress and Exhibition on Powder Metallurgy. European PM Conference Proceedings*, volume 3, pages 307–312, Shrewsbury, January 2005. The European Powder Metallurgy Association.
- [30] M. Hrairi and H. Chtourou. Predicting density distribution in green compacts using finite element simulations. *Australian Journal of Basic and Applied Sciences*, 5(3):60–68, March 2011.
- [31] C-Y. Wu and Y. Guo. Numerical modelling of suction filling using dem/cfd. *Chemical Engineering Science*, 73:231–238, May 2012.
- [32] Y. Guo. *A coupled DEM/CFD analysis of die filling process*. PhD thesis, The University of Birmingham, 2010.
- [33] P. Brewin and L. Federzoni. Pm modelling workshop: Conclusions of dienet. In *European Congress and Exhibition on Powder Metallurgy. European PM Conference Proceedings*, volume 3, pages 321–326. The European Powder Metallurgy Association, January 2005.
- [34] J. Cante, M. Riera, J. Oliver, J. Prado, A. Isturiz, and C. Gonzalez. Flow regime analyses during the filling stage in powder metallurgy processes: experimental study and numerical modelling. *Granular Matter*, 13(1):79–92, February 2011.
- [35] K. Weimar. *LS-DYNA User's Guide*.
- [36] Y. Guo, C.-Y. Wu, and C. Thornton. The effects of air and particle density difference on segregation of powder mixtures during die filling. *Chemical Engineering Science*, 66(4):661–673, 2011.
- [37] Y. Guo, C-Y. Wu, K.D. Kafui, and C. Thornton. Numerical analysis of density-induced segregation during die filling. *Powder Technology*, 197(1):111–119, 2010.
- [38] J. Wang, H. Teng, Z. Han, and M. R. Jensen. Discrete element method in ls-dyna ® (dem). November 2012. Unofficial Guide, ® Livermore Software Technology Corporation.

- [39] B. Gladman. *LS-DYNA KEYWORD USER'S MANUAL - VOLUME II*. Livermore Software Technology Corporation (LSTC).
- [40] K.W. Chu, J. Chen, B. Wang, A.B. Yu, A. Vince, G.D. Barnett, and P.J. Barnett. Understand solids loading effects in a dense medium cyclone: Effect of particle size by a cfd-dem method. *Powder Technology*, 320:594 – 609, 2017.
- [41] LSTC and DYNAmore Nordic. Basic tutorials: Ex. 9. fsi with the icfd solver.
- [42] B. Gladman. *LS-DYNA KEYWORD USER'S MANUAL - VOLUME III*. Livermore Software Technology Corporation (LSTC).
- [43] Paul Evans. Properties of air at atmospheric pressure.
- [44] B.Q. Li. *Discontinuous Finite Elements in Fluid Dynamics and Heat Transfer*. Computational Fluid and Solid Mechanics. Springer London, 2006.

# Appendix



## ARDUINO scripts

---



Hereunder the basic ARDUINO script utilized in the die filling experiments can be found. It uses a running average and a Gaussian filter to smooth the output data.

## Untitled

```
//  
// IR distance measuring unit using Gauss filtering and running average - SHARP  
//  
  
#include <math.h>  
  
const int steps =50; // Antal målinger der tages i betragtning af gauss-filteret.  
float smooth_x; // filtreret outputt  
  
float rolling[steps]; // Rullende array for (steps) sidste målinger  
  
// Beregning af normalfordelingen:  
  
float stepsize = 0.2; // Opløsning på gauss-kurven  
float gstartX = -4.0; // Startværdi på x-aksen  
float xval[steps]; // Værdi på X-aksen  
float nr[steps]; // nummer for datasættet  
float Gaussval[steps]; // værdi på y-aksen  
  
float smooth_speed;  
float speed_vec[2];  
float time_vec[2];  
  
float groll[steps];  
int grollnr;  
float gsum = 0.00;  
float Goutput=0;  
int k=1;  
int i=1;  
int doneOut=0;  
int doneIn=1;  
float curTime=300000;  
  
const int aversize = 1; //Mængden af målinger der tages løbende gennemsnit for.  
(Justerbar) RUNNING AVERAGE  
float avgarr[aversize]; // Rullende array der tages gennemsnit af  
int indexavg =0; // Indeks  
float sumavg =0; // Sum  
  
float x; // Bruges i Gauss-filter  
int time_begin =0;  
int IRpin = A1; // analog pin for reading the IR  
sensor  
// the setup function runs once when you press reset or power the board  
void setup() {
```

Untitled

```
Serial.begin(9600); // start the serial port ---
initialize baud rate to 9600
pinMode(2, OUTPUT);
pinMode(3, OUTPUT);

for(int nd_index =0; nd_index < steps; nd_index++){
    nr[nd_index] = nd_index; // skaber array med tal 1-40
    xval[nd_index] = gstartX+(nr[nd_index]*stepsize); // ganger hvert tal
i nr[] med stepsize så xval[]= (-4,-3.8,-3.6.. 3.8,40)
Gaussval[nd_index] =
(1/(sqrt(2*3.14159)))*exp(-1*(xval[nd_index]*xval[nd_index])/2); // Beregner
y-værdier for normalfordelingen samlet fra startX til -startX (-4..4).
}
digitalWrite(2, HIGH);
digitalWrite(3, HIGH); //both high -> lock
}

void loop() {
float volts = analogRead(IRpin)*0.0048828125; // value from sensor * (5/1024) -
if running 3.3.volts then change 5 to 3.3 --- read value from analog pin "IRpin"
float distance = 12.594*pow(volts, -1.057); // worked out from graph 65 =
theretical distance / (1/Volts)S - luckylarry.co.uk
if (distance>40){
distance=30;
}
if (distance<3){
distance=3;
}
// Gauss-filter -----

// Producerer et rolling array af længde=steps , der gemmer de 40 sidste
sensormålinger, array'et opdateres for hver sensormåling.
for(int r_index = 0; r_index < steps; r_index++){
rolling[r_index]= distance;
//Serial.println(rolling[steps]);
}

//Ganger hvert enty i rolling array med den tilhørende værdi på
normalfordelingskurven.
for(int g_index =0; g_index < steps ; g_index++){
groll[g_index] = (rolling[g_index])*(Gaussval[g_index]);
}
}
```

```

                                Untitled
for(int gsum_index = 0; gsum_index < steps; gsum_index++){
    gsum = groll[gsum_index]+ gsum ;} // Lægges alle værdier i
groll sammen.
Goutput = (gsum/5);
gsum =0; // Nulstiller summen

// Rolling average
sumavg = sumavg - avgarr[indexavg];
avgarr[indexavg] = Goutput;
sumavg = sumavg + avgarr[indexavg];
indexavg = indexavg+1;

if(indexavg >= aversize){indexavg =0;}
smooth_x = sumavg / aversize; // Det filtrerede output.
float time_start = millis();
speed_vec[i]=smooth_x;
time_vec[i]=time_start;
smooth_speed=((speed_vec[2]-speed_vec[1])/100)/((time_vec[2]-time_vec[1])/1000);

//Print results
//Serial.println("Gauss filtering is:");
//Serial.println(Goutput);
//Serial.println("Smooth filtering is:");
//Serial.println(smooth_x);
float time = millis();

Serial.print("\t"); //This is just a tab to move the text in a bit
Serial.print(k); // Sample number
Serial.print("\t");
Serial.print(time); //Time since start of program
Serial.print("\t");
Serial.print(smooth_x); //Measured distance (cm)
Serial.print("\t");
//Serial.print(smooth_speed); //Measured distance (m/s) (don't think, that you can
trust this. When you do the experiment - just put then sensor in front or behind the
shoe and look at the time it takes to go from distance 1 to distance 2.
Serial.println("\t");
k++;
if (i<2){
i++;}
else {
i=1;
}
if ((millis() % 10000 <=30) && (doneIn==1)){
digitalWrite(2, HIGH); //both high -> lock
doneIn=0;
outWards();

```

Untitled

```
Serial.print("Going Out");
Serial.print("\n");
}
if ((curTime+500 <= millis()) && (doneOut==1)){
  digitalWrite(3, HIGH); //both high -> lock
inWards();
doneOut =0;
  Serial.print("Going In");
  Serial.print("\n");
}
delay(10); // arbitrary wait time.
}
void outWards(){
  //digitalWrite(2, HIGH); //both high -> lock
digitalWrite(3, LOW); // outwards
doneOut=1;
curTime=millis();
}
void inWards(){
  //digitalWrite(3, HIGH); //both high -> lock
digitalWrite(2, LOW); //inwards
doneIn = 1;
}
```



## Numerical models' diagram

---

# B

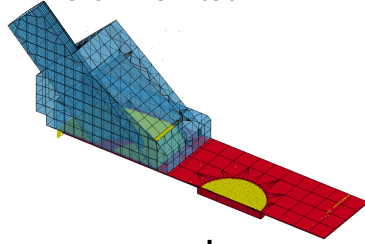
A diagram portraying the steps followed in the process of experimenting with different models. (\*) Section 6.5.7.

(\*\*) Paper by Chu et. al [40].

(\*\*\*) Section 6.4.2.

(\*\*\*\*\*) Section 6.5.4.

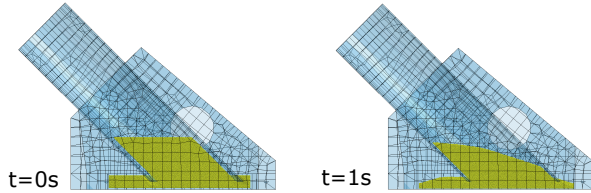
**Initial model from previous semester**  
DES: r=0.4 mm, n=92522  
Mat: \*MAT\_SOIL\_AND\_FOAM  
Sim Time: 2.2 s  
CPU Time: 1696 hr



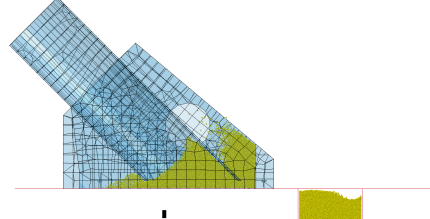
**Update parameters according to literature:**  
Mat of DES, surface coupling and DES interaction

**Split model:**  
One for initial fall of powder, and one for the filling process

**Step 1, powder falling**  
DES: r=0.4 mm, n=84655  
Sim Time: 1 s  
CPU Time: 204 hr



**Step 2, die filling**  
DES: r=0.4 mm, n=84655  
Sim Time: 0.23 s  
CPU Time: 32 hr



**Reduce size of DE:**  
Literature suggest up to 10 times

**78 times larger**  
DES: r=0.32 mm, n=232668  
Sim Time: 1 s  
CPU Time: 651 hr



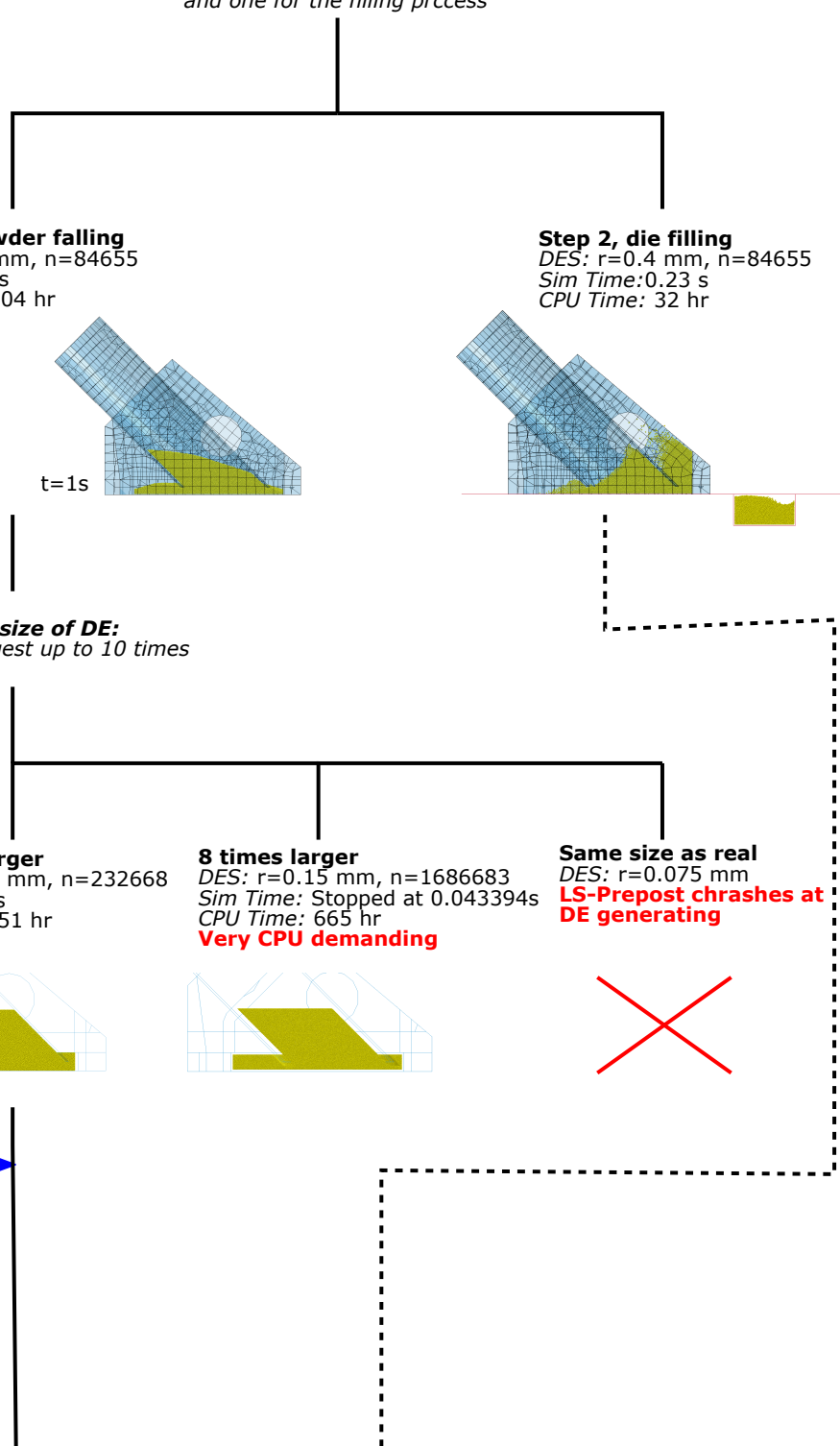
**8 times larger**  
DES: r=0.15 mm, n=1686683  
Sim Time: Stopped at 0.043394s  
CPU Time: 665 hr  
**Very CPU demanding**



**Same size as real**  
DES: r=0.075 mm  
**LS-Prepost crashes at DE generating**

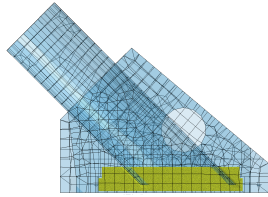


**Conducting initial experiments** →



**Change powder height according to experiments**

**Step 1 with powder height as in exp.**  
 DES:  $r=0.32$  mm,  $n=183169$   
 Sim Time: 1 s  
 CPU Time: 458 hr

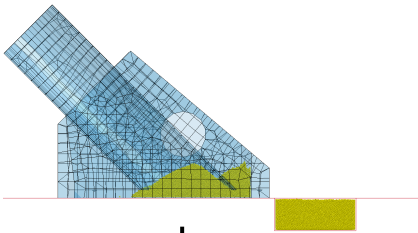


Dynain with DE after settling

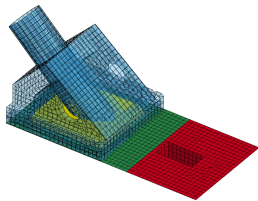
First obtaining of velocities from sensor

Model excl. DE  
 Change velocities of filling shoe according to sensor data

**Step 2 with powder height and velocities as in experiments, here RBBS**  
 DES:  $r=0.32$  mm,  $n=183169$   
 Sim Time: 0.45 s  
 CPU Time: 226 hr



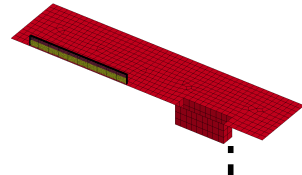
**Run full simulation to establish that half is sufficient**  
 See results in report (\*)



**Determination of best particle-particle interaction**  
 Litteratur states, that particle-particle interaction is the most uncertain parameter when enlarging particles, and that both density and system energy must be kept the same (\*\*)

Results for density

**Step 2 best setting for particle-particle interaction**  
 DES:  $r: 0.32$  mm,  $n=183169$   
 Sim Time: 0.45 s  
 CPU Time: 226 hr  
 Average density:  $3.828$  g/cm<sup>3</sup>



**Tester large DE, RBBS speed**  
 DES:  $r=0.32$  mm,  $n=1936$   
 Sim Time: 0.45 s  
 CPU Time: 1 hr 41 min



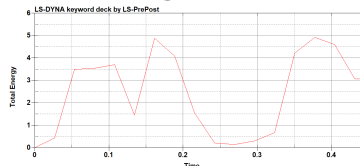
**Tester small DE, RBBS speed**  
 DES:  $r=0.15$  mm,  $n=24338$   
 Sim Time: 0.45 s  
 CPU Time: 39 hr 22 min



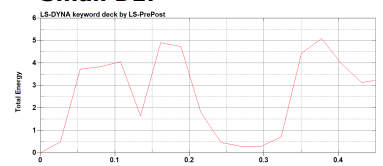
Iterations changing damping coefficients, and frictions, comparing with Tester small DE

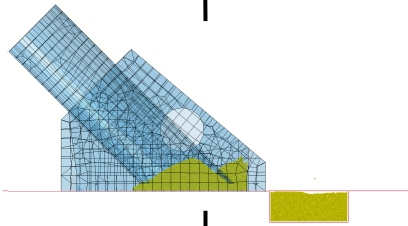
**Best setting for preserving total energy of the system:**  
 Normal damping: 0.125  
 Tangential damp: 0.125  
 Friction: 0.3  
 Rolling friction: 0.1

**Best setting:**



**Small DE:**





First obtaining of velocities from high speed camera

**Iterations raising friction and damping**  
 Literature study shows that higher friction between the particles results in less density (\*\*\*)

**Introducing contact death time between DE and shoe, and DE and sliding plane**  
 For reducing CPU hours by getting rid of the powder that are not in the die after the shoe returns

**Change velocities of filling shoe according to video data**

**Adding simulation time for securing that the powder settles before evaluating density**

**Investigation of material card (\*\*\*\*) for lowering CPU cost, comparing average density and total system energy, here RB**

Parameters: Normal and tangential damping=0.4  
 Friction=0.3 and rolling friction=0.1  
 DES: r=0.32 mm, n=183169

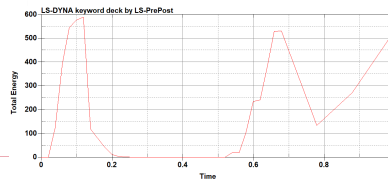
**Step 2 best setting for lowered density, with velocity from high speed videos, and introduced death of surface coupling, here RB**

Parameters: Normal and tangential damping=0.75  
 Friction and rolling friction=0.3

DES:r: 0.32 mm, n=183169  
 Sim Time: 0.84 s  
 CPU Time: 295 hr  
 Average density: 3.553 g/cm<sup>3</sup>

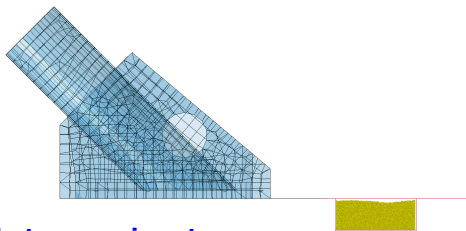
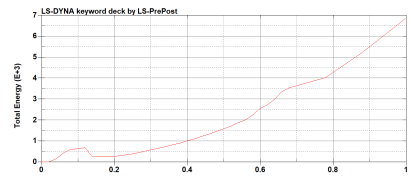
**\*MAT\_SOIL\_AND\_FOAM\_TITLE**

Sim Time: 1 s  
 CPU Time: 282 hr  
 Average density: 3.597 g/cm<sup>3</sup>  
**Reference**



**\*MAT\_RIGID\_TITLE**

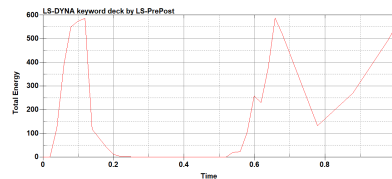
Sim Time: 1 s  
 CPU Time: 216 hr  
 Average density: 3.601g/cm<sup>3</sup>  
 No visible difference in powder flow



First comparison to flow obtained from high speed camera

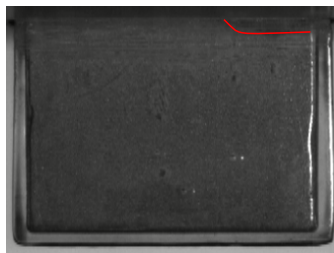
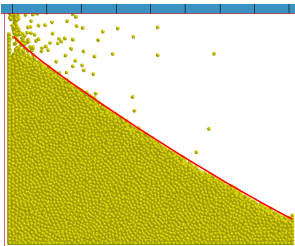
**\*MAT\_RIGID\_DISCRETE**

Sim Time: 1 s  
 CPU Time: 219 hr  
 Average density: 3.610 g/cm<sup>3</sup>  
 No visible difference in powder flow



**Step 2 evaluating flow compared to high speed videos, here ex. RB (40mm depth of die)**  
 Time=0.5, just before shoe starts retracting  
 Red line indicates line for powder

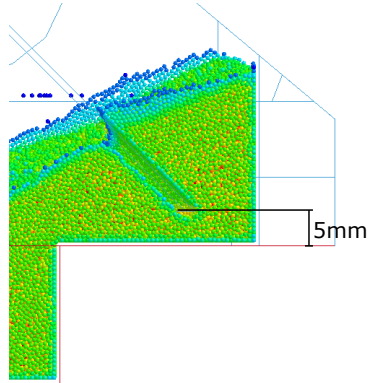
Direction of feeding shoe (outward)



**Raising tube from 5 mm to 10 mm**

Recognizing that due to increased particle size, the tube height could be acting like a narrow cavity, which could cause packing of particles -> less flow  
10 mm is the max height used in production

Direction of feeding shoe (outward) →



Raising the tube only resulted in a slight change

Iterations changing damping coefficients, and frictions for particle-particle interaction, and for DE surface coupling

Step 2 with the best parameters for flow, here ex. RB (40mm depth of die)

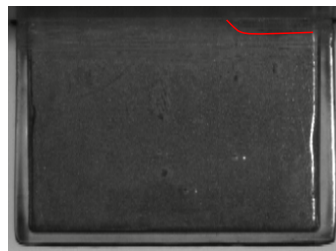
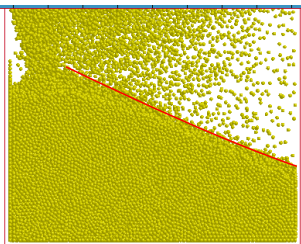
Parameters

DE coupling: normal and tangential damping=0.25  
friction=0.15 rolling friction=0.05  
DE-surface: friction and rolling friction=0.15  
damping=0.4

Time=0.5, just before shoe starts retracting

Red line indicates line for powder

← Direction of feeding shoe (outward)



Hand in



## ICFD numerical model keyword

---

C

The ICFD numerical model can be seen hereunder.

```

1  $$ LS-DYNA Keyword file created by LS-PrePost (R) V4.5.17 -- 02Apr2018
2  $$ Created on May-30-2018 (14:42:40)
3  *KEYWORD
4  *PARAMETER
5  $$ prm1 val1 prm2 val2 prm3 val3 prm4 val4
6  R T_end 0.8
7  R dt_plot 0.1
8  R rho_fluid 2.0
9  R mu_fluid 0.01
10 R dt_fluid 0.05
11 *INCLUDE
12 $$
13 Model.k
14 *INCLUDE
15 $$
16 ICFDmesh.k
17 *ICFD_BOUNDARY_NONSLIP
18 $$ pid
19 5
20 *ICFD_BOUNDARY_FREESLIP
21 $$ pid
22 7
23 *ICFD_BOUNDARY_PRESCRIBED_PRE
24 $$ pid lcid sf death birth
25 6 6 1.01.00000E28 0.0
26 *ICFD_CONTROL_DEM_COUPLING
27 $$ ctype bt dt sf
28 0 0.01.00000E28 1.0
29 *ICFD_CONTROL_TIME
30 $$ ttm dt cfl lcidsf dtmin dtmax dtinit tdeath
31 0.6 0.0 1.0 0 0.0 0.0 0.01.00000E28
32 *ICFD_MAT_TITLE
33 Air
34 $$ mid flg ro vis st
35 6 11.2040E-121.8210E-11 0.0
36 *ICFD_PART_TITLE
37 wall
38 $$ pid secid mid
39 5 5 6
40 *ICFD_PART_TITLE
41 outlet
42 $$ pid secid mid
43 6 5 6
44 *ICFD_PART_TITLE
45 symmetry
46 $$ pid secid mid
47 7 5 6
48 *ICFD_PART_VOL
49 $$ pid secid mid
50 1 5 6
51 $$ spid1 spid2 spid3 spid4 spid5 spid6 spid7 spid8
52 5 6 7 0 0 0 0 0
53 *ICFD_SECTION
54 $$ sid
55 5
56 *MESH_VOLUME
57 $$ volid
58 1
59 $$ pid1 pid2 pid3 pid4 pid5 pid6 pid7 pid8
60 5 6 7 0 0 0 0 0
61 *END
62

```

# Graphs and pictures from the experiments conducted

# D

Graphs introduced in Chapters 4 and 5 can be seen here in bigger dimensions to be more easily investigated.

Furthermore, the transparent 3D printed die used in Alexouli's [15] can be seen. The pictures are taken after it has been in use for a semester, so some scratches and build up powder can be distinguished.

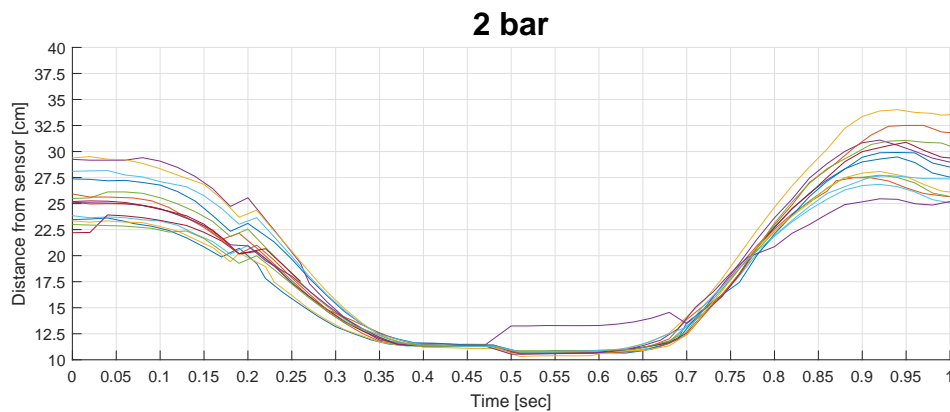


*Figure D.1.* Distance over time graphs from the displacements sensor for the experiments with 2 bar air input.

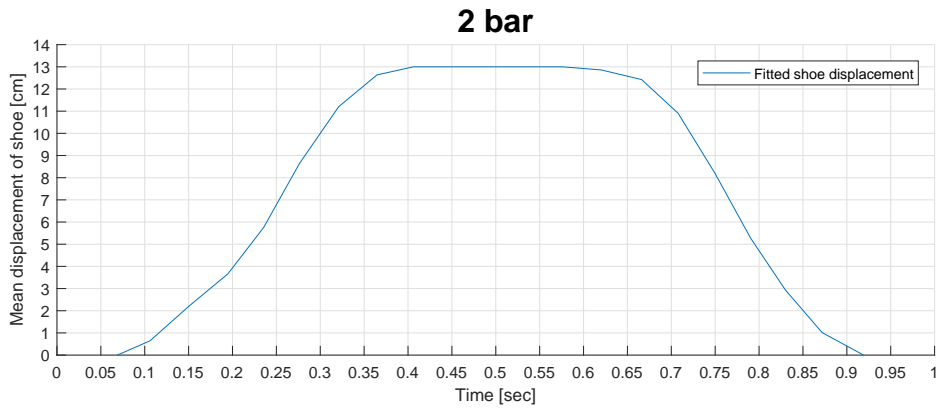


Figure D.2. Displacement graph from fitting the results above.

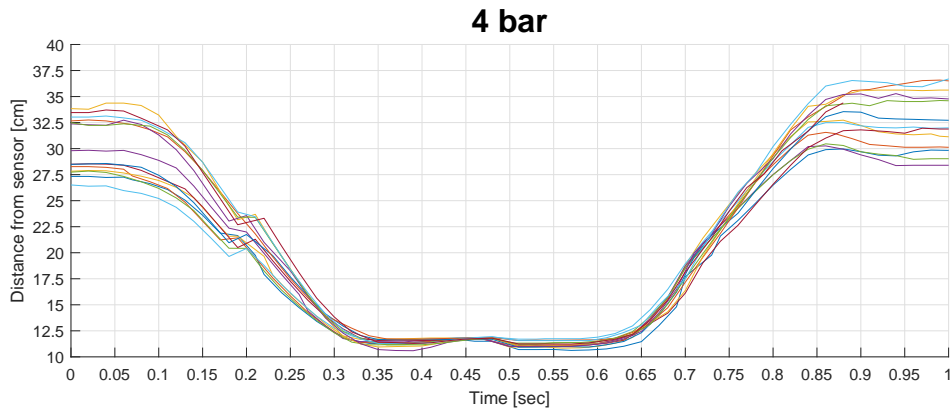


Figure D.3. Distance over time graphs from the displacements sensor for the experiments with 4 bar air input.

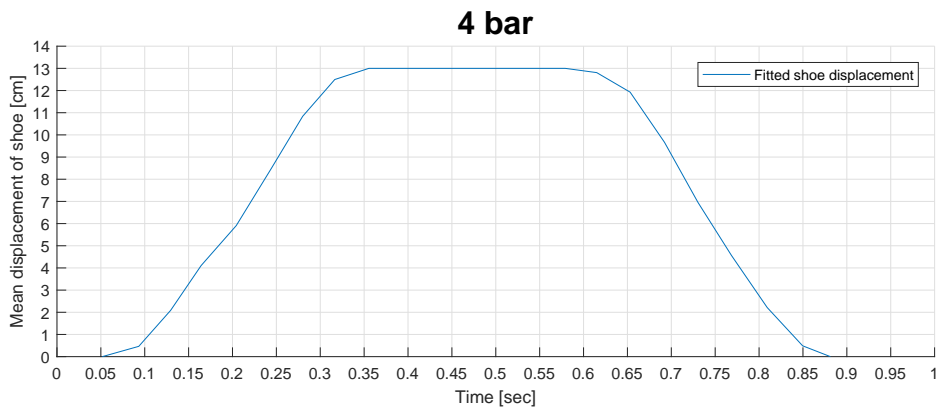
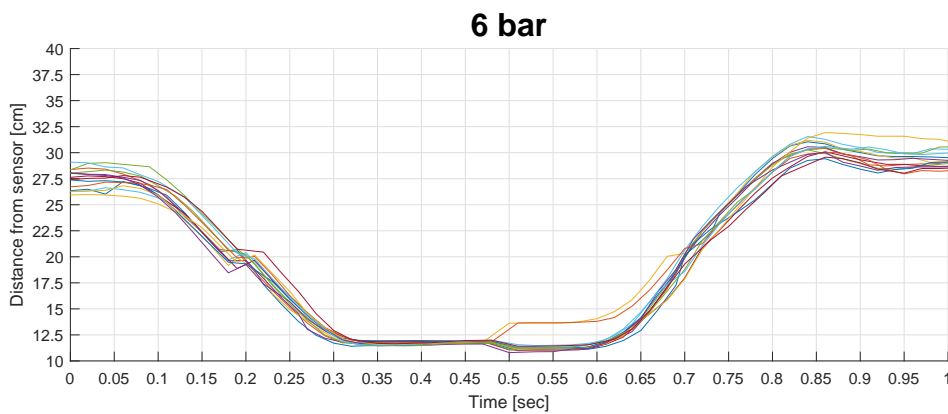
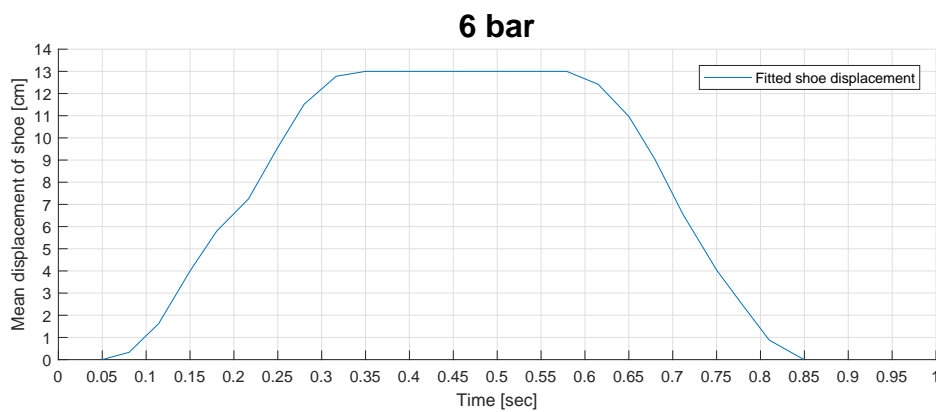


Figure D.4. Displacement graph from fitting the results above.



**Figure D.5.** Distance over time graphs from the displacements sensor for the experiments with 6 bar air input.



**Figure D.6.** Displacement graph from fitting the results above.

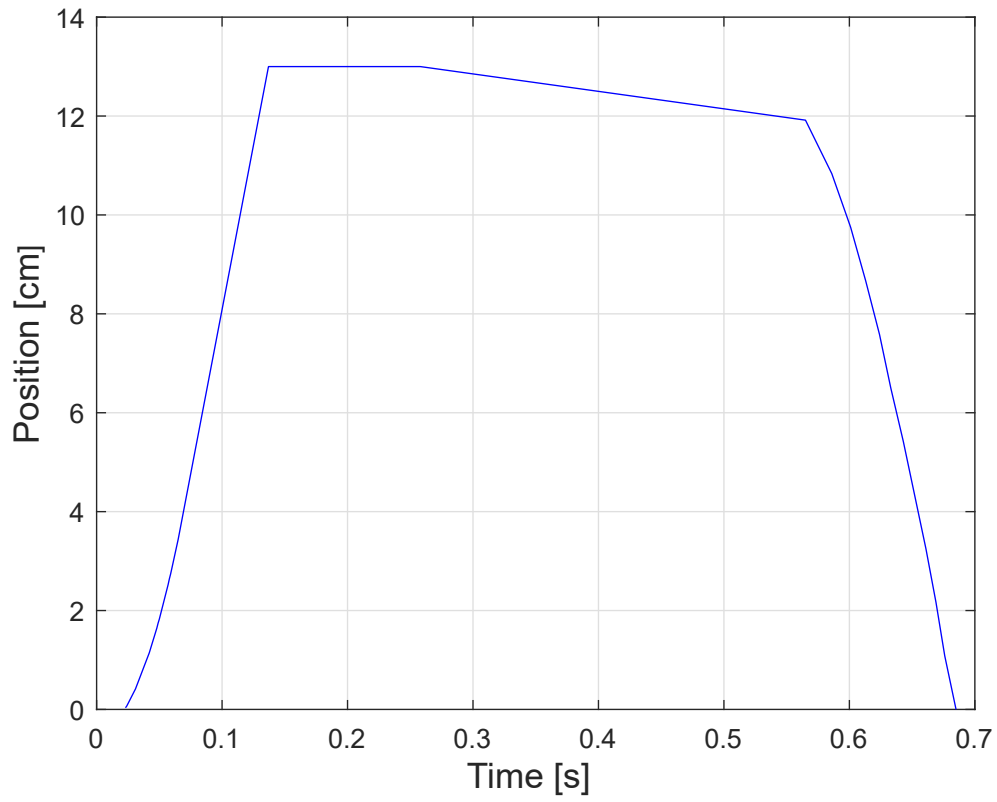


**Figure D.7.** Position over time graphs from analysing the high speed camera videos, for 4 bar air input.

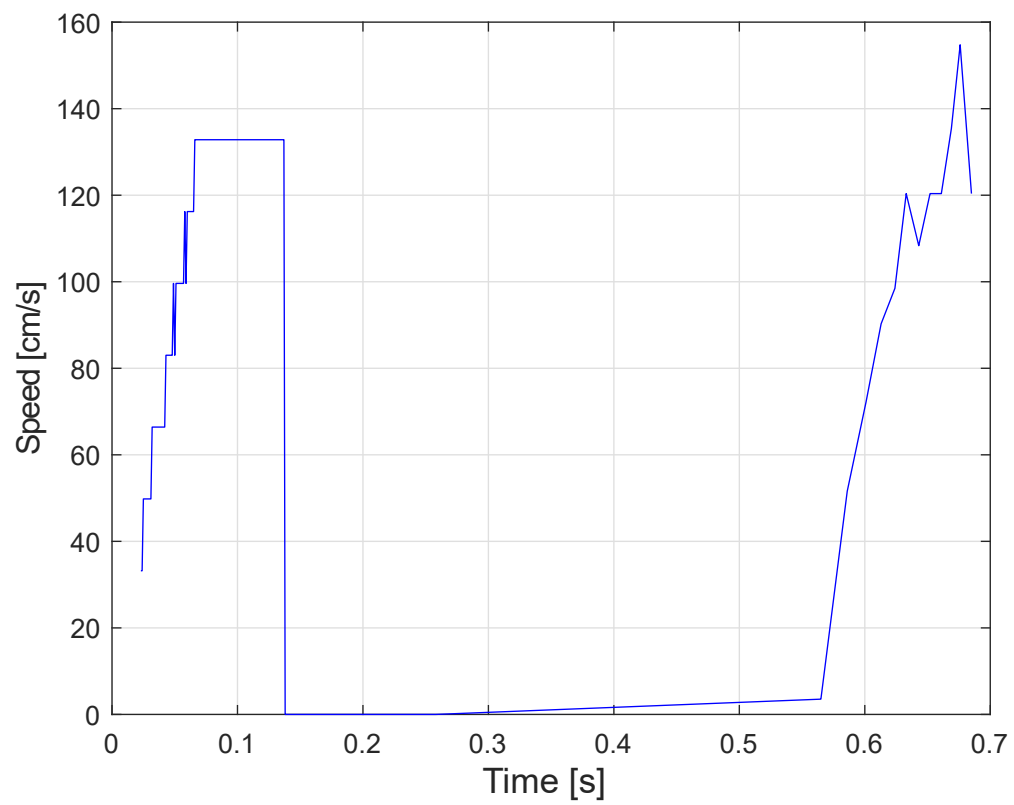


*Figure D.8.* Speed over time graphs from the displacements sensor for the experiments with 6 bar air input.

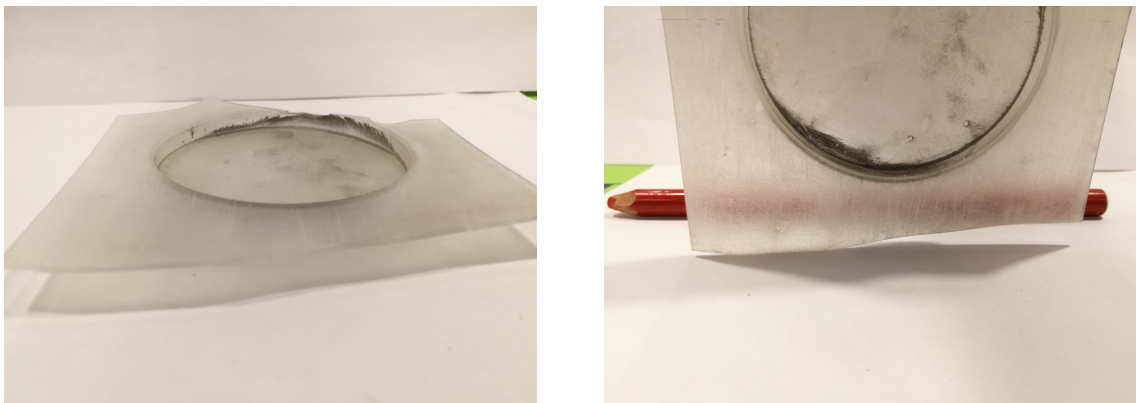


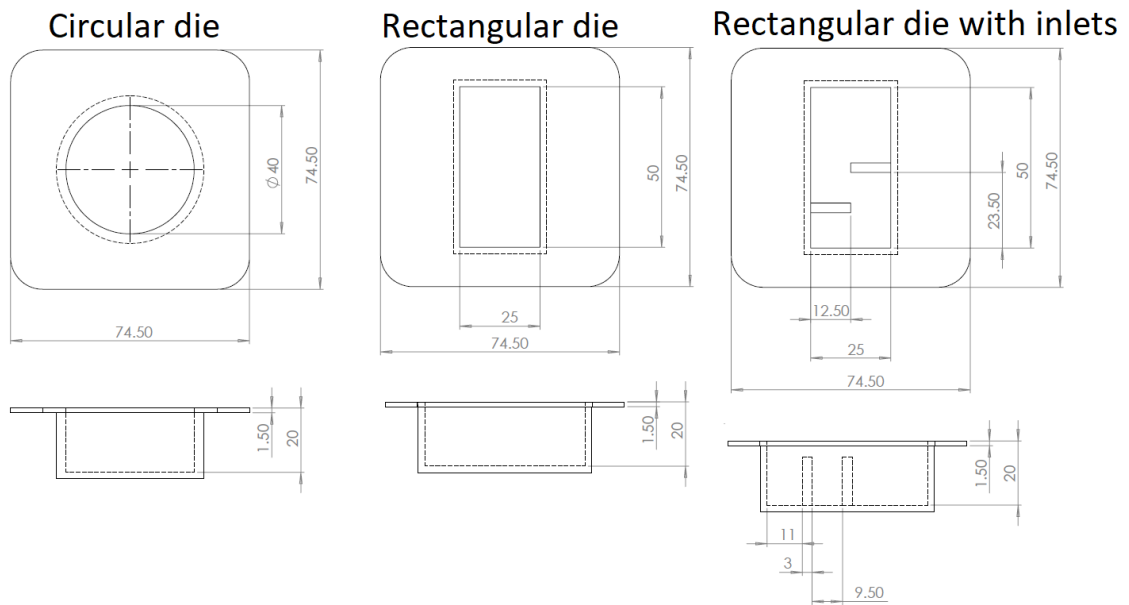
*Figure D.9.* Transparent dies without been grinded and coated.



# Die geometries

# E

In this Appendix detailed sketched of the basic dies geometries utilized in this study can be found. The transparent dies have one difference only, that they are 40 *mm* tall. All the dimensions are in *mm*.





## Numerical model keyword

---

F

In this Appendix the keyword file of the numerical model developed can be found.

Model

## LS-DYNA Keyword file created by LS-PrePost(R) V4.5.17 - 02Apr2018

## Created on May-30-2018 (14:39:06)

\*KEYWORD

\*TITLE

## title

LS-DYNA keyword deck by LS-PrePost

\*CONTROL\_DISCRETE\_ELEMENT

## ndamp tdamp fric fricr normk sheark cap mxnsc  
0.25 0.25 0.15 0.05 0.0 0.0 0 0

\*CONTROL\_OUTPUT

## npopt neecho nrefup iaccop opifs iprint ikedit iflush  
0 0 0 0 0.0 0 100 5000

## iprtf ierode tet10s8 msgmax ipcurv gmdt ip1dbl eocs  
0 0 2 50 0 0.0 0 0

## tolev newleg frfreq minfo solsig msgflg cdetol  
2 0 1 0 0 1 10.0

## phschng demden  
0 1

\*CONTROL\_TERMINATION

## endtim endcyc dtmin endeng endmas nosol  
0.6 0 0.0 0.0 0.0 0

\*CONTROL\_TIMESTEP

## dtinit tssfacs isdo tslimt dt2ms lctm erode ms1st  
0.0 0.9 0 0.0 0.0 4 0 0

## dt2msf dt2mslc imscl unused unused rmscl  
0.0 0 0 0.0

\*DATABASE\_ELOUT

## dt binary lcur ioopt option1 option2 option3 option4  
0.0 0 4 1 0 0 0 0

\*DATABASE\_GLSTAT

## dt binary lcur ioopt  
0.0 0 4 1

\*DATABASE\_NODOUT

## dt binary lcur ioopt option1 option2  
0.0 0 4 1 0.0 0

\*DATABASE\_BINARY\_D3PLOT

## dt lcdt beam npltc psetid  
0.0 4 0 0 0

## ioopt  
1

\*DATABASE\_BINARY\_DEMFOR

## dt lcdt beam npltc psetid  
0.0 4 0 0 0

\*BOUNDARY\_PRESCRIBED\_MOTION\_RIGID\_ID

## id heading  
1shoe\_movement

## pid dof vad lcid sf vid death birth  
2 1 2 1 1.0 0 8.0 0.0

Model

```

*LOAD_BODY_Z
$#   lcid      sf   lciddr      xc      yc      zc      cid
      5        1.0     0        0.0     0.0     0.0     0
*PART
$#                                     title
diePlane
$#   pid      secid      mid      eosid      hgid      grav      adpopt      tmid
      1        1        1        0        0        0        0        0
*SECTION_SHELL_TITLE
shell
$#   secid      elform      shrf      nip      propt      qr/irid      icomp      setyp
      1          2        1.0        5        1.0        0        0        1
$#   t1         t2         t3         t4         nloc      marea      idof      edgset
      1.0       1.0       1.0       1.0       0.0       0.0       0.0       0
*MAT_RIGID_TITLE
rigid_fully_constrained
$#   mid      ro      e      pr      n      couple      m      alias
      17.85000E-9  210000.0  0.3      0.0      0.0      0.0
$#   cmo      con1      con2
      1.0       7        7
$#lco or a1      a2      a3      v1      v2      v3
      0.0       0.0     0.0     0.0     0.0     0.0
*PART
$#                                     title
fillingShoe
$#   pid      secid      mid      eosid      hgid      grav      adpopt      tmid
      2        1        2        0        0        0        0        0
*MAT_RIGID_TITLE
rigid_y,z&rot_constrained
$#   mid      ro      e      pr      n      couple      m      alias
      27.85000E-9  210000.0  0.3      0.0      0.0      0.0
$#   cmo      con1      con2
      1.0       5        7
$#lco or a1      a2      a3      v1      v2      v3
      0.0       0.0     0.0     0.0     0.0     0.0
*PART
$#                                     title
slidingPlane
$#   pid      secid      mid      eosid      hgid      grav      adpopt      tmid
      3        1        1        0        0        0        0        0
*PART
$#                                     title
powder
$#   pid      secid      mid      eosid      hgid      grav      adpopt      tmid
      4        2        3        0        0        0        0        0
*SECTION_SOLID_TITLE
solid_des
$#   secid      elform      aet

```

Model

```

      2      2      0
*MAT_RIGID_DISCRETE_TITLE
rigidDES
$#   mid      ro      e      pr
      47.75000E-9  205000.0  0.28
*DEFINE_BOX_TITLE
des_box
$#   boxid      xmn      xmx      ymn      ymx      zmn      zmx
      1      -10.0      270.0      -10.0      72.0      -41.0      150.0
*DEFINE_DE_ACTIVE_REGION
$#   id      type      xm      ym      zm
      1      1      0.0      0.0      0.0
*DEFINE_DE_TO_SURFACE_COUPLING
$#   slave      master      stype      mtype
      4      1      3      1
$#   frics      fricd      damp      bsort      lcvx      lcvy      lcvz      wearc
      0.15      0.15      0.4      10      0      0      0      1.5
$#   w1      w2      w3      w4      w5      w6      w7      w8
*DEFINE_DE_TO_SURFACE_COUPLING
$#   slave      master      stype      mtype
      4      2      3      1
$#   frics      fricd      damp      bsort      lcvx      lcvy      lcvz      wearc
      0.15      0.15      0.4      10      0      0      0      1.5
$#   w1      w2      w3      w4      w5      w6      w7      w8
$#   sfp      sft      unused      unused      unused      cid_rcf      bt      dt
      1.0      1.0      0      0      0      0      0.0      0.225
*DEFINE_DE_TO_SURFACE_COUPLING
$#   slave      master      stype      mtype
      4      3      3      1
$#   frics      fricd      damp      bsort      lcvx      lcvy      lcvz      wearc
      0.15      0.15      0.4      10      0      0      0      1.5
$#   w1      w2      w3      w4      w5      w6      w7      w8
$#   sfp      sft      unused      unused      unused      cid_rcf      bt      dt
      1.0      1.0      0      0      0      0      0.0      0.225
*DEFINE_CURVE_TITLE
shoe_displacement
$#   lcid      sidr      sfa      sfo      offa      offo      dattyp      lcint
      1      0      1.0      10.0      0.0      0.0      0      0
$#
      a1      o1
      0.001      0.0
      0.03      1.181818
      0.043      2.363636
      0.054      3.545455
      0.063      4.727273
      0.072      5.909091
      0.08      7.090909
      0.088      8.272727
      0.096      9.454545

```

Model

0.105	10.63636
0.115	11.81818
0.131	13.0
0.136	13.0
0.16	11.81818
0.172	10.63636
0.181	9.454545
0.189	8.272727
0.197	7.090909
0.205	5.909091
0.211	4.727273
0.217	3.545455
0.224	2.363636
0.23	1.181818
0.238	0.0
8.0	0.0

\*DEFINE\_CURVE\_TITLE

timestep

\$#	lcid	sidr	sfa	sfo	offa	offo	dattyp	lcint
	4	0	1.0	1.0	0.0	0.0	0	0
\$#		a1		o1				
		0.0		0.02				
		0.225		0.02				
		0.225001		0.1				
		8.0		0.1				

\*DEFINE\_CURVE\_TITLE

gravity

\$#	lcid	sidr	sfa	sfo	offa	offo	dattyp	lcint
	5	0	1.0	1.0	0.0	0.0	0	0
\$#		a1		o1				
		0.0		9810.0				
		100.0		9810.0				

\*DEFINE\_CURVE\_TITLE

No\_Movement

\$#	lcid	sidr	sfa	sfo	offa	offo	dattyp	lcint
	6	0	1.0	1.0	0.0	0.0	0	0
\$#		a1		o1				
		0.0		0.0				
		8.0		0.0				

\*ELEMENT\_SHELL

\$#	eid	pid	n1	n2	n3	n4	n5	n6	n7	n8
-----	-----	-----	----	----	----	----	----	----	----	----

\*ELEMENT\_DISCRETE\_SPHERE\_VOLUME

\$#	nid	pid	volume	inertia	radii
-----	-----	-----	--------	---------	-------

\*NODE

\$#	nid	x	y	z	tc	rc
-----	-----	---	---	---	----	----

\*END

